UNIVERSITY OF CALIFORNIA,
IRVINE

An Isothermal, Low-resource Diagnostic Tool for Detection of SARS-CoV-2 Viral RNA and Discrimination between Relevant COVID-19 Strains in Vulnerable Communities

DISSERTATION

submitted in partial satisfaction of the requirements
for the degree of

DOCTOR OF PHILOSOPHY

in Biomedical Engineering

by

Alfonso Hyuntaek Shin

Dissertation Committee:
Distinguished Professor Emeritis Marc Madou, Chair
Adjunct Professor Lawrence Kulinsky
Associate Professor Elliot Hui

2022

DEDICATION

Dedicated to my family. Nam, Elizabeth, Andy, Angelina, Yvonne, Allie and Ozzy I look forward to the future where I can support you like you have supported me through another chapter of my life.

TABLE OF CONTENTS

LIST OF FIGURES

LIST OF TABLES

ACKNOWLEDGEMENTS

I would like to thank Professor Marc Madou who had served as my principal investigator for 5 years, who has supported me through many years and has inspired me to work toward a passion in development in diagnostics, especially with a viewpoint for those less fortunate to have readily accessible healthcare and medicine. His guidance has helped me achieve many of my goals and motivated me to think about science from a new perspective.

I would like to thank Professor Lawrence Kulinsky, who took me under his wing after Professor Madou's retirement and showed just as much attention and effort into my work as he did his students that he had initially accepted into his group. Without his guidance, much of the work of this dissertation would not have been accomplished.

I would like to thank Professor Elliot Hui, who regularly provided me with his perspective of this work and future direction that led to the development of this dissertation despite his limited time.

I would like to thank Professor Sunny Jiang, who first provided us with initial funding with our projects with Dr. Hamsa Gowda that would eventually become the current iteration that has been shared in this dissertation. Her expertise in diagnostics and generosity with her time were critical in the development of this work.

I would like to thank AMDI Autonomous Medical Devices Inc. for their generous funding that made the completion of this thesis possible.

VITA

Alfonso Hyuntaek Shin

2016	B.S. in Chemical Biology, University of California, Berkeley
2016-17	Research Assistant, Madou Lab, University of California, Irvine
2017-19	Master of Science in Biomedical Engineering, University of California, Irvine
2020-22	Doctor of Philosophy in Biomedical Engineering, University of California, Irvine

FIELD OF STUDY

Molecular Diagnostics Devices

PUBLICATIONS

An Isothermal Low-resource Cost Amplification Method for Differentiation of SARS-CoV-2 Wuhan Virus from Relevant Variant Strains Utilizing Detection of Genomic RNA (Prepared for Submission)

Guided Electrokinetic Self-Assembly of Polystyrene Microbeads As a Method of Detection and Post-concentration for Detection of SARS-CoV-2 Virus (In Preparation for Submission)

Signal Enhancement of Lateral Flow Detection Using Centrifugal Microfluidics (In Preparation for Submission)

PATENTS

Filed September 30th, 2021: ISOTHERMAL RNA SIGNAL AMPLIFICATION SYSTEM FOR SCREENING OF COVID-19 VARIANTS (UC Case no. 2022-717)

Filed April 15th, 2022: A BURSTABLE LIQUID STORAGE PACKAGE FOR BIOLOGICAL MATERIALS AND VALVE SUBSTITUTION (Application No.: 17/721,826)

Filed April 16th, 2022: A RECIRCULATION MECHANISM USING ELASTIC MEMBRANE (Application No.: 17/721,651)

ABSTRACT OF THE DISSERTATION

An Isothermal, Low-resource Cost Diagnostic Tool for Detection of SARS-CoV-2 Viral RNA and Discrimination between Relevant COVID-19 Strains in Vulnerable Communities

By

Alfonso Hyuntaek Shin

Doctor of Philosophy in Biomedical Engineering

University of California, Irvine, 2022

Distinguished Professor Emeritis Marc Madou, Chair

Since the emergence of the coronavirus SARS-CoV-2 in 2019, unprecedented rates of transmission coupled with alarmingly high mortality rates have remained the focus of the current healthcare climate. Despite the development of vaccines designed to combat virulence and the severity of the symptoms, the global healthcare crisis has continued through to 2022. Additionally, existing golden standard RNA-based diagnostics such as RT-PCR require expensive instrumentation, careful handling and extensive training, services that may not be immediately available to some vulnerable communities and limit their response during an epidemic. These issues have become increasingly evident with continued transmission stemming from mutation of the virus, resulting in a multitude of different lineages with varying degrees of infectivity, endangering the efficacy of existing solutions.

To address these shortcomings in the global response, an RNA-based diagnostic tool has been developed that provides an isothermal and easy-to-handle option for screening samples for the presence of the Wuhan strain of the SARS-CoV-2 virus (Wuhan-Hu-1) and differentiation from the UK (B.1.1.7) variant. In this work, two key steps have been incorporated for detection of regions of interest: 1) upstream isothermal amplification of key regions using Reverse

Transcription-Recombinase Polymerase Amplification (RT-RPA), and 2) a proof-read step using duplex-specific nuclease that mediates further signal amplification only in the presence of a perfect DNA:RNA duplex. We further demonstrate compatibility with alternative low-resource signal enhancement strategies with a signal concentration method utilizing electro-osmotic concentration of bead-based fluorescence and detection on lateral flow nitrocellulose strips. The potential of this novel nuclease-based fluorescent assay is demonstrated as a user-friendly alternative for screening between relevant SARS-CoV-2 strains through detection of key regions within the ORF1a and S genes necessary to distinguish between the aforementioned strains (Wuhan-Hu-1, B.1.1.7).

INTRODUCTION

Since the emergence of the coronavirus SARS-CoV-2 in 2019, unprecedented rates of transmission coupled with alarmingly high mortality rates have remained the focus of the current healthcare climate.[1] Despite the development of vaccines designed to combat virulence and severity of the symptoms, the global healthcare crisis has continued through to 2022. Additionally, existing gold standard RNA-based diagnostics require expensive instrumentation, sterile handling of infectious patient sample to avoid contamination and extensive training with sophisticated instrumentation for sample preparation and analysis, services that require trained personnel and expensive tools that may not be immediately available to all communities.[2] These issues have become increasingly evident with continued transmission stemming from mutation of the virus, resulting in a multitude of different lineages with varying degrees of infectivity, endangering the efficacy of existing solutions.[3] Access to systems that enable low resource, reliable screening options with minimal handling have become a critical component in monitoring variant trends within populations to contain the spread of disease and deter the prolongation and potential re-escalation of the global crisis.

[1]Cascella, Marco, et al. "Features, evaluation, and treatment of coronavirus (COVID-19)." *Statpearls [internet]* (2022).
[2]Song, Qi, et al. "Point-of-care testing detection methods for COVID-19." *Lab on a Chip* 21.9 (2021): 1634-1660.
[3]Vasireddy, Deepa, et al. "Review of COVID-19 variants and COVID-19 vaccine efficacy: what the clinician should know?." *Journal of Clinical Medicine Research* 13.6 (2021): 317.

Limiting Factors for COVID-19 in Vulnerable Communities:

While COVID-19 typically results in development of mild illness, approximately 14% of those effected require hospitalization and another 5% require intensive care unit support.[4] SARS-CoV-2 has impacted communities to a greater degree than previous epidemics such as SARS-CoV and MERS-CoV due to several key characteristics of the virus, including higher rates of infectivity resulting from aerosol transmission and recombination leading to new variants, and long asymptomatic incubation periods within the host.[5] Infection with COVID-19 has also displayed varying degrees of symptoms and infectivity, leading to underreporting of cases globally. The Center for Disease Control and Prevention estimates that 86% of cases prior to travel restrictions implemented on January 23rd, 2020 during the initial emergence of the virus were undocumented. Even after instatement of COVID-19 protocols, the CDC estimates that only 1 in 4 COVID-19 infections in the United States were reported during the time frame of February 2020 to September 2021.[6] These staggering numbers are further amplified in communities without regular access to clinical screening and healthcare to contain the spread of contagion.[7]

This issue is exacerbated in vulnerable communities with limitations on available standards of healthcare, resulting in a potential outbreaks within a community leading to greater disease transmission from untreated cases.[8] Inaccessibility to common screening options in these communities is driven by multiple factors including high cost of instruments and reagents necessary to perform laboratory tests, decentralization of healthcare in regions with a lack of

[4] WHO Clinical Management of Severe Acute Respiratory Infection (SARI) When COVID-19 Disease is Suspected: Interim guidance. 2020. https://apps.who.int/iris/bitstream/handle/10665/331446/WHO-2019-nCoV-clinical-2020.4-eng.pdf?sequence=1&isAllowed=y (accessed 7 November 2022)
[5] Ludwig, Stephan, and Alexander Zarbock. "Coronaviruses and SARS-CoV-2: a brief overview." *Anesthesia and analgesia* (2020).
[6] National Center for Immunization and Respiratory Diseases (NCIRD), Division of Viral Diseases, Aug. 12 20222.
[7] "Symptoms of COVID-19." Center for Disease Control and Prevention. Mar. 22, 2022
[8] Giri, Anil K., and Divya RSJB Rana. "Charting the challenges behind the testing of COVID-19 in developing countries: Nepal as a case study." *Biosafety and Health* 2.02 (2020): 53-56.

infrastructure, and limited training and expertise with complicated instrumentation and protocols required to operate these tests.[9] These issues all contribute to the inability to contain an outbreak within a community, leading to a higher risk of mortality due to insufficient means of diagnosis and treatment, as well as lapses in data for understanding trends to formulate a proper public health response. Due to these limitations, there is a clear need for simple screening options with limited instrumentation that facilitate screening of large vulnerable populations to minimize the burden of disease.

Evolution of SARS-CoV-2 and Sequence Differentiation Between Variants:

Despite the presence of an exonuclease enzyme in coronaviruses that reduce replication error rate by 15-fold to 20-fold, further diversity of the virus has emerged through recombination resulting from infection of a host by variants with different mutations.[10,11,12,13] Incidentally, this has complicated phylogenetic classification of emergent SARS-CoV-2 lineages due to the high degree of similarity between existing and emerging viral strains.[14] Geographical classification of variants has also been largely unsuccessful due to their emergence in multiple countries and

[9] World Health Organization. "Global atlas of medical devices." (2017).
[10] Minskaia, E. et al. Discovery of an RNA virus 3'→5' exoribonuclease that is critically involved in coronavirus RNA synthesis. *Proc. Natl Acad. Sci. USA* **103**, 5108–5113 (2006).
[11] Eckerle, L. D. et al. Infidelity of SARS-CoV Nsp14-exonuclease mutant virus replication is revealed by complete genome sequencing. *PLoS Pathog.* **6**, e1000896 (2010).
[12] Duffy, S., Shackelton, L. A. & Holmes, E. C. Rates of evolutionary change in viruses: patterns and determinants. *Nat. Rev. Genet.* **9**, 267–276 (2008).
[13] Tao, Kaiming, et al. "The biological and clinical significance of emerging SARS-CoV-2 variants." *Nature Reviews Genetics* 22.12 (2021): 757-773.
[14] guia, R. T. et al. A human coronavirus evolves antigenically to escape antibody immunity. *PLoS Pathog.* **17**, e1009453 (2021).

inconsistencies in reported sequencing in different countries.[15,16,17] For this reason, variants are classified according to lineage and component mutations and are largely defined by different subsets of mutations.[18,19]

Variant B1.1.7 also known as the alpha variant, contains spike mutations including the RBD mutation N501Y, P681H and NTD deletions at positions 69–70 and 144. The 69-70 base deletion has been noted to impede sequence amplification of the genomic region in commonly used diagnostic PCR assays, resulting in S-gene target failure.[20,21] During the initial stages of the COVID-19 pandemic, molecular assays were developed to target these mutation regions of the B1.1.7 variant genome in order to differentiate with the Wuhan-hu-1 strain. Established assays have utilized detection of the conserved nucleocapsid (N1) region, 3675-3677 deletion of the open reading frame 1a (ORF1a) region, and 69-70 deletion of the spike region with S-gene target failure indicative of the spike deletion as a method to differentiate the Wuhan-hu-1 strain from newly emerging B1.1.7 strain reaching sensitivities down to 1 copy/ µl.[22,23]

[15] Morel, B. et al. Phylogenetic analysis of SARS-CoV-2 data is difficult. *Mol. Biol. Evol.* **38**, 1777–1791 (2020).
[16] Mavian, C. et al. Sampling bias and incorrect rooting make phylogenetic network tracing of SARS-COV-2 infections unreliable. *Proc. Natl Acad. Sci. USA* **117**, 12522–12523 (2020).
[17] Rambaut, A. et al. A dynamic nomenclature proposal for SARS-CoV-2 lineages to assist genomic epidemiology. *Nat. Microbiol.* **5**, 1403–1407 (2020).
[18] Volz, E. et al. Assessing transmissibility of SARS-CoV-2 lineage B.1.1.7 in England. *Nature* **593**, 266–269 (2021).
[19] Allen, H. et al. Increased household transmission of COVID-19 cases associated with SARS-CoV-2 variant of concern B.1.617.2: a national case–control study. *Knowledge Hub* (2021).
[20] Faria, N. R. et al. Genomics and epidemiology of the P.1 SARS-CoV-2 lineage in Manaus, Brazil. *Science* **372**, 815–821 (2021).
[21] Borges, Vítor, et al. "Tracking SARS-CoV-2 VOC 202012/01 (lineage B. 1.1. 7) dissemination in Portugal: insights from nationwide RT-PCR Spike gene drop out data." *Euro. Surveill* 26 (2021): 2100131.
[22] Vogels, Chantal BF, et al. "PCR assay to enhance global surveillance for SARS-CoV-2 variants of concern." *MedRxiv* (2021).
[23] Morel, B. et al. Phylogenetic analysis of SARS-CoV-2 data is difficult. *Mol. Biol. Evol.* **38**, 1777–1791 (2020).

Methods of Detection for COVID-19:

Detection of COVID-19 infection can be divided into three main methods targeting different analyte; 1) antibody-based detection targeting antibodies produced during immune response, 2) antigen detection targeting presence of viral protein within sample, and 3) nucleic acid amplification (NAAT) testing targeting a specific sequence of the virus, each with their own advantages over one another.[24,25,26] In antibody testing, humoral response to SARS-CoV-2 includes production of IgM, IgG, and IgG antibodies directed against S and N proteins and can be detected one to three weeks following infection.[23,27] Antibody testing had originally been used extensively as a means of point-of-care screening due to fast turnaround times and low cost to manufacture.[28,29] However, antibodies can exist in a host with resolving or past SARS-CoV-2 infection, indicating that this method is not reflective of active infection with SARS-CoV-2.[21,26] Additionally, due to the requirement of an active immune response in the host, antibody testing can be unsuitable for detection of viral genome during early stages of infection.[30,31,32]

[24] Jacofsky, David, Emilia M. Jacofsky, and Marc Jacofsky. "Understanding antibody testing for COVID-19." *The Journal of arthroplasty* 35.7 (2020): S74-S81.
[25] Hall VJ, Foulkes S, Charlett A, Atti A, Monk EJM, Simmons R, et al. SARS-CoV-2 infection rates of antibody-positive compared with antibody-negative health-care workers in England: a large, multicentre, prospective cohort study (SIREN). Lancet. 2021 Apr 17;397(10283):1459-69.
[26] Liu, Guoqiang, and James F. Rusling. "COVID-19 antibody tests and their limitations." *ACS sensors* 6.3 (2021): 593-612.
[27] Lumley SF, O'Donnell D, Stoesser NE, Matthews PC, Howarth A, Hatch SB, et al. Antibody status and incidence of SARS-CoV-2 infection in health care workers. N Engl J Med. 2020 Dec 23;384:533-40.
[28] Qu, Jiuxin, et al. "Profile of immunoglobulin G and IgM antibodies against severe acute respiratory syndrome coronavirus 2 (SARS-CoV-2)." *Clinical Infectious Diseases* 71.16 (2020): 2255-2258.
[29] Wölfel, Roman, et al. "Virological assessment of hospitalized patients with COVID-2019." *Nature* 581.7809 (2020): 465-469.
[30] Grifoni A, Weiskopf D, Ramirez SI, Mateus J, Dan JM, Moderbacher CR, et al. Targets of T cell responses to SARS-CoV-2 coronavirus in humans with COVID-19 disease and unexposed individuals. Cell. 2020 Jun 25;181(7):1489-501 e15.
[31] Robbiani DF, Gaebler C, Muecksch F, Lorenzi JCC, Wang Z, Cho A, et al. Convergent antibody responses to SARS-CoV-2 in convalescent individuals. Nature. 2020 Aug;584(7821):437-42.
[32] Suthar MS, Zimmerman MG, Kauffman RC, Mantus G, Linderman SL, Hudson WH, et al. Rapid generation of neutralizing antibody responses in COVID-19 patients. Cell Rep Med. 2020 Jun 23;1(3):100040.

Unlike antibody-based detection, antigen and nucleic-acid amplification testing directly target the virus within the host and possess the ability to verify active infection. Antigen tests measure viral presence in sample through detection of key surface proteins and hold several key advantages in comparison to NAAT testing, including faster sample-to-answer times (15-30 minutes), point-of-care employment, and lower demands for instrumentation and personnel training at lower costs. However, antigen testing suffers from lower sensitivity with limits of detection up to 10,000 times higher than NAAT or molecular testing and are prone to false-negative results, a critical issue when screening large patient samples.[33,34]

Among COVID-19 diagnostic techniques, NAAT testing or molecular detection has provided the genetic specificity needed to accurately detect the virus.[35] Nucleic acid-based detection such as reverse transcription polymerase chain reaction (RT-PCR) has become standardized for clinical screening in diagnostics due to two key advantages over other relevant viral detection methods; 1) the ability to evaluate presence of active virus (a feature that is not possible with antibody-based detection methods, and 2) improved sensitivity over antigen-based detection techniques resulting from nucleic acid amplification.[36,37] Among COVID-19 diagnostics, molecular detection also provides the genetic specificity needed to accurately detect and differentiate viral strains. While RT-PCR has served as the gold standard for COVID-19 detection, it still suffers from assay complexity, expensive instrumentation, and requires trained personnel that complicate deployment in decentralized laboratory settings. More specifically, RT-PCR

[33] Corman, Victor M., et al. "Comparison of seven commercial SARS-CoV-2 rapid point-of-care antigen tests: a single-centre laboratory evaluation study." *The Lancet Microbe* 2.7 (2021): e311-e319.
[34] Arnaout, Ramy, et al. "SARS-CoV2 testing: the limit of detection matters." *BioRxiv* (2020).
[35] Tahamtan, Alireza, and Abdollah Ardebili. "Real-time RT-PCR in COVID-19 detection: issues affecting the results." *Expert review of molecular diagnostics* 20.5 (2020): 453-454.
[36] Liu, Guoqiang, and James F. Rusling. "COVID-19 antibody tests and their limitations." *ACS sensors* 6.3 (2021): 593-612.
[37] Giri, Anil K., and Divya RSJB Rana. "Charting the challenges behind the testing of COVID-19 in developing countries: Nepal as a case study." *Biosafety and Health* 2.02 (2020): 53-56.

requires a thermocycler, complex reagent storage, and trained personnel, limiting adoption by vulnerable communities that are often most impacted by an outbreak.[38] For rapid detection and tracking of COVID-19 and its variants within communities in potentially resource-limited locations, point-of-care tests are urgently needed for patient screening.

Isothermal Amplification Techniques for Low-resource Detection Methods:

While techniques for RNA-based low resource-cost or point-of-care screening currently exist and have been successfully deployed, many are susceptible to common issues including false-positive results that impact the reliability of the detection method. Isothermal techniques such as loop-mediated isothermal amplification (LAMP) and recombinase polymerase amplification (RPA) can be impacted by nonspecific amplification resulting from low operating temperatures causing poor annealing of primers, leading to inaccurate diagnosis and ineffective treatment.[39] In other works, researchers have utilized highly specific detection methods in conjunction with isothermal amplification strategies, including clustered regularly interspaced short palindromic repeats (CRISPR)/Cas technologies for targeted recognition and cleavage activity in the presence of target analyte.[40,41,42] However, due to the sequence-specific nature of CRISPR/Cas-mediated detection, multiplexing of such platforms can pose a challenge when targeting multiple regions of the SARS-CoV-2 genome, requiring unique CRISPR/cas pairs for each target analyte and

[38] Rezaei, Meysam, et al. "Point of Care Diagnostics in the Age of COVID-19." *Diagnostics* 11.1 (2020): 9.

[39] Becherer, L. et al. Loop-mediated isothermal amplification (LAMP)—review and classification of methods for sequence-specific detection. *Anal. Methods* 12, 717–746 (2020).

[40] Sun, Yangyang, et al. "One-tube SARS-CoV-2 detection platform based on RT-RPA and CRISPR/Cas12a." *Journal of translational medicine* 19.1 (2021): 1-10.

[41] Chen, Janice S., et al. "CRISPR-Cas12a target binding unleashes indiscriminate single-stranded DNase activity." *Science* 360.6387 (2018): 436-439.

[42] Gootenberg, Jonathan S., et al. "Nucleic acid detection with CRISPR-Cas13a/C2c2." *Science* 356.6336 (2017): 438-442.

complicating sample preparation.[43] Further enhancements in assay design are necessary to improve specificity while maintaining the sensitivity of existing RNA-based detection schemes with consideration for non-specific nucleases should be considered for their role in multiplexing strategies for molecular detection.

DSN Mechanism of Specific DNA Cleavage:

Finding an effective amplification strategy that combines both the specificity needed for variant tracking and the simplicity needed for point-of-care diagnostics is key for the future of COVID-19 detection and monitoring. With numerous discoveries of new classes of nucleases, enzymatic manipulation of nucleic acids has become integral to common biochemical assay techniques, enabling simplified assay conditions, high specificity and incorporation into common multiplexing designs.[44] With the ability to contribute to improving sensitivity, specificity, and multiplexing, nuclease-based detection methods are ideal for application in molecular detection of viral genome with sequence-based species differentiation. More comprehensive understanding of the preferential activity of these nucleases has extended the technique's relevance to a wider range of target analytes ranging from miRNA to DNA, inspiring novel designs for molecular diagnostic applications.[45]

One such enzyme is duplex-specific nuclease (DSN), a unique class of nonspecific duplex-cleaving nucleases originating from the cellular mechanisms of Paralithodes camtschaticus (Red King Crab) that has been utilized for RNA-based diagnostics due to its sequence-independent

[43] Gootenberg, Jonathan S., et al. "Multiplexed and portable nucleic acid detection platform with Cas13, Cas12a, and Csm6." *Science* 360.6387 (2018): 439-444.
[44] Gerasimova, Yulia V., and Dmitry M. Kolpashchikov. "Enzyme-assisted target recycling (EATR) for nucleic acid detection." *Chemical Society Reviews* 43.17 (2014): 6405-6438.
[45] Ye, Jiawei, et al. "Research advances in the detection of miRNA." *Journal of pharmaceutical analysis* 9.4 (2019): 217-226.

DNA cleaving activity and inactivity toward RNA.[46] Additionally, DSN has been found to display preferential activity toward DNA in duplexes while exhibiting minimal cleaving activity in the presence of mismatched pairs. This selective activity of the enzyme enables improved probe specificity while mediating signal enhancement through linear amplification from nuclease-mediated cleavage of the reporter probe-target complex.[47] With its compatibility with current point-of-care methods while improving assay specificity, the use of DSN is appropriate for application in molecular detection of viral RNA and sequence-based variant differentiation.[48] These properties of DSN have spurred recent investigation into the nuclease's potential for signal amplification and target specificity in RNA detection in COVID-19 diagnostics.[49]

[46] Shagin, Dmitry A., et al. "A novel method for SNP detection using a new duplex-specific nuclease from crab hepatopancreas." *Genome research* 12.12 (2002): 1935-1942.
[47] Qiu, Xiaopei, et al. "Duplex-specific nuclease-mediated bioanalysis." *Trends in biotechnology* 33.3 (2015): 180-188.
[48] Tan, Lin, et al. "Duplex-specific nuclease-mediated target recycling amplification for fluorescence detection of microRNA." *Analytical Methods* 11.2 (2019): 200-204.
[49] Liu, Meiqing, et al. "SARS-CoV-2 RNA detection with duplex-specific nuclease signal amplification." *Micromachines* 12.2 (2021): 197.

Figure 1: Schematic of Duplex-specific Nuclease-mediated Mismatch Discrimination Scheme. The image highlights the mismatch discrimination capabilities of DSN by including the presence of target and non-target RNA. The associated signal can be adapted for measurement on different detection platforms making this technique very versatile. Scheme: a) RNA (target) is introduced into a solution with a complementary ssDNA modified with a reporter (e.g. fluorophore) and allowed to hybridize to form a DNA-RNA duplex. b) DSN is then introduced and cleaves the ssDNA in the duplex, releasing both the reporter and intact RNA target back into solution. Thus, the target RNA can be recycled and hybridized with remaining uncleaved ssDNA reporter probes. As this cycle repeats, more cleaved reporters are accumulated in solution and are collected for downstream detection.[50]

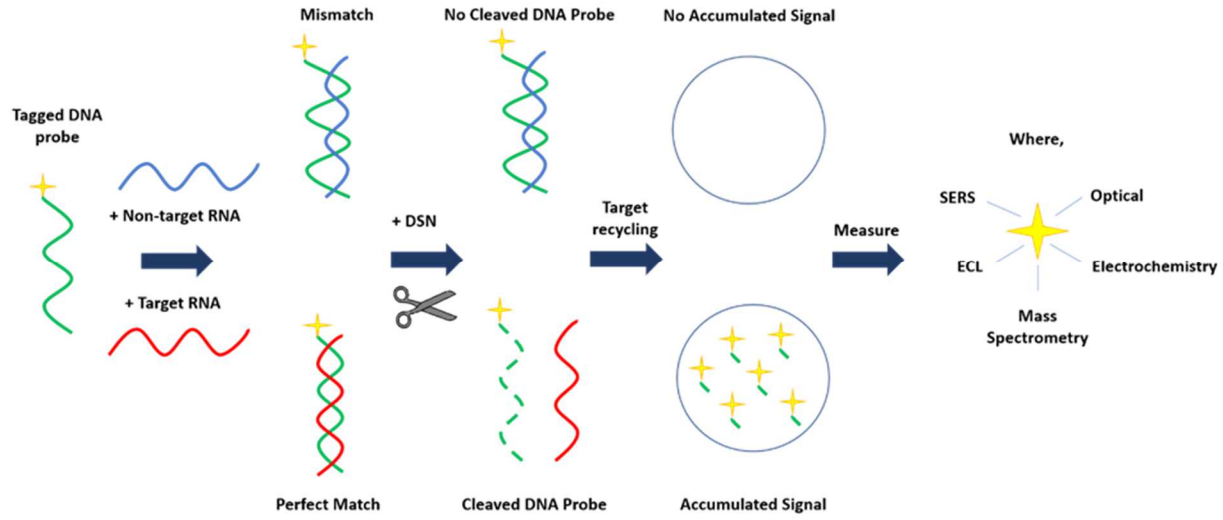

[50] Gong, Shaohua, et al. "Duplex-specific nuclease-assisted CRISPR-Cas12a strategy for MicroRNA detection using a personal Glucose meter." *Analytical Chemistry* 93.30 (2021): 10719-10726.

Current Applications for DSN Discrimination for Detection of miRNA:

Duplex-specific nuclease's unique cleaving activity has garnered interest in identifying single mismatched bases in genomic DNA studies as well as in sequence-specific miRNA detection, a common biomarker used in cancer and other disease-related diagnostics. miRNAs are typically short, 20-24 bp non-coding sequences that influence multiple biological pathways, including many related to cancer.[51,52] However, miRNA families exhibit sequence similarity and thus accurate sequence differentiation is needed for related disease detection.

By taking advantage of the lack of nuclease activity in the presence of mismatched pairs, DSN-mediated strategies have been employed for improving specificity and mismatch discrimination when detecting trace amounts of miRNA.[53,54] In a 2016 work by Miao et al., a biosensor targeting miR-29a-3p, a biomarker related to influenza, demonstrated successful distinction of the target when tested against six closely related miRNAs, demonstrating DSN's ability to discriminate up to a single base-pair mismatch.[53] Due to these intrinsic capabilities of DSN to distinguish mismatches and prevent nonspecific amplification, multiplexed detection mechanisms have also been well explored.[53,55,56] Xu et al., utilized sequence specific 3D tetrahedron-structured probes to simultaneously target three different miRNAs (miRNA-26a, miRNA-16, and miRNA-21) and coupled them with varying fluorescent dyes for optical

[51] Liu, Meiying, et al. "Label-free optical detection of single-base mismatches by the combination of nuclease and gold nanoparticles." *Biosensors and Bioelectronics* 26.11 (2011): 4294-4300.
[52] Jansson, Martin D., and Anders H. Lund. "MicroRNA and cancer." *Molecular oncology* 6.6 (2012): 590-610.
[53] Xu, Fang, et al. "Ultrasensitive and multiple disease-related microRNA detection based on tetrahedral DNA nanostructures and duplex-specific nuclease-assisted signal amplification." *ACS Applied Materials & Interfaces* 8.49 (2016): 33499-33505.
[54] Miao, Peng, et al. "Nuclease assisted target recycling and spherical nucleic acids gold nanoparticles recruitment for ultrasensitive detection of microRNA." *Electrochimica Acta* 190 (2016): 396-401.
[55] Wang, Ye, et al. "Duplex-specific nuclease-amplified detection of MicroRNA using compact quantum dot–DNA conjugates." *ACS applied materials & interfaces* 10.34 (2018): 28290-28300.
[56] Zhang, Shixi, et al. "Multiplex miRNA assay using lanthanide-tagged probes and the duplex-specific nuclease amplification strategy." *Chemical Communications* 52.99 (2016): 14310-14313.

detection.[53] These examples highlight how DSN-mediated strategies can improve the accuracy of target identification and simplify detection post-amplification.

Due to the linear nature of DSN-mediated amplification, this strategy is not commonly highlighted as a primary contributor for improving sensitivity. Instead, techniques utilizing DSN have been used in conjunction with alternative amplification schemes. Aside from being compatible with unique assay designs, DSN-mediated techniques can be easily incorporated into a multitude of different detection platforms ranging from optical and electrochemical detection to mass spectrometry and SERS due to the adaptability of the signal amplification format.[57,58,59,60] DSN's compatibility with miRNA has already shown great promise, providing some insight into possible compatibility with other RNA-based targets. The platform flexibility and assay compatibility have the potential for seamless integration of detection of other similar targets such as COVID-19 RNA.

Flexibility of DSN Platform for Detection in Low Resource-cost Diagnostics:

In addition to the flexibility of DSN-mediated assays when combined with other amplification strategies and detection mechanisms, these assays have also already been designed and implemented for low resource-cost applications. First, the isothermal nature of DSN removes the need for a thermocycler, minimizing temperature monitoring challenges and increasing usability outside of a standard laboratory. Additionally, groups have been able to reduce assay

[57] Wu, Yudong, et al. "Recent advances in duplex-specific nuclease-based signal amplification strategies for microRNA detection." *Biosensors and Bioelectronics* 165 (2020): 112449.
[58] Li, Xue-Mei, et al. "A dual-amplified electrochemical detection of mRNA based on duplex-specific nuclease and bio-bar-code conjugates." *Biosensors and Bioelectronics* 65 (2015): 245-250.
[59] Kuang, Yuqiong, et al. "Duplex-specific nuclease-mediated amplification strategy for mass spectrometry quantification of MiRNA-200c in breast cancer stem cells." *Analytical chemistry* 91.14 (2019): 8820-8826.
[60] Pang, Yuanfeng, et al. "Fe3O4@ Ag magnetic nanoparticles for microRNA capture and duplex-specific nuclease signal amplification based SERS detection in cancer cells." *Biosensors and Bioelectronics* 79 (2016): 574-580.

time down to 30 minutes - 1 hour as well as demonstrate one step or one-pot assays making it competitive with other developed point-of-care diagnostics.[61,62] Furthermore, integrating these assays onto more user-friendly platforms for rapid and easy detection has been highlighted by several groups. More specifically, microRNA detection incorporating DSN-based methods have been demonstrated on lateral flow and microfluidic platforms, tools that have been successfully utilized in point-of-care settings.[63,64]

With the emergence of different lineages of the original SARS CoV-2 virus, it becomes increasingly necessary to maintain a diligent approach to tracking changes in susceptibility. While highly successful forms of prevention and treatment have been developed in the past year, rates of mutation within the virus have resulted in a growing number of virulent strains, raising concerns regarding effectiveness of existing preventative tools in the near future.[65] Availability and ease of access to rapid screening tools will be vital for combating future waves to minimize the impact to public health. DSN offers a unique solution as a point-of-care screening tool with its ability to discriminate between point mutations within target regions, enabling accurate differentiation of existing and future variants with high sequence homology.

In this work, we have developed a novel method for variant screening of SARS-CoV-2 utilizing a combination of isothermal techniques in reverse-transcriptase recombinant-polymerase

[61] Wei, Hongjuan, et al. "Duplex-specific nuclease signal amplification-based fluorescent lateral flow assay for the point-of-care detection of microRNAs." *Analyst* 146.2 (2021): 558-564.
[62] Shandilya, Ruchita, et al. "Point-of-care diagnostics approaches for detection of lung cancer-associated circulating miRNAs." *Drug Discovery Today* 26.6 (2021): 1501-1509.
[63] Ying, Na, et al. "Lateral flow nucleic acid biosensor for sensitive detection of microRNAs based on the dual amplification strategy of duplex-specific nuclease and hybridization chain reaction." *PloS one* 12.9 (2017): e0185091.
[64] Wang, Nan, et al. "Recent advances in the rapid detection of microRNA with lateral flow assays." *Biosensors and Bioelectronics* (2022): 114345.
[65] Mercatelli, Daniele, and Federico M. Giorgi. "Geographic and genomic distribution of SARS-CoV-2 mutations." *Frontiers in microbiology* 11 (2020): 1800.

amplification (RT-RPA) and duplex-specific nuclease (DSN) mediated SNP detection following T7 transcription. By using sequencing data from previous testing, distinct regions of the viral sequence have been identified for differentiating predominant variants around the world. We demonstrate the efficacy of this technique by targeting three key portions of the SARS-CoV-2 viral genome; a conserved region of the open-reading frame region, and two unique variable regions of the open-reading frame and spike regions. We are able to identify infection with SARS-CoV-2 through detection of the conserved ORF1a region and differentiate between two common SARS-CoV-2 strains (Wuhan/**Wuhan-Hu-1**, European/**B1.1.7**) from detection or lack thereof of the variable ORF1ab region (Del3675-3677) and Spike region (Del69-70). Following amplification of target regions using RT-RPA and conversion to RNA using T7 transcription, we have incorporated detection using FRET-quenching DNA probes specific for all three regions. We have incorporated DSN-mediated sequence-specific cleavage of fluorescent probes in order to improve the specificity of the assay while mediating linear amplification in presence of target RNA, providing a quantifiable signal to evaluate the presence of multiple key regions that can be used to determine the viral variant present in the sample.

Additionally, we have demonstrated the compatibility of our technique with relevant low-resource cost sample-to-answer methods without the use a traditional fluorescent plate reader through preliminary analysis of lateral flow-based detection and electrokinetic assembly of beads using electro-osmosis. Using alternative methods for signal analysis to conventional fluorescent detection, we have exhibited the flexibility of this device for adaptation and deployment in vulnerable communities with limited access to standardized healthcare.

CHAPTER 1: Development of Duplex-specific nuclease-based Molecular Testing for SARS-CoV-2 Wuhan Strain and Differentiation with B1.1.7 Variant

Materials and Methods:

Probes and Primers:

RPA primers were designed to flank target sequences of the conserved and variable regions for amplification. Fret-based DNA probes were designed to target and hybridize with the amplified regions of the RPA products, with the probes complementary to the mutant regions of the variable sequences. Sequences for SARS-CoV-2 Wuhan-Hu-1 and B1.1.7 strains were obtained from GenBank® and designed using the Primer-BLAST tool from NCBI.[66] DNA probe melting temperatures were calculated using the IDT OligoAnalyzer™ tool. Nucleic acid sequences and GenBank® accession codes are provided in Table S1.[21,67]

Primer and probe pairs for RT-RPA amplification and DSN detection targeting the ORF1a region and spike region of the SARS-CoV-2 genome were designed based on previous work using RT-RPA amplification of SARS-CoV-2 by Patchsung et al. in conjunction with the Primer-BLAST designing tool from NCBI.[65,68] Each probe and primer pair were designed to be unique to the associated target region within the 29kb SARS-CoV-2 genome with the melting temperature of the DNA probes at 54-55^{o}C to prevent non-specific hybridization resulting in false-positive signal while minimizing the prevalence of self- and hetero-dimers. In order to take advantage of

[66] Ye, Jian, et al. "Primer-BLAST: a tool to design target-specific primers for polymerase chain reaction." *BMC bioinformatics* 13.1 (2012): 1-11.
[67] Rosenberg, Alan H., et al. "Vectors for selective expression of cloned DNAs by T7 RNA polymerase." *Gene* 56.1 (1987): 125-135.
[68] Patchsung, Maturada, et al. "Clinical validation of a Cas13-based assay for the detection of SARS-CoV-2 RNA." *Nature biomedical engineering* 4.12 (2020): 1140-1149.

duplex-specific nuclease's sequence-specific cleavage activity, The conserved region of the ORF1a region was designed to be consistent between the Wuhan-Hu-1 and B1.1.7 strains while the variant regions of the ORF1a region and spike region contain key mutations of 9 and 6 base-pairs, respectively. During the detection phase, DNA probes in complementary DNA:RNA complexes were designed to be cleaved using DSN to separate fluorescent tags from the quencher ends while DNA in non-complementary DNA:RNA complexes are left intact, producing quantifiable signal only in the presence of amplified target.

Primer Sequence Design:

Primer sequences for the two strains targeted in this work (Wuhan-hu-1/B1.1.7) were retrieved from NCBI Genbank (GISAID ID: MN908947.3) and GISAID (GenBank ID: EPI_ISL_710528), respectively. Targeted regions for primers for RT-RPA amplification for both strains were designed based on previous work by Patchsung et al. for RT-RPA amplification of SARS-CoV-2 and modified using the Primer-BLAST designing tool from NCBI.[67] Primer pairs were designed according to RT-RPA manual provided by TwistDx with the following conditions: 1) 30-35 nucleotides in length, 2) below 70% but above 30% GC content, 3) minimized number of mononucleotide repeats or repeating patterns of nucleotides, and 4) primers that would yield an amplicon length from ~100 to ~200 base-pairs. Primers were also designed to function for RT-RPA amplification of target regions for both strains in order to only require addition of one set of primers regardless of the strain contained within sample. Using this approach, the resulting amplicons of the variant regions would contain differing sequences due to the amplification of the mutant region. Additionally, primer stringency was validated using the Primer-BLAST tool from NCBI and aligned against the genome of both viral strains to minimize non-specific interaction

during RT-RPA amplification. To perform downstream T7 transcription following RT-RPA, it is also necessary to incorporate a promoter sequence that is recognized by T7 polymerase to initiate transcription of the resulting amplicon into RNA.[69] For this reason, the T7 promoter sequence was included upstream of the forward primer sequence so that the resulting amplicon would contain the promoter sequence at the 5' end.

Probe Sequence Design:

Probe sequences were designed for each region using IDT Oligoanalyzer with a target melting temperature of 54-55^{o}C while also minimizing hairpin and self-dimer structures at a prevalence of <0.1% at the probe melting temperatures. Probes for the conserved open reading frame region were designed to be consistent between both strains to allow detection using the same probe to signify positive infection with either of these SARS-CoV-2 strains. Probes of the variant regions were designed to contain the mutation region located within the center of the probe sequence with a maximum of 12 matched base-pairs located before and after the mutant region. This requirement was in line with previous work highlighting the ability of DSN to distinguish single-nucleotide mutations within a 15 base-pair region of a DNA:RNA complex. Sequences were then validated using BLAST sequence alignment tool with an upper limit of 10 matched base-pairs for both Wuhan and B1.1.7 strains to rule out nonspecific hybridization with remaining viral genomic RNA remaining in sample following RT-RPA amplification[70]. Probes for each target region were labeled with a different fluorescent tag at unique excitation and emission wavelengths and quenched using the corresponding quenchers Table S1. By using probes with unique excitation

[69] Sun, Yangyang, et al. "One-tube SARS-CoV-2 detection platform based on RT-RPA and CRISPR/Cas12a." *Journal of translational medicine* 19.1 (2021): 1-10.
[70] Altschul, S.F., Gish, W., Miller, W., Myers, E.W. & Lipman, D.J. (1990) "Basic local alignment search tool." J. Mol. Biol. 215:403-410.

and emission wavelengths, detection of all three target regions within the same sample is possible and would allow differentiation between the presence of the two strains.

Figure 2a: Key Mutations of B1.1.7 SARS-CoV-2 Variant and Detection Strategy for Differentiation from Wuhan-Hu-1 Strain. Image courtesy from Gordon et al., Nature 2020[71]

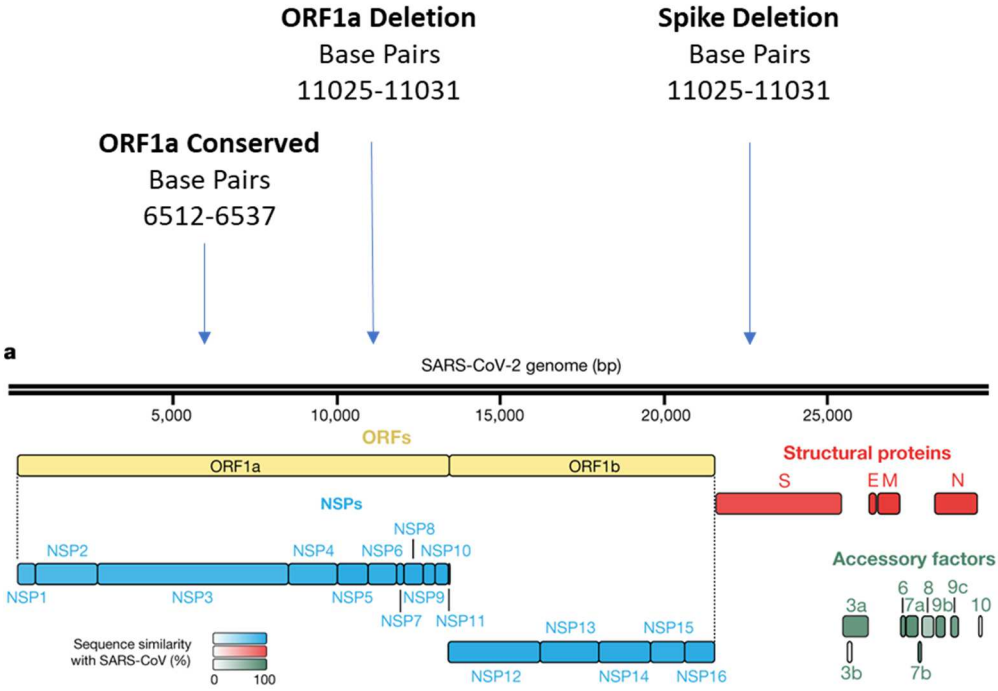

Figure 2b: Target Regions of SARS-CoV-2 Genome for Differentiation Between Wuhan-hu-1 and B1.1.7 Strains

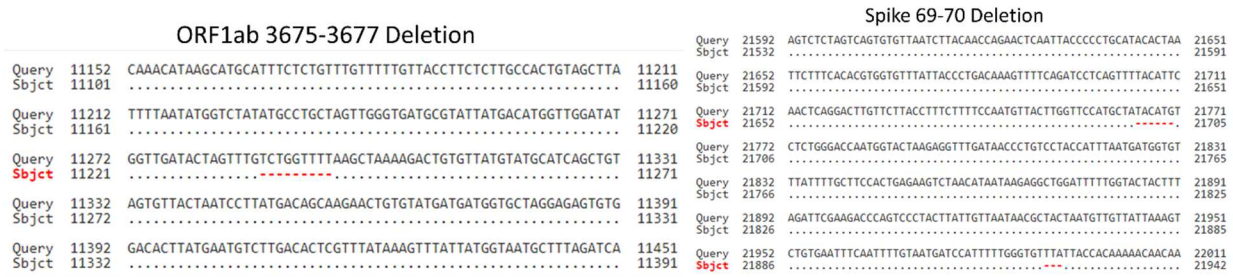

[71] Gordon, David E., et al. "A SARS-CoV-2 protein interaction map reveals targets for drug repurposing." *Nature* 583.7816 (2020): 459-468.

Figure 3a: Multiplexing Scheme For DSN-mediated Detection. Theoretical excitation and emission wavelengths with relative intensity (%) generated in Thermofisher SpectraViewer[72]

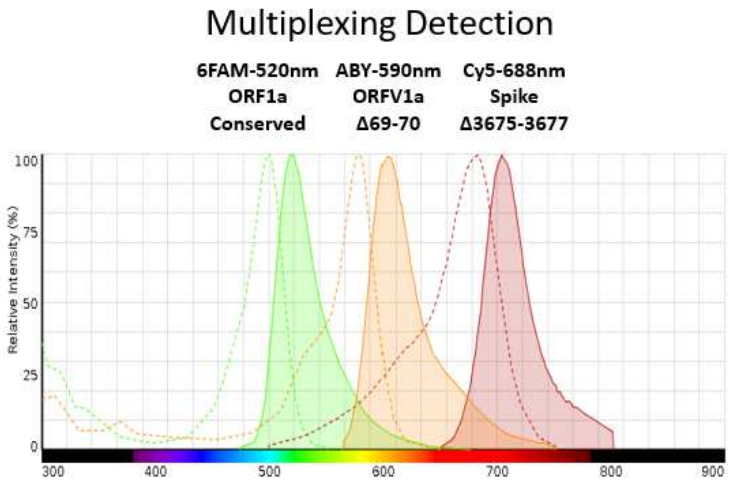

Figure 3b: Signal Interpretation Strategy of Multiplexed Assay for SARS-CoV-2 Variant Discrimination

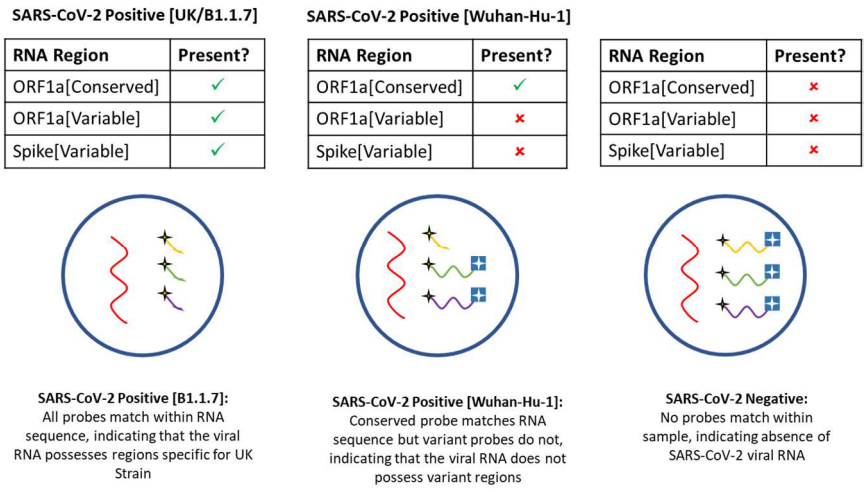

[72] "Guide for Using the Fluorescence Spectraviewer." *Thermo Fisher Scientific - US*, Thermo Fisher Scientific Inc., https://www.thermofisher.com/us/en/home/life-science/cell-analysis/fluorophores/guide-fluorescence-spectraviewer.html.

Probe Melting Temperatures:

While melting temperature of primers used in RT-RPA is insignificant due to the nature of the polymerase used in this reaction, melting temperatures of the primers are of great importance for two critical reasons; 1) maintaining availability of unbound probes that would allow RNA target recycling during the DSN reaction, and 2) minimizing probe-dimers from forming that DSN could potentially cleave, resulting in false-positive fluorescent signal. For these reasons, presence of these secondary structures were theoretically maintained at <0.1% at the operating temperature of 55ºC through IDT Oligoanalyzer and was also maintained with any non-specific dimers formed with the resulting amplicons from each RT-RPA amplification reaction to avoid cross-reactivity of probes.

Table 1: Melting temperatures of DNA Probes. ORFC = open reading frame, SPK = spike. Regions of deletion of B1.1.7 RNA are underlined in red text.

Viral Strain	Probe	Sequence	T_m (ºC)
Wuhan-hu-1	SPK Variable	Cy5 5' CCAGAGACATGTATAGCA 3' BHQ	55.1
	ORFC Variable	ABY 5' TTTAGCTTAAAACCAGACAAACTAGTAT 3' QSY	54.3
	ORFC Conserved	FAM 5' CCAACCTCTTCTGTAATTTTTAAAC 3' QSY	55.9
B1.1.7			
	ORFC Variable	ABY 5' TCTTTTAGCTTCAAACTAGTAT 3' QSY	54.8
	SPK Variable	Cy5 5' TCCCAGAGATAGCATG 3' BHQ	54.8

DSN and Primer/Probe Dilution Preparation:

Prior to the experiments, duplex-specific nuclease (DSN) was prepared from lyophilized sample according to the manufacturer (Evrogen) by addition of 50 mM Tris-HCl on the basis of 5 μl of the buffer for each 10 DSN units followed by an equal part 100% glycerol (to 50% final glycerol concentration). DSN enzyme was then further diluted at 1:9 ratio with 50 mM Tris-HCl (pH 8.0, Evrogen) to working concentrations of 0.1U μl^{-1}. Lyophilized DNA probes and primers

were resuspended in UltraPure™ DNase/RNase-Free Distilled Water (Thermofisher Scientific) to 100 μM stock concentrations and further diluted to working concentrations of 1μM and 10μM, respectively (Thermofisher Scientific/IDT).

Reverse Transcriptase-Recombinase Polymerase Amplification (RT-RPA):

RT-RPA was adapted and performed from a similar protocol described in work by Patchsung, Jantarug et al.[67] Using the TwistAmp Basic Kit from TwistDx, one lyophilized RPA pellet was resuspended with 29.5 μl rehydration buffer. The resuspended RPA pellet was then separated into three 1.5 ml Eppendorf tubes with approximately 10 μl in each. 1 μl forward primer (10 μM, Invitrogen), 1 μl reverse primer (10μM, Invitrogen), and 1 μl Protoscript® II reverse transcriptase (200 U μl^{-1}, NEB) were added to each tube. Dilutions of 6.5 μl RNA of Wuhan-Hu-1 or B.1.1.7 controls (10^6 copies/sample, Twist Biosciences) were then incorporated into tubes followed by addition of 1 μl MgOAc (280 mM, TwistDx) to initiate the reaction. Tubes were incubated at 37^{o}C for 60 minutes on a heat block before placing on ice for 5 minutes followed by centrifugation at 5000 rpm for 15 seconds.

T7 Transcription:

Reaction mixtures were pre-prepared in 1.5 ml Eppendorf tubes with 2 μl T7 RNA polymerase buffer (10X, NEB), 1 μl ribonucleotide solution mix (25 mM, NEB), 1 μl SUPERase•In™ RNase inhibitor (20 U μl^{-1}, Thermofisher Scientific), 12 μl UltraPure™ DNase/RNase-Free Distilled Water (Thermofisher Scientific) and placed on ice. 2 μl of RT-RPA product were then added to corresponding tubes followed by addition of 2 μl of T7 RNA

polymerase (50U μl^{-1}, NEB). Tubes were then incubated at 37°C for 60 minutes on a heat block before placing on ice for 5 minutes followed by centrifugation at 5000 rpm for 15 seconds.

DSN Reaction and Fluorescent Detection:

Reaction mixtures were prepared in 0.5 ml Eppendorf tubes with 6 µl DNA probe (1 µM, Thermofisher Scientific/IDT), 1 µl SUPERase•In™ RNase inhibitor (20 U μl^{-1}, Thermofisher Scientific), 2 µl duplex-specific nuclease (0.1U μl^{-1}, Evrogen), and 3 µl of 10X reaction buffer consisting of 500 mM Tris-HCl, 50 mM $MgCl_2$, 10 mM DTT (Evrogen). 4 µl T7 transcription product were then added followed by addition of UltraPure™ DNase/RNase-Free Distilled Water (Thermofisher Scientific) to a final reaction volume of 30 µl with buffer concentration of 50 mM Tris-HCl, 5 mM $MgCl_2$, 1 mM DTT. Samples were incubated at 55°C for 25 minutes followed by addition of 30 µl of EDTA (10 mM, Evrogen) and incubation at 55°C for 5 minutes. Samples were then aliquoted into a 384-well plate and read in the SPECTRAmax® GEMINI XS fluorescent plate reader.

<u>Validation of Design for DSN-mediated Detection of SARS-CoV-2 Strains:</u>

Validation of Duplex-specific Nuclease Enzyme Activity and Specificity Conditions:

Initial testing of the DSN enzyme's activity and specificity conditions were conducted using probes targeting the ORF1a conserved region and synthetic 25nt complementary DNA and RNA to determine the activity of the DSN enzyme in the presence of DNA and RNA duplexes. In previous works, DSN has been found to have high fidelity with the ability to differentiate mismatched complexes down to 10 base-pairs for DNA:DNA hybrids and 15 base-pairs for DNA:RNA hybrids[9]. To test the specificity of the enzyme, noncomplementary targets were also

tested with a 10 base-pair mismatch located within the 25nt sequence for both synthetic DNA and RNA targets. Five previously confirmed conditions from previous works were tested to determine conditions for DSN enzyme recognition of molecular duplexes that trigger DNA cleavage. Solutions containing different analyte are listed in order from left to right in Figure 4 to test the following conditions; 1) minimal activity in presence of single-stranded DNA, 2) activity in presence of duplexed DNA, 3) minimal activity in presence of mismatched DNA, 4) activity in presence of duplexed DNA: RNA complex, and 5) minimal activity in presence of mismatched DNA:RNA complex. Samples were incubated at 55ºC in the absence or presence of DSN for 30 minutes and endpoint fluorescent signal was compared to determine cleaving activity of the enzyme with the presence of different DNA complexes.[73,74] Sample 1 and sample 5 saw little change in signal after the addition of DSN enzyme, while sample 2 and sample 4 saw significant increase in signal of up to 252% and 194% with addition of enzyme. Notably, sample 3 with addition of non-specific DNA did exhibit a significant increase in signal, demonstrating the limited recognition of longer mismatched DNA:DNA duplexes by DSN in comparison to mismatched DNA:RNA duplexes (sample 5).

[73] Yin, Bin-Cheng, Yu-Qiang Liu, and Bang-Ce Ye. "One-step, multiplexed fluorescence detection of microRNAs based on duplex-specific nuclease signal amplification." *Journal of the American Chemical Society* 134.11 (2012): 5064-5067.

[74] Anisimova, Veronika E., et al. "Isolation, characterization and molecular cloning of duplex-specific nuclease from the hepatopancreas of the Kamchatka crab." *BMC biochemistry* 9.1 (2008): 1-12.

Figure 4: Validation of activity conditions of DSN. Incubation was performed using 5'FAM-3'QSY labeled open-reading-frame conserved probes with synthetic 25nt targets. Samples were incubated with and without 0.1 U DSN for 30 minutes and read in the SPECTRAmax® GEMINI XS fluorescent plate reader with excitation wavelength of 485 nm and emission wavelength of 538 nm. From left to right: 1) 100 nM probe with nonspecific sheared duplex DNA, 2) 100 nM probe with addition of 50 nM complementary DNA, 3) 100 nM probe with addition of 50 nM noncomplementary DNA, 4) 100 nM probe with addition of 50 nM complementary RNA, 5) 100 nM probe with addition of 50 nM noncomplementary RNA.

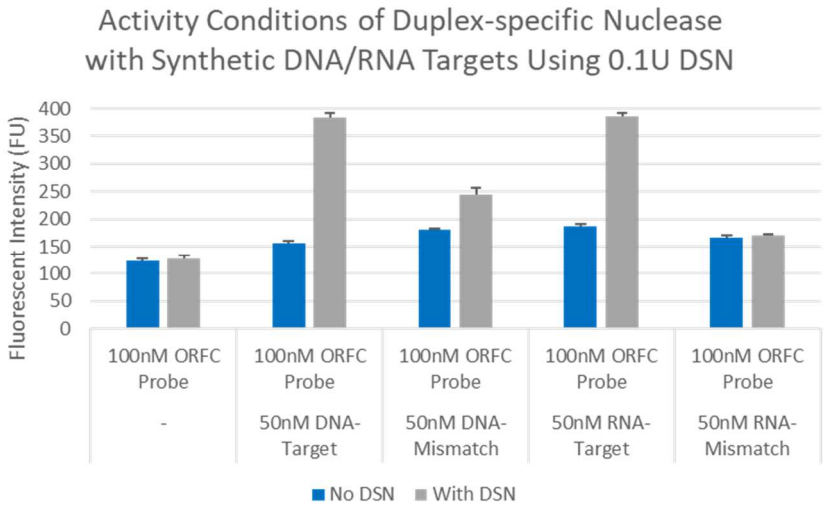

These results validated the expected function of the DSN enzyme as listed in previous works, with clear activity in the presence of complementary DNA:DNA or DNA:RNA complexes and minimal or absence of activity in the presence of off-target analyte. Notably, there is significant enzymatic activity of DSN in the presence of noncomplementary DNA:DNA hybrids, indicating potential limitations of the enzyme with specificity when working with amplified DNA target regions. This phenomenon is reflected in previous papers outlining the characterization of the enzyme.[66] However, the lack of activity in the presence of mismatched DNA:RNA pairs of up

to 10 base-pairs as well as single-stranded probe DNA indicates the suitability of DSN for distinguishing the 6 and 9 base-pair mutations located within the ORF1a and spike regions being tested in this work.

Hairpin Probe vs. TaqMan Probe Design

Considerations between DNA hairpin probe design and DNA TaqMan probe design were evaluated and increase in DSN signal was measured for each case. DNA hairpin probes were constructed with a CCGCG tail at the 5' end and a complementary region on the 3' end and a melting temperature of the hairpin structure at ~58.2^{o}C. Both types of probes were constructed with a FAM fluorescent tag located at the 5' end and the associated quencher at the 3' end. Samples were incubated at probe concentrations of 100 nM with a dilution range of synthetic complementary RNA mimicking the target sequence of the conserved open reading frame region with a final concentration of 100 nM DNA probe, 50 mM Tris-HCl, 5 mM $MgCl_2$, 1 mM DTT, and a varying range of RNA. Samples were incubated with 0.1 U DSN for 30 minutes and fluorescent signal was obtained in the SPECTRAmax® GEMINI XS fluorescent plate reader with excitation wavelength of 485 nm and emission wavelength of 538 nm.

Figure 5: Design and Melting Point of Hairpin Probes Targeting ORFC Region. Hairpin probes are designed with complementary tail end regions to facilitate closing of the ends while containing complementary DNA sequences within the hairpin loop. Melting temperatures are designed to maintain hairpin structure under incubation conditions of 55°C to prevent non-specific cleavage by DSN.

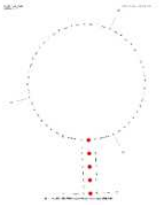

5'FAM-CCGCGCCAACCTCTTCTGTAATTTTTAAACCGCGG–IBQ-1 3'

Hairpin Tail End: CCGCG/CGCGG

Complementary Region: CCAACCTCTTCTGTAATTTTTAAAC

Fluorescent Tag/Quencher: FAM/IBQ

Structures

structure	Image	ΔG (kcal.mole^{-1})	T_m (°C)	ΔH (kcal.mole^{-1})	ΔS (cal.K^{-1}mole^{-1})	Output
1		-0.4	58.2	-41.5	-125.24	Ct Det

Testing to compare hairpin probe design and TaqMan probe design for compatibility with the DSN-mediated detection scheme was conducted using 100 nM DNA probe targeting the open reading frame conserved region together with a dilution range of target RNA ranging from 2.5 nM to 50 nM concentrations to determine the achievable sensitivity with each method. Samples were incubated using 0.25 U DSN at the melting temperatures of both probes of 55°C for 30 minutes. Samples were then quenched with 10mM EDTA and read using the SPECTRAmax® GEMINI XS fluorescent plate reader with an excitation and emission wavelength of 485nm and 538nm, respectively.

Table 2: ORFC Probes for hairpin vs. TaqMan probe suitability with DSN-mediated amplification

Taqman Probe	FAM 5' CCAACCTCTTCTGTAATTTTTAAAC 3' IBQ
Hairpin Probe	FAM 5' CCGCGCCAACCTCTTCTGTAATTTTTAAACCGCGG 3' QSY
Target RNA (Wuhan-hu-1)	GUUUAAAAAUUACAGAAGAGGUUGG
Non-target RNA (Wuhan-hu-1)	ACUAGUUUGUCUGGUUUUAAGCUAA

Figure 6a: Signal Intensity of DSN-mediated Amplification of Hairpin Probes. Samples were incubated with RNA dilutions of ORFC region. Signal intensity following DSN-mediated amplification of hairpin probes in presence of complementary RNA targeting the open-reading frame conserved region at concentrations of 2.5 nM, 10 nM, 25 nM, and 50nM were measured. Increases in signal intensity are observed at all concentrations within the dilution range aside from 2.5 nM which demonstrates similar signal intensity to negative control (DNA probe with addition of complementary RNA).

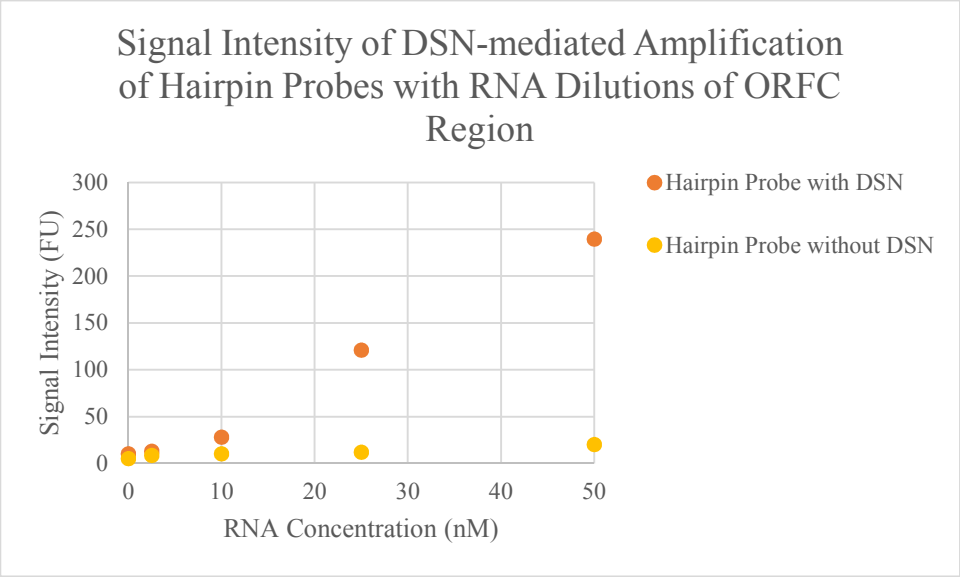

Figure 6b: Signal Intensity of DSN-mediated Amplification of Taqman Probes. Samples were incubated with RNA Dilutions of ORFC Region. Signal intensity following DSN-mediated amplification of TaqMan probes in presence of complementary RNA targeting the open-reading frame conserved region at concentrations of 2.5 nM, 10 nM, 25 nM, and 50 nM were measured. Increases in signal intensity are observed at all concentrations within the dilution range including 2.5 nM, indicating a superior limit-of-detection to hairpin probe model.

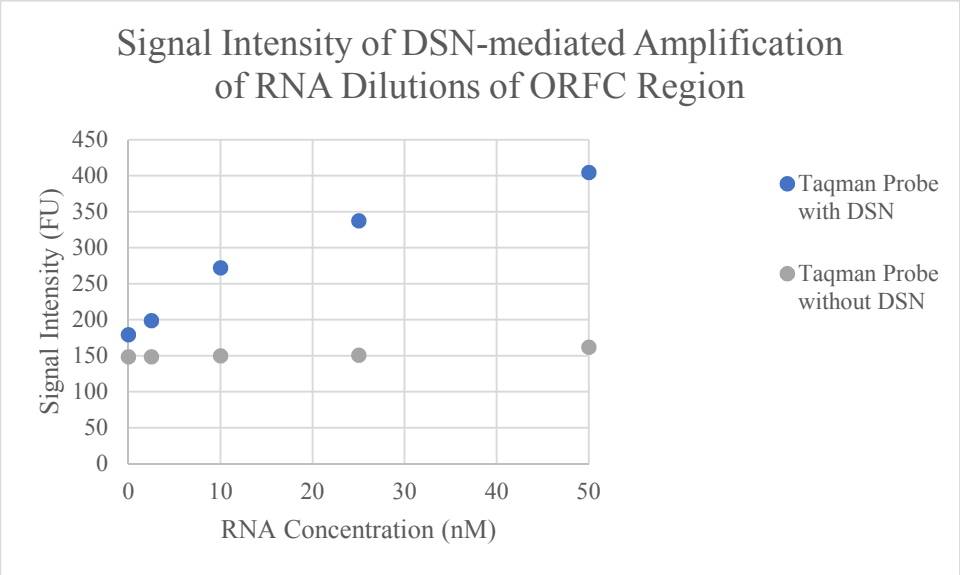

Figure 6c: Corrected Signal Intensity of DSN-mediated Amplification of Hairpin and Taqman Probes. Samples were incubated with RNA Dilutions of ORFC Region. Difference in signal intensity was measured prior to and following DSN-mediated amplification of TaqMan probes in presence of complementary RNA targeting the open-reading frame conserved region at concentrations of 2.5 nM, 10 nM, 25 nM, and 50 nM. Despite the increase in background signal with the use of TaqMan probe design in comparison to the hairpin probe design, improved limit of detection of the TaqMan probes justify their use in future experiments for detection of additional regions of interest.

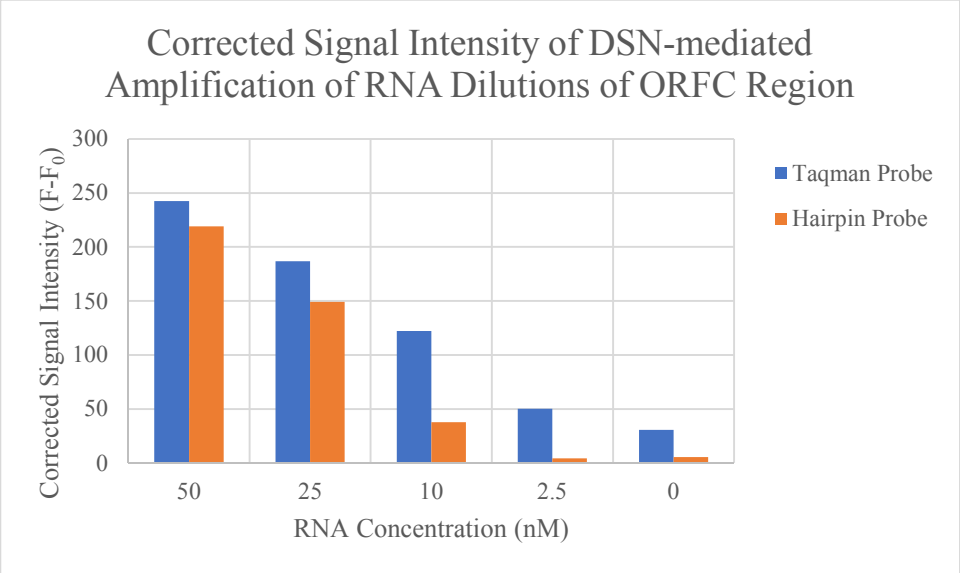

Fluorescent signal was measured from incubated samples with and without the addition of DSN enzyme. While background signal from the hairpin design probes were significantly lower than that of the TaqMan probes (~3.34%-12.5%) due to more efficient FRET quenching, signal change following addition of DSN was nonsignificant for samples with 2.5 nM RNA and lower in comparison at all concentrations within the dilution range in comparison to respective TaqMan probe samples. Additionally, TaqMan probe detection demonstrated an improved sensitivity with

significant signal change down to 2.5 nM RNA. The use of TaqMan probes in the development of a multiplexed system is also preferred due to the simplicity in design in comparison to unique hairpin tail-ends that would also require comparable melting temperatures with one another while minimizing non-specific interactions with non-target RNA and tail-ends of hairpin probes in solution. For these reasons, a TaqMan-based probe design was utilized in future testing for detection of target regions of RNA from the SARS-CoV-2 genome.

DSN Signal and Fidelity based on Temperature, DSN Concentration, Time:

While there are extensive studies on the necessary conditions for optimal DSN digestion efficiency with respect to Mg^{2+} concentration and pH, it was necessary to determine additional factors including incubation times, DSN concentrations, and temperature ranges that would be compatible with our experimental design as well as optimal concentrations of enzyme for effective DNA digestion.

DSN Incubation Time Variations on DSN Activity:

It is critical to determine the optimal incubation times with DSN in order to minimize the reaction time of the assay while avoiding depletion of hybridized DNA probe resulting in non-specific dnase activity on remaining single-stranded probes in sample. In order to determine the role of incubation times with DSN for our studies, an experiment was conducted using 100 nM DNA targeting the open reading frame conserved region along with 50 nM target RNA at 55ºC for a range of incubation times with a final volume of 30 µl of 100 nM DNA probe, 50 nM target and non-target RNA, 50 mM Tris-HCl, 5 mM $MgCl_2$, and 1 mM DTT together with 0.25 U DSN. Following incubation, samples were quenched with 10 mM EDTA to a final volume of 60 µl and

heated for 5 minutes at 55ºC. Samples were then compared to a positive control incubated with 20U DNase I for 8 hours overnight to determine DSN digestion efficiency.

Figure 7a: DSN Enzyme Activity as a Factor of Incubation Time. TaqMan probes were incubated with 0.25 U in presence of complementary and non-complementary RNA targeting the open-reading frame conserved region with incubation times of 15, 30, 45, and 60 minutes. The positive control is defined as maximum signal attainable from 100% efficiency in DSN cleavage following DNase I incubation of 100 nM DNA probe. Negative control is defined as the minimum signal attainable from 0% efficiency in DSN cleavage with 100 nM DNA probe in solution only. DSN amplification of complementary duplexes is significant at time points of 30, 45, and 60 minutes with nonsignificant increase in signal at 15 minutes. DSN selectivity is effective at all time points aside from 60 minutes, where a 13.47% increase in signal is observed.

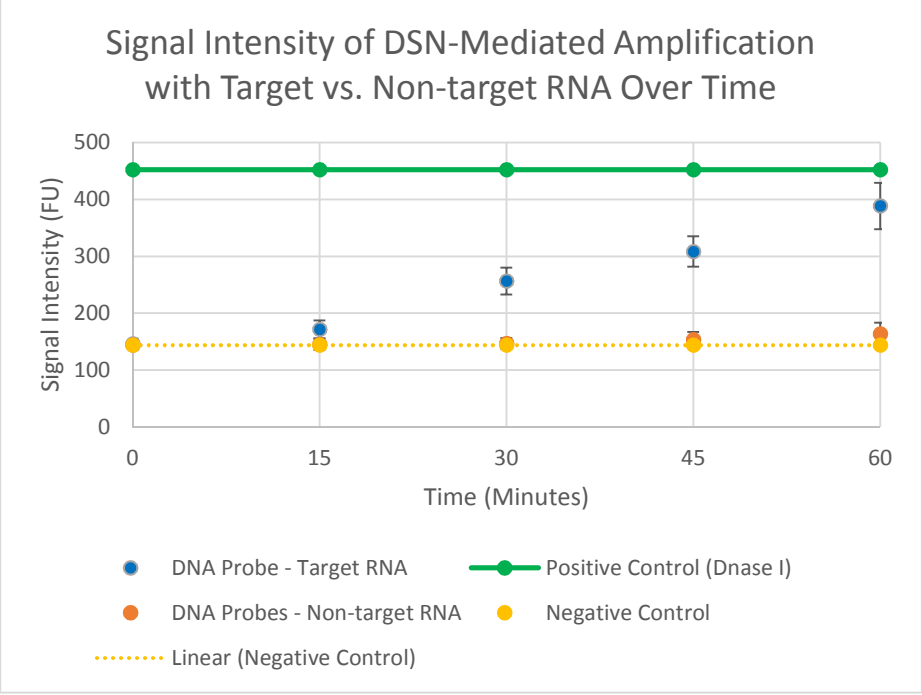

Figure 7b: Signal-to-noise Ratio of DSN Enzyme Activity as a Factor of Incubation Time. TaqMan probes were incubated with 0.25 U DSN in presence of complementary and non-complementary RNA targeting the open-reading frame conserved region with incubation times of 15, 30, 45, and 60 minutes. Signal-to-noise ratio is calculated as the fluorescent signal following DSN amplification divided by the signal of the baseline. The signal-to-noise ratio of 1.0 indicates no increase in signal relative to the baseline. Increase in signal-to-noise ratio apparent for sample containing non-complementary RNA at 45-minute and 60-minute incubation times of 6.50% and 13.47%, respectively. Increase in signal-to-noise ratio for 15 minutes and 30 minutes were minimal at under 2% with .78% and 1.70%, respectively.

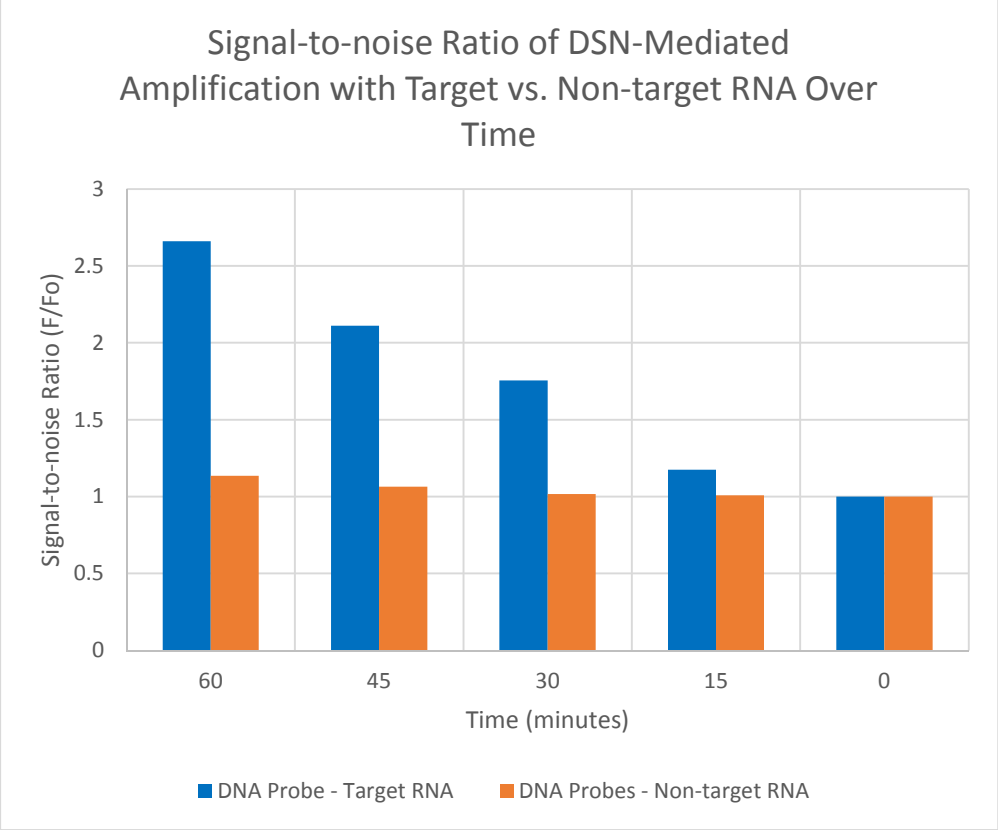

Following incubation, samples containing target RNA demonstrated the greatest increase in signal from the 15-minute to the 30-minute timepoint with a relative plateau over the remaining 30 minutes. The marginal increase in signal at the 15-minute timepoint can be explained as the "hot start" point of reaction, where the reaction tube had not reached sufficient temperature for significant DSN digestion efficiency. In order to evaluate non-specific DSN activity in the presence of non-target RNA, signal-to-noise ratio was calculated by the change in signal relative to the baseline (F/F_0). Samples incubated with non-target RNA exhibited minimal increase in signal-to-noise of under 5% increase over the baseline up to the 30-minute timepoint, but an increase was observed following the 45-minute timepoint of 14.61% and 30.29% for the 45-minute and 60-minute timepoints, respectively. From these results, it can be concluded that the 30-minute timepoint is the most advantageous for this experimental setup due to sufficient signal increase from DSN activity coupled with minimal change of less than 5% signal change over the baseline in the presence of non-target RNA.

DSN Concentration Dependency on DSN Activity:

In order to determine the role of DSN concentration for our studies, a dilution range of the enzyme from 0.1 U to 1 U was incubated with 100 nM DNA targeting the open reading frame conserved region along with 50 nM target RNA at 55^{o}C for 30 minutes with a final concentration of 100 nM DNA probe, 50 mM Tris-HCl, 5 mM $MgCl_2$, and 1 mM DTT. Samples were then compared to a positive control incubated with 20U DNase I for 8 hours overnight to determine DSN digestion efficiency.

Signal change resulting from DSN digestion was evaluated by comparing it to a negative control containing 100 nM DNA probe and 50 nM target RNA only. Corrected signal was

calculated by subtracting the baseline signal resulting from the negative control from the signal following DSN digestion. Signal change was apparent at all concentrations of DSN within the tested dilution range. However, the most significant increase in signal occurred from an increase from 0.1 U to 0.25 U DSN, with incrementally smaller increases in signal thereafter.

In order to determine the role of enzyme concentration on DSN fidelity, a similar experiment was conducted using the same dilution range but with non-target RNA specific for the open reading frame variable region of the SARS-CoV-2 Wuhan-hu-1 genome. Due to the ability of DSN to cleave single-stranded DNA when in the absence of double-stranded product, it was hypothesized that greater concentrations of enzyme may result in non-specific cleavage of unbound DNA probes. As shown by the results, dnase activity was nonsignificant following incubation with 0.25 U DSN but demonstrated increases in fluorescence at greater enzyme concentrations of 0.5 U and 1 U DSN. Following exhaustion of double-stranded non-specific DNA added to the reaction to improve probe stringency, higher concentrations of DSN enzyme resulted in unintentional cleavage of quenched DNA probes resulting in an increase in false-positive signal. To maintain high specificity in DSN digestion and conserve enzyme while maintaining a significant signal increase from DSN digestion, future experiments utilized 0.25 U for DSN-mediated reactions.

Figure 8a: DSN Enzyme Activity as a Factor of DSN Concentration. Corrected signal intensity is calculated as signal prior to incubation of DSN subtracted from signal following incubation with DSN. Sample digested with DNase I is considered change in signal at maximum DSN efficiency. The greatest change in signal between DSN concentrations is observed at 0.25 U DSN.

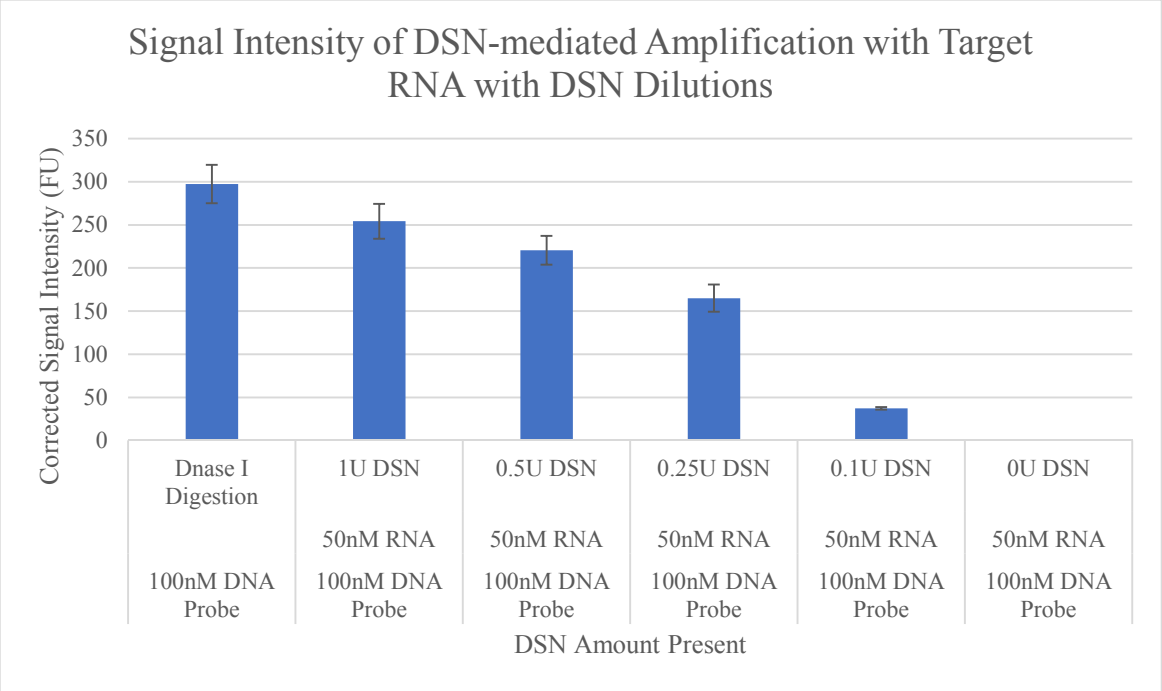

Figure 8b: DSN Enzyme Activity with Non-target RNA as a Factor of Enzyme Concentration. Corrected signal intensity is calculated as signal prior to incubation of DSN subtracted from signal following incubation with DSN. Sample digested with DNase I is considered change in signal at maximum DSN efficiency. Sample with minimal change in signal between DSN concentrations is observed at 0.25 U DSN.

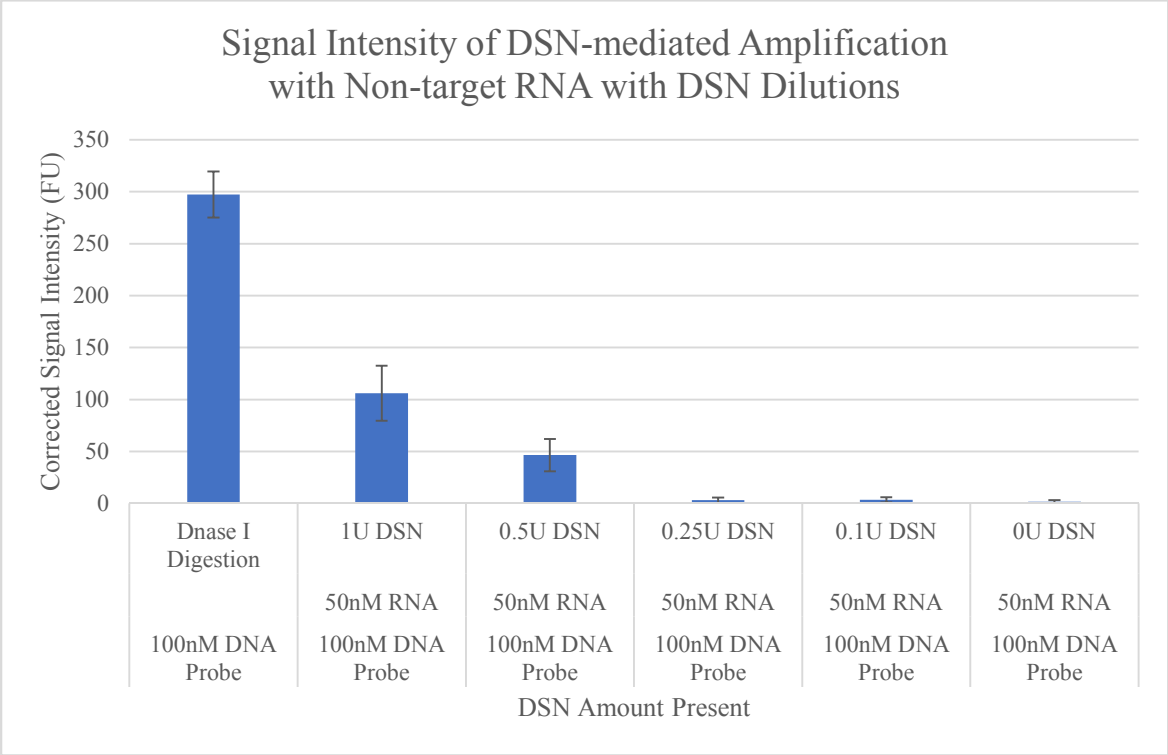

Incubation Temperature Variance on DSN Activity:

The next trial was to determine the role of temperature in DSN digestion efficiency and fidelity. Samples were prepared containing 100 nM probe targeting the open reading frame conserved region and incubated with 50 nM target or non-target RNA along with 0.25 U DSN at a temperature range from 40ºC to 60ºC. The temperature range was designed to contain the functional temperature required for RT-RPA and T7 transcription as well as the melting temperature of the designed TaqMan probes in order to determine feasibility of the DSN reaction in a one-pot assay with the aforementioned upstream amplification steps while maintaining greater than 50% DSN digestion efficiency.

Figure 9: DSN Enzyme Activity as a Factor of Incubation Temperature. Samples were incubated with 0.25 U DSN with complementary and non-complementary RNA at 40, 45, 50, 55, and 60ºC to investigate the influence of temperature on DSN activity and fidelity. Temperatures at or greater than the melting temperature of the complementary complex demonstrated minimal change in non-specific DNA cleavage. Corrected signal intensity is calculated as signal prior to incubation of DSN subtracted from signal following incubation with DSN.

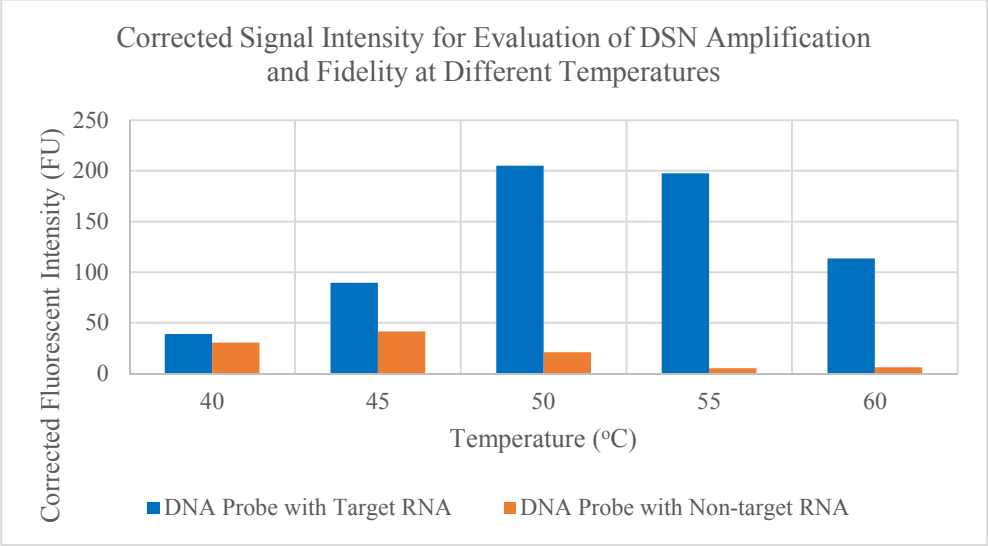

Within the temperature range tested, samples containing target RNA demonstrated an increase in fluorescence at all temperature ranges with the greatest increase within the 50-55^{o}C range, in agreement with previous expectations due to greater DSN digestion efficiency of ~75-80%. Additionally, due to the melting temperature of the probes of about 55^{o}C, it is also expected that greater concentrations of the probe-RNA complex were present due to temperature-mediated removal of existing secondary structures and dimer interactions. At a greater temperature of 60^{o}C, DSN approaches optimal digestion efficiency but demonstrated lower signal due to lower concentrations of available probe-RNA complex.

Surprisingly, significant non-specific cleavage of DNA continued to occur at temperatures below the melting point of the probe, indicating that undesirable dimers existed in solution and that DSN demonstrated significant activity toward these complexes despite base-pair lengths of less than 15 nucleotides. Due to the characteristics of DSN demonstrating preferential activity toward DNA in double-stranded complexes, it can be concluded that the improvement in selectivity at temperatures at and above the melting temperature of the DNA strand (55^{o}C) can be attributed to probe DNA existing in the single-stranded form in the presence of non-target RNA. Additionally, the ideal conditions for optimal DSN activity at 55^{o}C can be attributed to a greater percentage of DNA probes existing in the double-stranded complex with target RNA, leading to DSN recognition of the complex resulting in specific DNA probe cleavage. These results indicate that existing TaqMan probe design is not compatible with RT-RPA and T7 transcription in a one-pot assay at the 40^{o}C incubation temperature and require incubation at 55^{o}C in order to achieve high specificity in the presence of non-specific RNA.

Introduction of Point-mutations for improved DSN Fidelity:

Due to these inconsistencies in DSN fidelity at lower reaction temperatures, alternative strategies were first evaluated in an effort to maintain a 37-42^{o}C isothermal temperature consistent with the necessary reaction temperatures for RT-RPA and T7 transcription stages. Previous work by Zhang et al. characterized the ability of DSN to recognize and cleave DNA into 6-8 base-pair fragments following digestion in the presence of perfectly matched sequence.[75] By introducing point-mutations at positions 6 and 21 of the DNA probe sequence, we hypothesized that at lower working temperatures DSN would recognize the 14 base-pair complement located between the point-mutations when hybridizing with target RNA and maintain dnase activity. Conversely, the mismatch introduction would inhibit DSN activity in the presence of off-target RNA by incorporating at least one mismatch sequence every 7 base-pairs within the non-specific hybrid. Comparison with probe without point mutations at positions six and 21 were used to test reaction stringency with the introduction of point-mutations and was performed using the variable open reading frame region using the probes listed in table 3. Point-mutation probes targeting the open reading frame variable region of the B1.1.7 SARS-CoV-2 strain were designed with comparable melting temperatures with the original probes at 56.1^{o}C in order to maintain comparable incubation temperatures for both trials.

[75] Zhang, Kai, et al. "Sensitive detection of microRNA in complex biological samples by using two stages DSN-assisted target recycling signal amplification method." Biosensors and Bioelectronics 87 (2017): 358-364.

Table 3: DNA Probe Sequences for DSN Point-mutation Recognition Testing

Point-mutation Probe (B1.1.7)	AGTCTATTAGCTTCAAACTACTATC
Standard Probe (B1.1.7)	TCTTTTAGCTTCAAACTAGTAT
Target RNA (B1.1.7)	GAUACUAGUUUGAAGCUAAAAGACU
Non-target RNA (Wuhan-hu-1)	GAUACUAGUUUGUCUGGUUUUAAGCUAAAAGACU

* Position of Deletion
* Position of Point Mutation

Figure 10: Base-pair Matching of Standard TaqMan vs. Point-mutation Probes

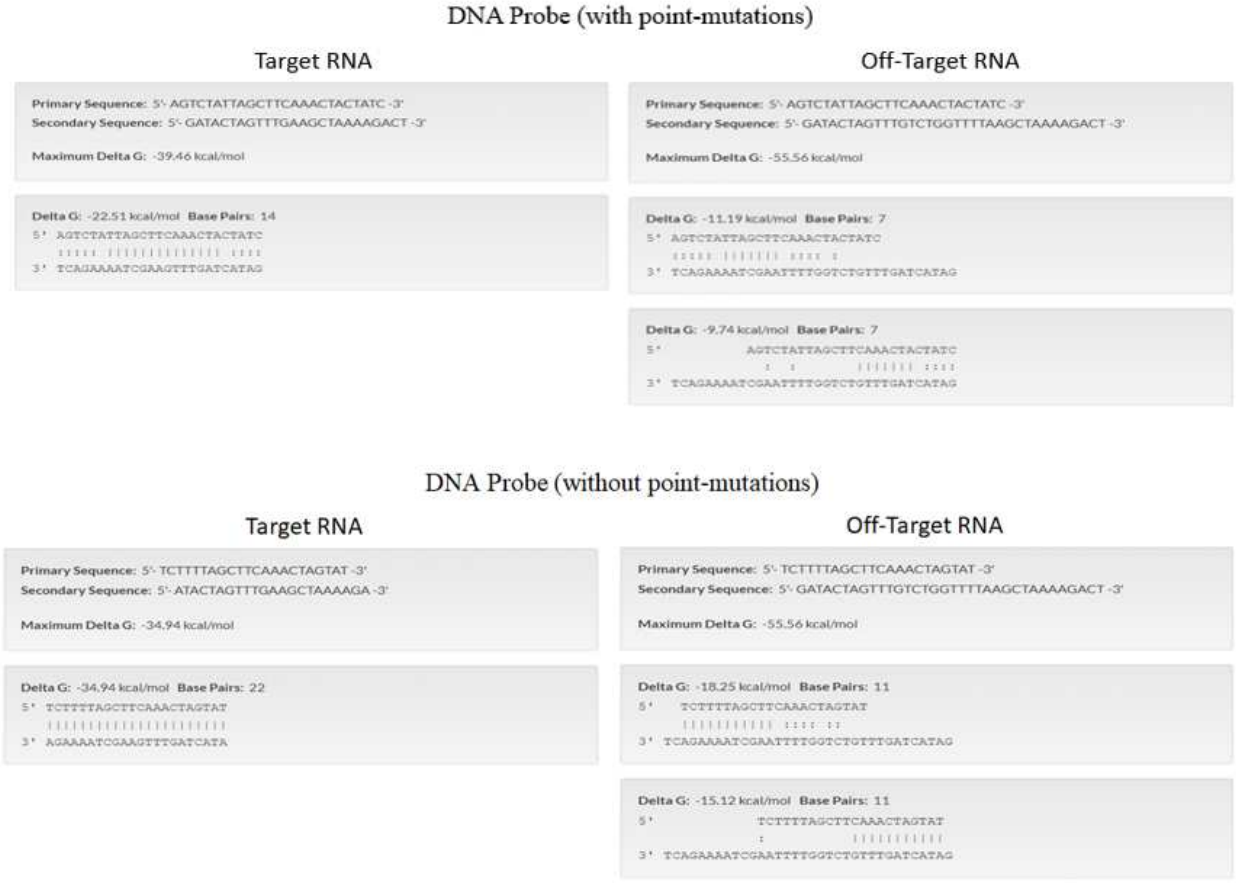

In order to evaluate DSN fidelity with the standard and point-mutation based probe designs, samples were prepared at 0.2 µM concentrations in a total volume of 30 µl. Following addition of a dilution range of target or non-target synthetic RNA to the sample, 0.25 U DSN was added to associated tubes in a final reaction volume of 30 µL with a final concentration of 100 nM DNA probe, 50 mM Tris-HCl, 5 mM $MgCl_2$, 1 mM DTT, and a varying range of RNA. Samples were incubated at 40ºC for 30 minutes to mimic the incubation temperatures required for one-pot reactions with RT-RPA and T7 transcription. Following incubation, the DSN reaction was quenched with the addition of 30 µL 10mM EDTA and incubated for 5 minutes at 40ºC. Fluorescent signal was measured using the SPECTRAmax® GEMINI XS fluorescent plate reader with an excitation and emission wavelength of 544 nm and 590 nm, respectively.

At the incubation temperature of 40ºC, there was significant DNA cleavage in both sets of samples containing standard and point-mutation probes in the presence of target RNA at the higher range of the dilution at 10 nM and 20 nM RNA. At the lower range of 5 nM RNA concentration, change in signal following DSN was comparable to that of the negative control. This could be due to the lower operating temperature of the incubation falling outside of the ideal temperature for DSN activity, resulting in hindered dnase activity even in the presence of complementary hybrids and limiting sensitivity of the assay. This issue with sensitivity could also be attributed to a lower melting temperature of the intended DNA:RNA complex due to containing only a 14 base-pair contiguous segment that is complementary to the target RNA as opposed to the 22 base-pair region of the standard probes. However, only the standard probes exhibited a significant increase in signal intensity in the presence of higher concentrations of non-target RNA at 10 nM and 20 nM, indicating that non-complementary hybrids had formed during incubation due to unsuitably high melting temperatures of secondary structures resulting in false-positive signal. In contrast, the set

of point-mutation probes exhibited nonsignificant change in signal in the presence of non-target RNA at all concentrations within the dilution range, indicating that the introduction of the point mutation at the 6 and 21 position of the probe sequence was successful in limiting presence of non-complementary hybrids by lowering melting temperature as well as preventing DSN dnase activity due to recognition of the mismatch introduction. While the point-mutation probes are a suitable option for highly specific detection, they are limited in their role in improving sensitivity and are also only relevant at a significantly lower incubation temperature than the optimal conditions for DSN activity due to the lower melting temperatures resulting from artificial insertion of mutation regions. For these reasons, further experiments were conducted using the standard probes at higher melting temperatures of 55^{o}C to minimize the presence of interfering secondary structures while approaching the optimal temperature conditions for DSN.

Figure 11a: 40°C DSN Incubation of TaqMan vs. Point-mutation Probes with Target RNA. Signal intensity of standard TaqMan vs. point-mutation probes following DSN incubation at 40°C in the presence of complementary RNA. Standard and point-mutation probes exhibit significant increase in signal intensity following addition of DSN in the presence of complementary RNA.

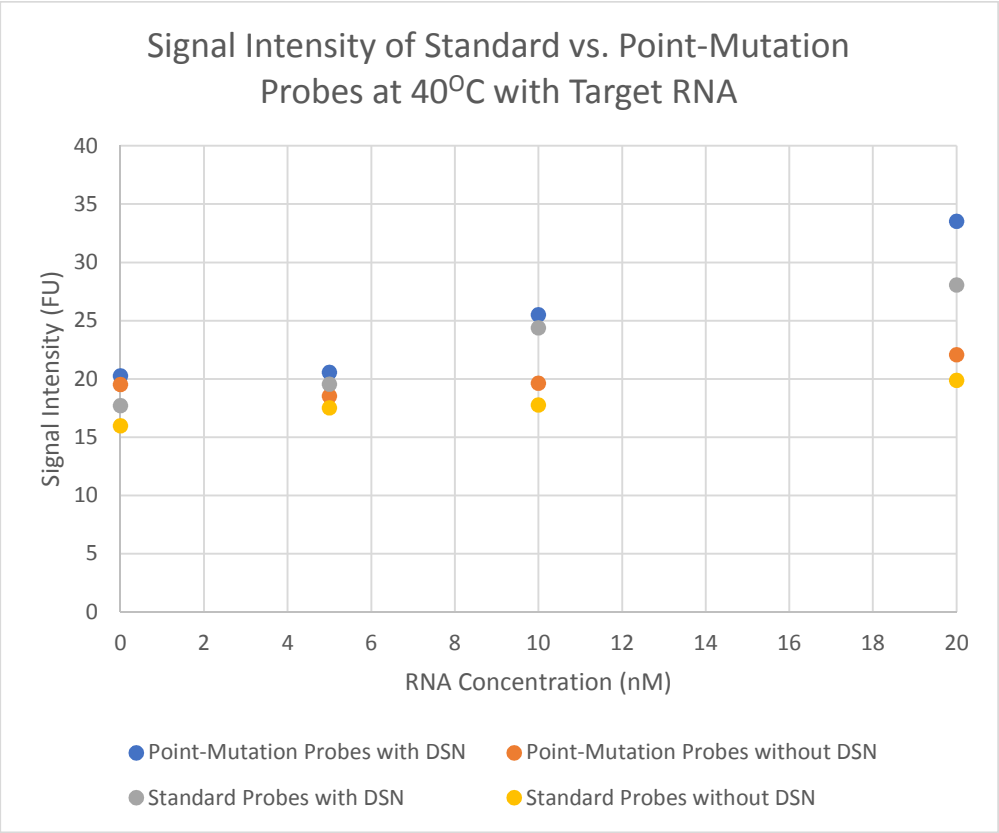

Figure 11b: 40ºC DSN Incubation of TaqMan vs. Point-mutation Probes with Non-target RNA. Signal intensity of standard TaqMan vs. point-mutation probes following DSN incubation at 40ºC in the presence of non-complementary RNA. Only point-mutation probes exhibit nonsignificant increase in signal intensity following addition of DSN in the presence of non-complementary RNA, indicating greater discrimination of off-target RNA at lower operating temperatures.

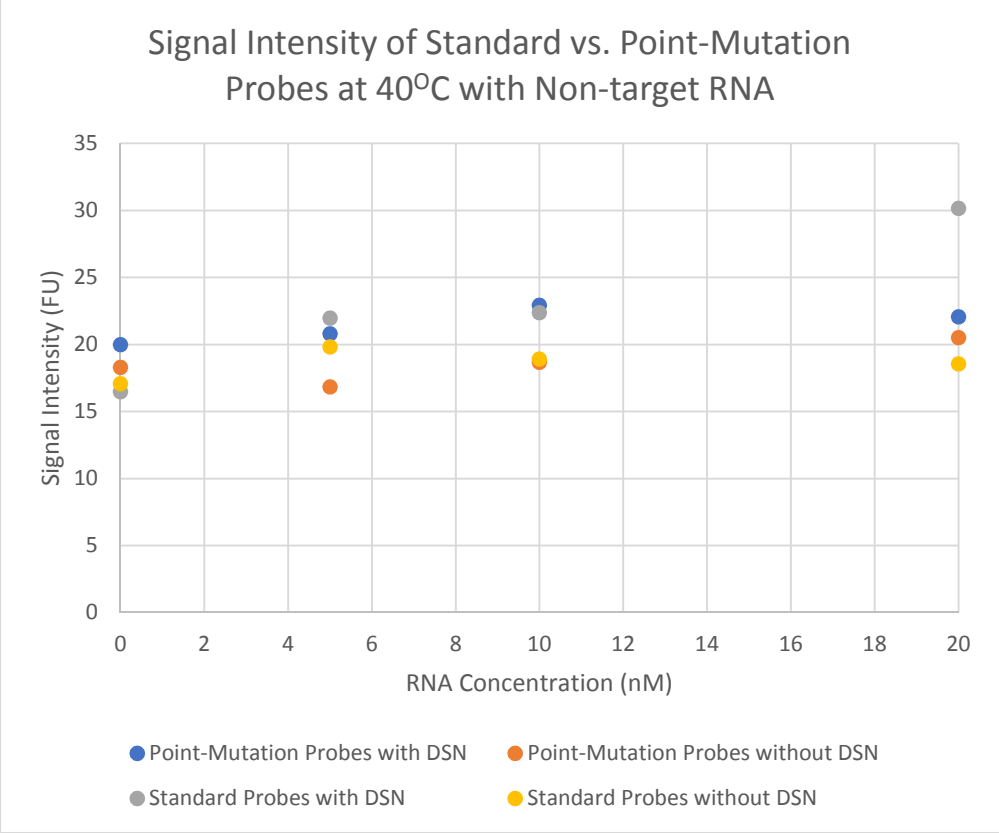

Using the standard probes constructed for detection of the open reading frame variable region, similar reaction conditions were applied while increasing the incubation temperature to 55ºC based on the melting temperature of the probes. Similar to the results seen from the point-mutation probes, samples containing target-RNA exhibited significant increase in signal at the upper concentrations within the dilution range but maintained signal increase at the lower concentration as well indicating greater DSN activity resulting from greater incubation

temperatures. Additionally, DSN activity in the presence of non-target RNA was minimal at all concentrations within the dilution range, indicating that higher incubation temperature was critical in removing significant secondary structures resulting from non-complementary hybridization that impacted false-positive signal. Future experiments were conducted using these conditions of standard TaqMan probes with an incubation temperature of 55°C to achieve a balance in sensitivity and high discrimination for mismatched RNA targets in sample.

Figure 12a: 55°C DSN Incubation of TaqMan Probes. Signal intensity of standard TaqMan probes following DSN incubation at 55°C in the presence of complementary and non-complementary RNA. DSN exhibits high selectivity of DNA:RNA complexes at higher operating temperatures close to the melting temperature of the standard probes, indicating incubation temperature plays a critical role on DSN fidelity.

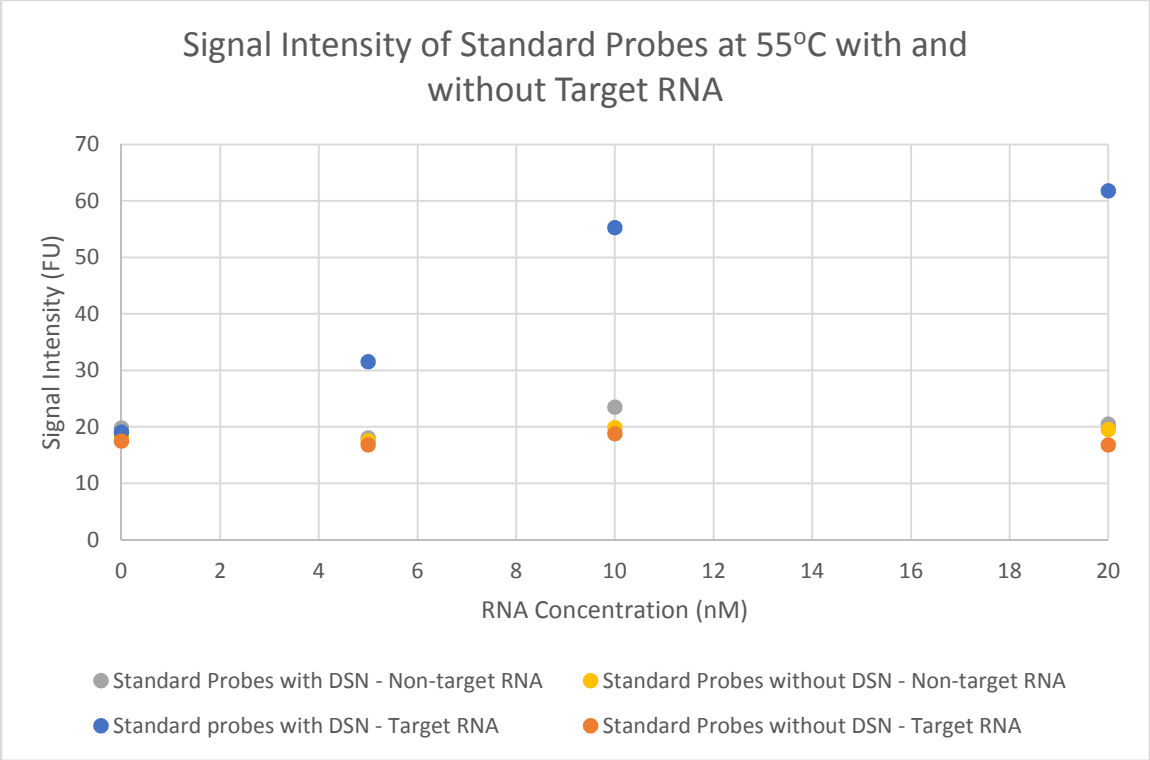

Figure 12b: Corrected Signal Intensity of 55ºC DSN Incubation of TaqMan Probes. Corrected signal intensity of standard TaqMan probes following DSN incubation at 55ºC in the presence of complementary and non-complementary RNA. Corrected signal intensity is calculated as signal prior to incubation of DSN subtracted from signal following incubation with DSN. DSN exhibits high selectivity of DNA:RNA complexes at higher operating temperatures close to the melting temperature of the standard probes, indicating incubation temperature plays a critical role on DSN fidelity.

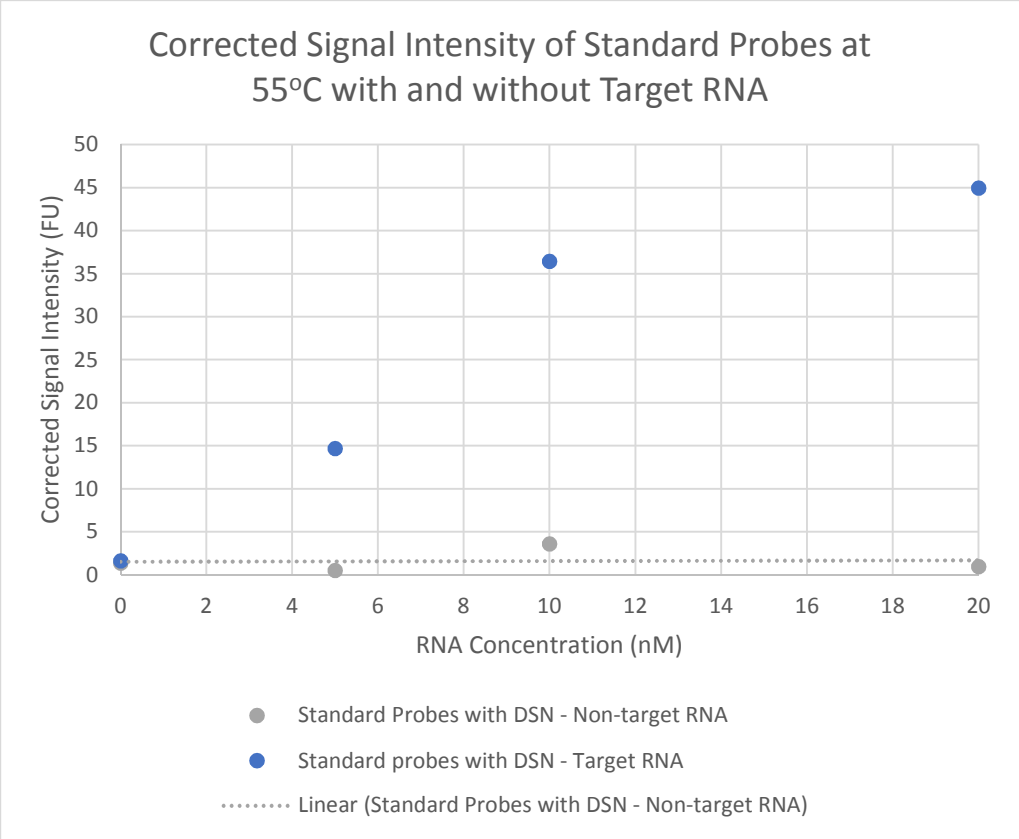

DSN Detection of Target Regions Using Wuhan-Hu-1 and B1.1.7 Synthetic RNA Genome:

Validation of probes for detection of target regions using synthetic RT-RPA fragments:

Due to potential issues with secondary structure inhibiting probe hybridization and cross-reactivity of probes to other amplified target regions in the sample, probes were tested with the addition of synthetic ~100nt RNA fragments to mimic the RT-RPA/T7 transcription amplification products. Probes targeting the ORF1a conserved, ORF1a variable, and the spike variable regions were labeled with FAM, ABY, or Cy5 fluorescent labels and prepared at concentrations of 50 nM each. Probes were then incubated with target and off-target RNA fragments along with 0.25 U DSN to determine cross-reactivity as well as potential nonspecific enzymatic activity by DSN in the presence of mismatched heteroduplexes. Additionally, samples were read at each fluorescent channel of interest to verify minimal overlap of signal emission for multiplexing potential of probe sets.

Table 4: Synthetic RT-RPA fragments for Multiplexing Experiments. Sequences designed in Primer-BLAST[66]

SARS-CoV-2 Strain	RNA Region	Theoretical RT-RPA Fragment
Wuhan-Hu-1 GenBank® Accession Code: MN908947.3	Open Reading Frame Conserved Region	5'GUAGGAGACAUUAUACUUAAACCAGCAAAUAAUAGUUUAAAAAUUACAGAAGAGGUUGGCCACACAGAUCUAAUGGCUGCUUAUGUAGACAAUU 3'
	Open Reading Frame Variable Region	5'GUGAUGCGUAUUAUGACAUGGUUGGAUAUGGUUGAUACUAGUUUGUCUGGUUUUAAGCUAAAAGACUGUGUUAUGUAUGCAUCAGCUGUAGUGUUACUAAU 3'
	Spike Variable Region	5'GACUUGUUCUUACCUUUCUUUUCCAAUGUUACUUGGUUCCAUGCUAUACAUGUCUCUGGGACCAAUGGUACUAAGAGGUUUGAUAACCCUGUCCUACCAUUUAAUGAUGGUGUUUAUUUUG 3'
B.1.1.7 GenBank® Accession Code: EPI_ISL_710528	Open Reading Frame Conserved Region	5'GUAGGAGACAUUAUACUUAAACCAGCAAAUAAUAGUUUAAAAAUUACAGAAGAGGUUGGCCACACAGAUCUAAUGGCUGCUUAUGUAGACAAUU 3'
	Open Reading Frame Variable Region	5'GUGAUGCGUAUUAUGACAUGGUUGGAUAUGGUUGAUACUAGUUUGAAGCUAAAAGACUGUGUUAUGUAUGCAUCAGCUGUAGUGUUACUAAU 3'
	Spike Variable Region	5'GACUUGUUCUUACCUUUCUUUUCCAAUGUUACUUGGUUCCAUGCUAUCUCUGGGACCAAUGGUACUAAGAGGUUUGAUAACCCUGUCCUACCAUUUAAUGAUGGUGUUUAUUUUG 3'

*: Deletion region in variant probe targeting B1.1.7 underlined in red

Figure 13: DSN Detection of Synthetic Fragment RNA vs. Theoretical RT-RPA RNA. Signal intensity of detection of ~25bp synthetic RNA fragment vs. theoretical RT-RPA fragment. Signal intensity of detection of complementary RT-RPA RNA following incubation with DSN exceeded that of the synthetic fragment, indicating relevance as a RNA target for DSN-mediated experiments.

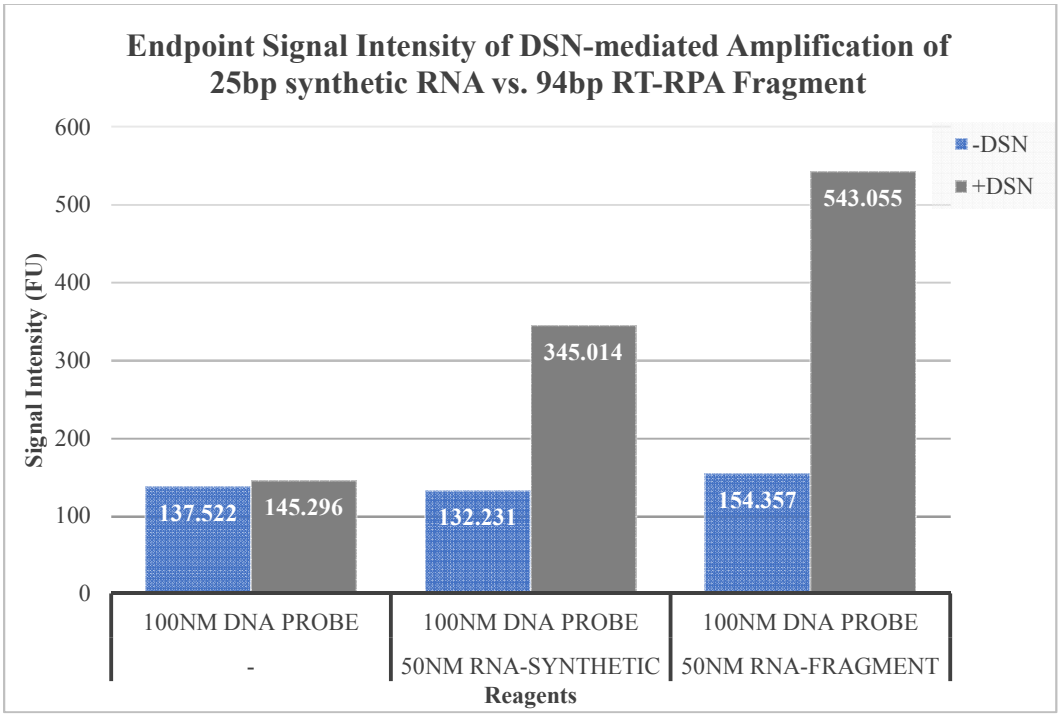

Signal intensity following addition of DSN demonstrated an increase in signal for both samples containing a region of complementary RNA. Interestingly, the signal increase was 82.7% greater for sample consisting of the theoretical RT-RPA fragment. While secondary structures can inhibit accessibility with probe-based detection, longer sequences are also more stable due to stacking and hydrogen bond interactions and increased folding structure stability[76]. In essence, the

[76] Trotta, Edoardo. "On the normalization of the minimum free energy of RNAs by sequence length." *PloS one* 9.11 (2014): e113380.

RT-RPA fragment contributed greater stability without severely inhibiting hybridization reactions, an advantage to detection using RT-RPA products.

Figure 14: Cross-reactivity Testing of Multiplexed Probe Sets. Cross-reactivity testing of probes and DSN activity were explored in the presence of mismatched, off-target RNA. Probe sets are incubated with target RNA or mismatched RNA at concentrations of 10 nM and 25 nM to confirm minimal spectral overlap of fluorescent signal between probes. Mismatched RNA is composed of an equal ratio of the other off-target RNA fragments. With the set of three probes targeting different regions of the SARS-CoV-2 genome, minimal increase in signal in observed across channels while increase in signal is only observed in the presence of complementary RNA.

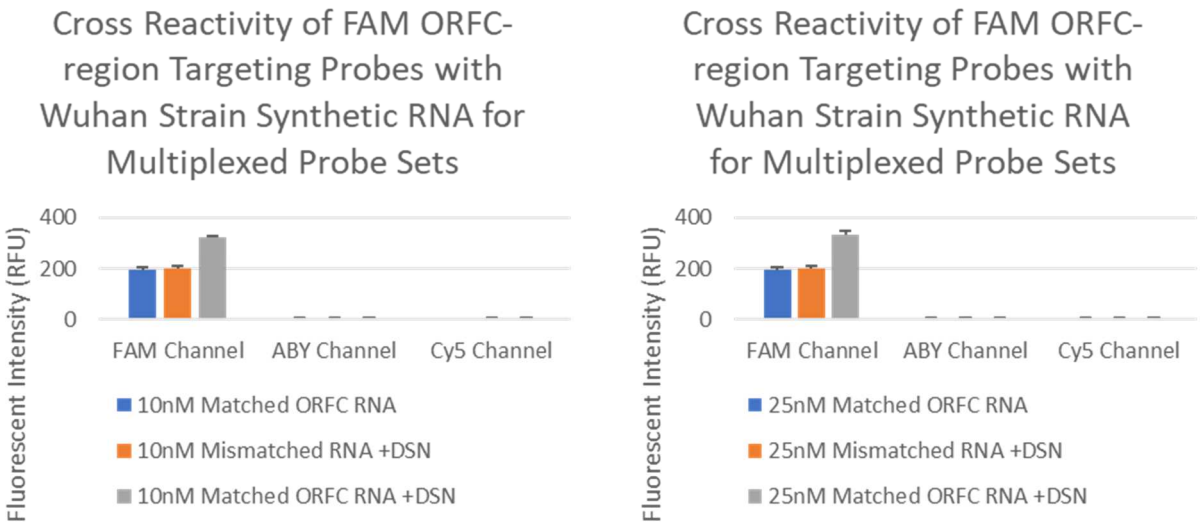

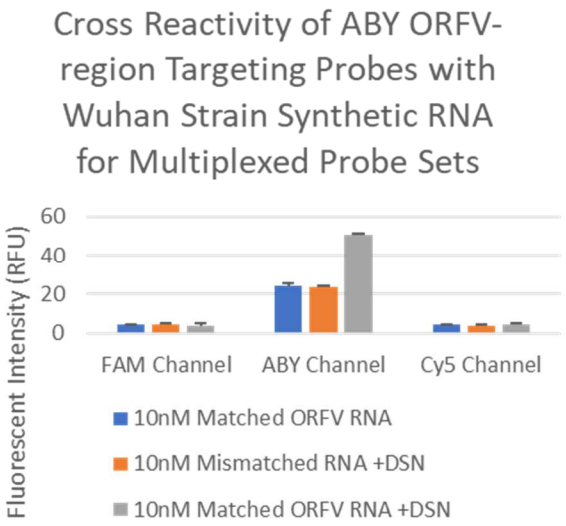

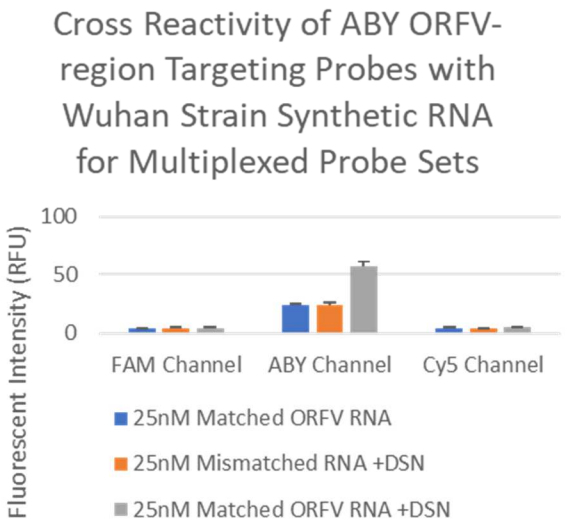

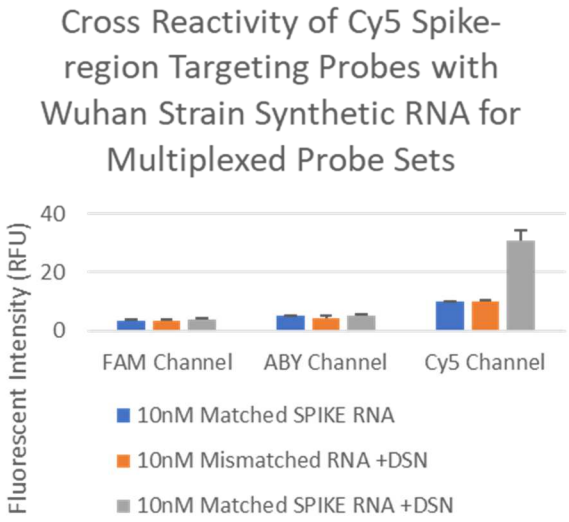

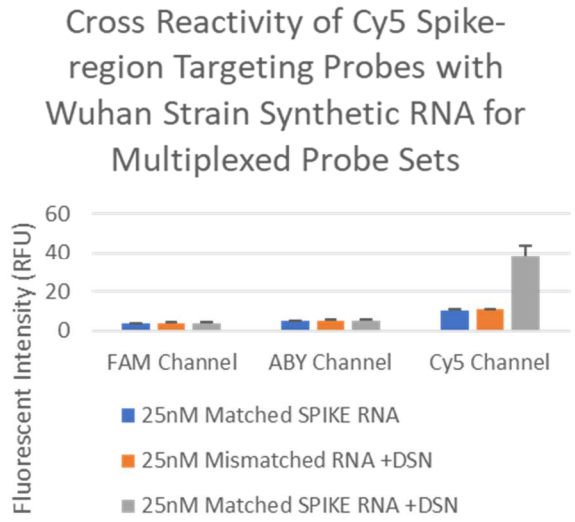

Each probe set was found to exhibit a noticeable increase in signal in the presence of complementary RNA as well as a minimal change in signal relative to sample without DSN enzyme upon the addition of the two other off-target RNA at equal concentrations. Additionally, signal differences between these samples were negligible outside of the relevant channel, indicating that there was insignificant spectral overlap between fluorophores. With minimal disturbance of fluorescent signal in neighboring channels in the presence of positive signal, we

determined that this fluorescent probe set does not exhibit significant signal crosstalk between probes as well as negligible non-specific signal amplification in the presence of DSN and mismatched DNA: RNA complexes. In conclusion, the experimental probe set demonstrated here is capable of simultaneous detection of the three target regions in multiplexed experiments.

Workflow of the Duplex-specific Nuclease-mediated Detection Platform:

The workflow for amplification and detection of key SARS-CoV-2 regions is noted below in Figure 4. Samples containing synthetic SARS-CoV-2 RNA were diluted in RNase-free water and prepared with the RT-RPA mix for amplification at 37^{o}C followed by T7 transcription at 37^{o}C. Following individual amplification and transcription of target regions, 4 µl of T7 transcription RNA product of each region were added together at equal volumes for a total volume of 12 µl of target RNA in a single tube. Samples were then mixed with probes at a final concentration of 0.1 µM each and duplex-specific nuclease mix at a final concentration of 0.25 U and incubated at 55^{o}C for 30 minutes. Following incubation, samples were analyzed in SPECTRAmax® GEMINI XS fluorescent plate reader at excitation/emission wavelengths of 485 nm/538 nm (FAM), 544 nm/590 nm (ABY), and 635 nm/675 nm (Cy5).

Figure 15: Total Assay Workflow for SARS-CoV-2 Detection. This assay utilizes RT-RPA with T7 transcription followed by DSN amplification for detection of SARS-CoV-2 strains Wuhan-Hu-1 and B1.1.7. Using synthetic RNA mimicking the viral genome of SARS-CoV-2 Wuhan-Hu-1 and B1.1.7 strains, target regions are amplified using RT-RPA. RT-RPA DNA products are then transcribed into RNA through T7 transcription and detected with relevant probes through DSN amplification. Fluorescent readout is then measured on the SPECTRAmax® GEMINI XS fluorescent plate reader.

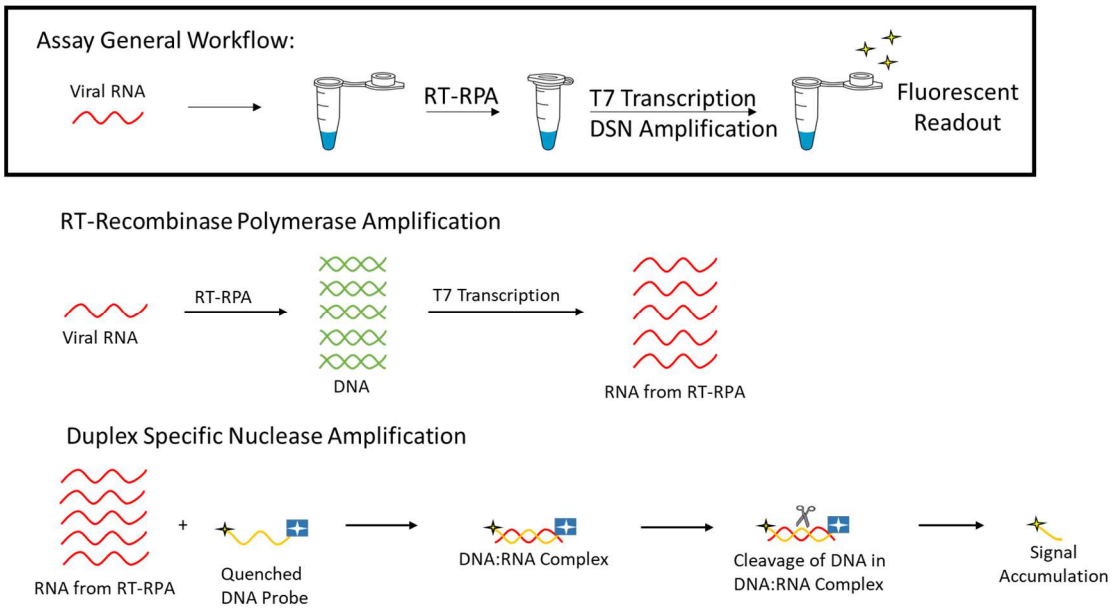

DSN specificity of variable region detection of RT-RPA/T7 RNA versus RT-RPA DNA:

Due to the increased sample-to-answer times resulting from addition of a transcription step after RT-RPA ranging from 1 to 16 hours for lower sample concentrations with compromised amplification efficiency, it is important to evaluate the necessity of T7 transcription for the downstream detection phase. This step is necessary for two reasons, 1) to increase signal by mediating linear amplification through target recycling of the amplified RNA, and 2) to improve specificity by avoiding nonspecific DSN activity observed in the DNA: DNA complexes from

previous experiments. To achieve this, samples with concentrations ranging from 10^2-10^4 copies were amplified using either RT-RPA only or with RT-RPA followed by T7 transcription. Samples were then incubated using the DSN detection protocol with corresponding probes for the target amplified regions of interest.

Figure 16: DNA vs. RNA Specificity of Detection of Variable Regions. DSN specificity in the presence of RT-RPA/T7 RNA product versus RT-RPA DNA product for detection of ORF1a and spike variant regions. Following RT-RPA and T7 transcription, samples were incubated for 30 minutes at 55°C with a mix containing 0.25 U DSN.

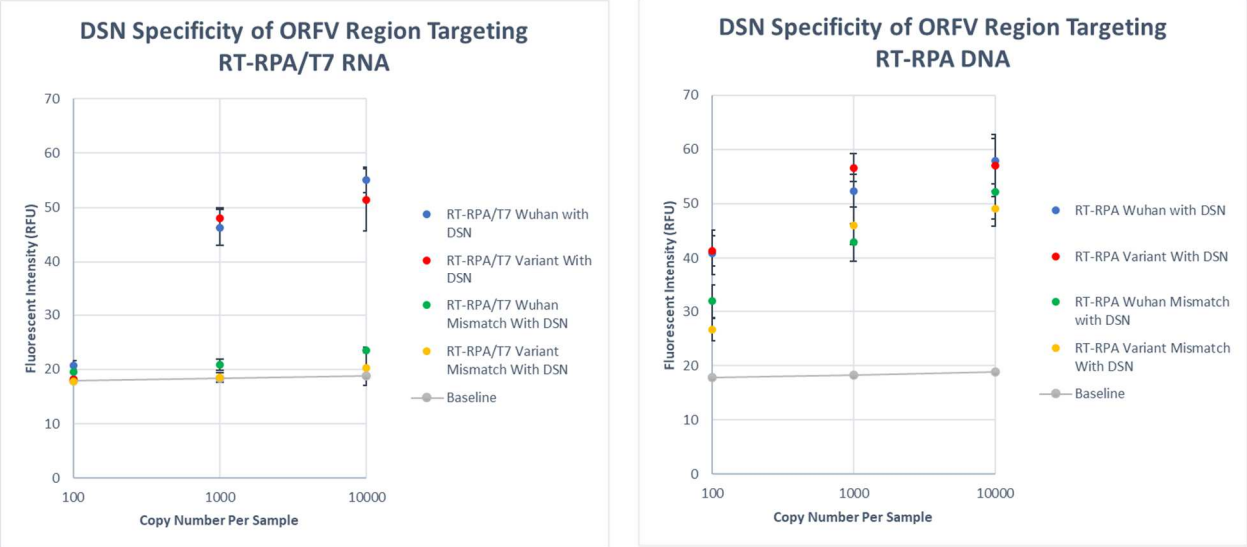

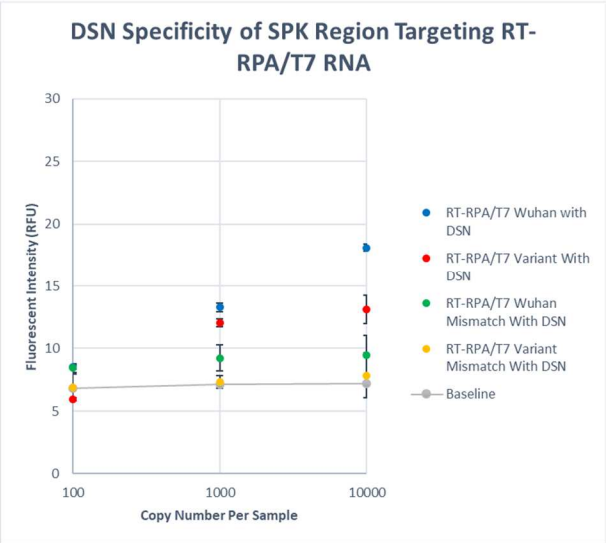

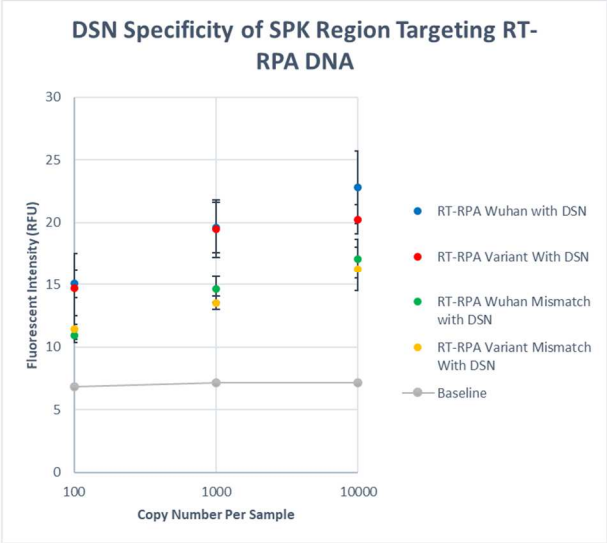

As previously described, DSN has greater specificity recognizing matched DNA:RNA complexes with less nonspecific activity than with DNA:DNA complexes. This phenomenon was also observed for detection of both the ORF1a and spike variable regions after transcribing RT-RPA amplified DNA into RNA. RNA samples were prepared and incubated with the previously stated conditions with the inclusion of the T7 transcription step while DNA samples were prepared and incubated by eliminating downstream T7 transcription prior to DSN incubation and signal readout using the SPECTRAmax® GEMINI XS fluorescent plate reader. The baseline was established as the signal intensity of 0.1μM probe only without the addition of target DNA/RNA. Signal increase over this baseline of each sample is listed in the supplementary data Fig S1.

For detection of the variable ORF1a and spike regions, signal intensity readout was comparable between the non-transcribed DNA and transcribed RNA samples following addition of DSN. However, nonspecific detection of RT-RPA DNA ranged from 61.18% to 143.87% increase over the baseline signal while detection of transcribed RT-RPA product demonstrated higher specificity at each concentration range for both regions with a maximum of 9.57% increase over baseline signal. Signal difference between RT-RPA product with and without T7 transcription

was negligible, indicating that DSN amplification occurs in the presence of both duplexes. Despite the increase in sample-to-answer times from inclusion of the T7 transcription stage, we have concluded it is vital for successful variant differentiation when using the DSN-mediated cleavage technique due to this significant gap in DSN specificity when targeting complexes in samples containing RT-RPA/T7 amplified RNA and RT-RPA amplified DNA. Failure to do so would result in compromised integrity of the DSN mediated reaction resulting in false-positive signal in the presence of non-specific variant target.

Figure 17a: DSN Detection and Specificity of ORF1a Conserved Region. DSN detection was performed following RT-RPA amplification and T7 transcription. T-tests were performed relative to mismatch RNA values and were assigned based on the following p-values: ***<0.005, **<0.01, *<0.05, nonsignificant (N.S.)>0.1.

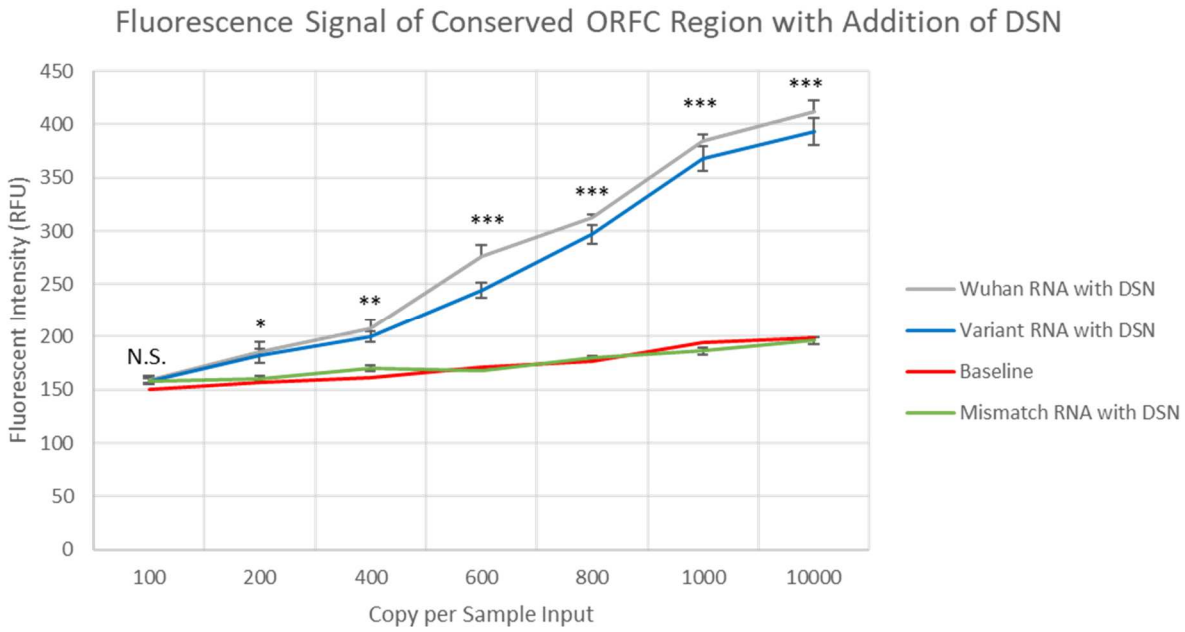

Figure 17b: DSN Detection and Specificity of Variable Regions. DSN detection and specificity of ORF1a and spike variable target regions following RT-RPA amplification and T7 transcription. T-tests were performed relative to mismatch RNA values and were assigned based on the following p-values: ***<0.005, **<0.01, *<0.05, nonsignificant (N.S.)>0.1.

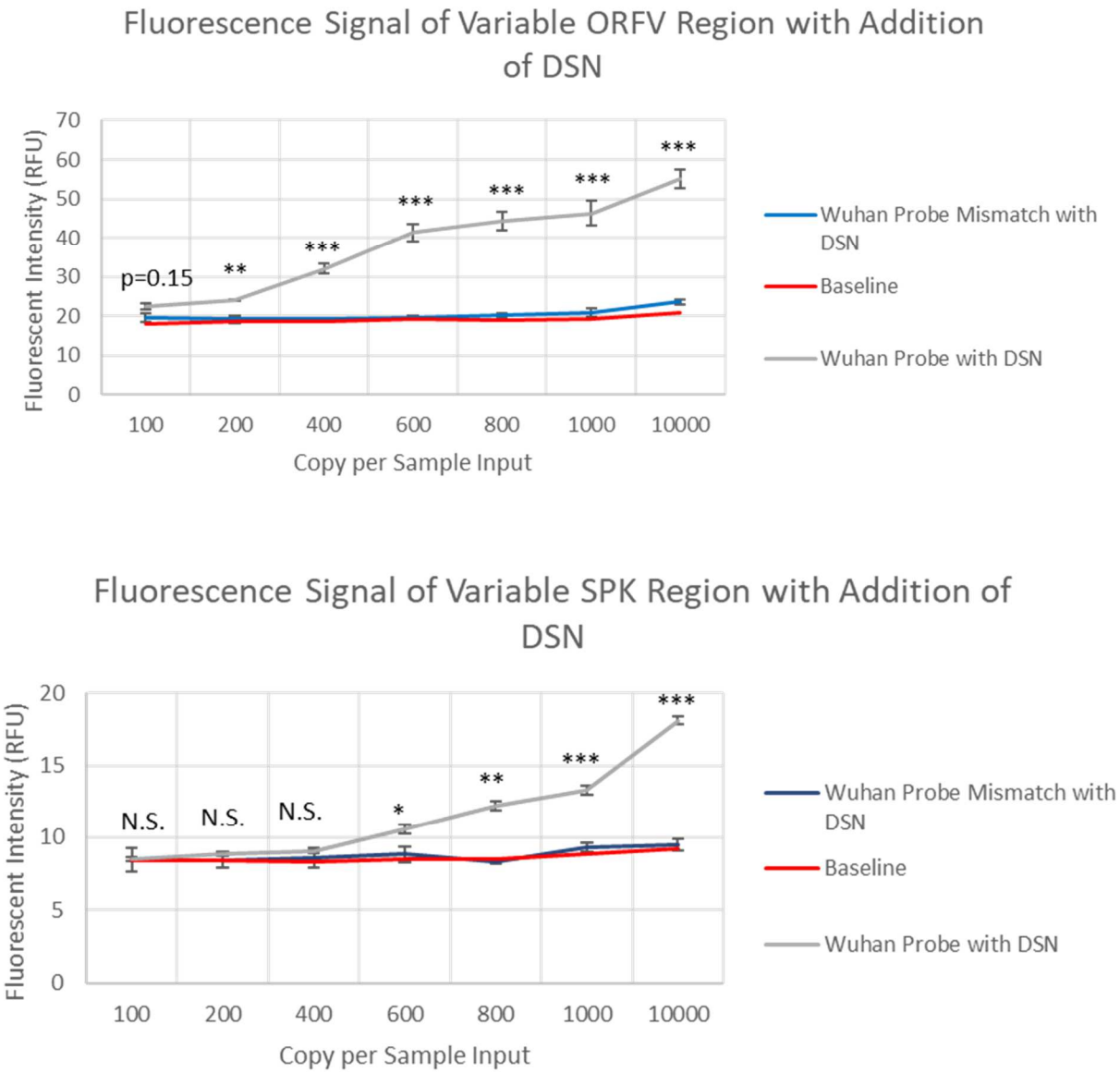

In order to determine the efficacy of this DSN-based technique in differentiating variants at varying initial sample concentrations prior to amplification, samples were prepared at varying dilutions of 100, 200, 400, 600, 800, 1,000, and 10,000 synthetic SARS-CoV-2 genomic RNA copies per sample and amplified using RT-RPA and T7 transcription. Samples were then incubated with 0.25 U DSN master mix to determine DSN specificity at a higher and lower-end initial concentration representing lower limits of detection of best-in-class assays for molecular testing during the early stages of the pandemic.[77] Sample preparation and target amplification of synthetic Wuhan-Hu-1 and B1.1.7 variant RNA was performed using previously listed methods for RT-RPA amplification followed by T7 transcription. DSN incubation was conducted at 55^{o}C for 30 minutes with 0.25 U DSN mix and read in the SPECTRAmax® GEMINI XS fluorescent plate reader at corresponding fluorescent excitation/emission wavelengths.

Detection of each variable target region was performed using T7 transcribed RNA of RT-RPA amplified product and sensitivity of the technique at each previously listed initial concentration of variable ORF1a and spike regions are portrayed in Figure 17b. Detection and differentiation of both Wuhan-hu-1 and B1.1.7 strain RNA was sensitive for the ORF1a variable and spike regions down to 200 and 600 copies, respectively. Additionally, detection of the conserved ORF1a region from both Wuhan and UK variant samples was sensitive down to 200 copies and is portrayed in figure S2 in the supplementary data. A baseline was established as the signal of 100 nM probe to discern the increase in signal resulting from DSN specific cleavage of quenched fluorescent probes in the presence of matched DNA: RNA duplexes. In order to evaluate the efficacy of the DSN technique in differentiating target and mismatched RNA analyte in sample, T-tests were performed relative to mismatch RNA values and were annotated based on the

[77] Arnaout, Ramy, et al. "SARS-CoV2 testing: the limit of detection matters." *BioRxiv* (2020).

following p-values: ***<0.005, **<0.01, *<0.05, nonsignificant (N.S.)>0.1. Additional information portraying the difference in signal following DSN detection of target and non-target RNA of the Wuhan and UK variant with DNA probe is listed in figure S3 in the supplementary data.

For both regions targeted in the ORF1a region, signal change in presence of DSN enzyme was insignificant in comparison to samples with complementary RNA and was effective in differentiating target ORF1a variant region down to 200 copies/sample. Due to the inaccessibility of the region containing the 69-70 amino acid deletion, efficiency of reverse-transcriptase based amplification has been noted to become negatively impacted resulting in S-gene target failure.[78] In order to compensate for this issue, RT-RPA amplification and T7 transcription were performed for 2 and 16 hours respectively to improve RNA yield of the spike target region. However, sensitivity of the assay was still compromised with significantly lower fluorescence and greater nonspecific signal in the presence of off-target RNA. Despite these issues, detection of the spike region was successful down to 600 copies/sample with significant differentiation between viral strains.

[78] Brown, Kevin A., et al. "S-gene target failure as a marker of variant B. 1.1. 7 among SARS-CoV-2 isolates in the greater Toronto area, December 2020 to March 2021." *Jama* 325.20 (2021): 2115-2116.

CHAPTER 2: Nitrocellulose-based Lateral Flow Testing for Viability with DSN-mediated SARS-CoV-2 Detection

Streptavidin Spotting on Nitrocellulose Strips for Lateral Flow Detection:

Compatibility of nitrocellulose-based lateral flow was tested using streptavidin-spotted lateral flow strips in order to determine the working range for binding of DNA and the achievable limit of detection using image analysis. Nitrocellulose strips (Thermofisher Scientific) were first tested to determine acceptable streptavidin spotting concentrations for sufficient reaction with biotinylated DNA probes. Strips were spotted with 1 μL of streptavidin at concentrations of 0.1, 0.5, and 1 mg/uL and dried in a dessicator at 25^{o}C for 24 hours. Strips were then blocked by submersion in 400 uL of GVS blocking buffer for 30 minutes and rinsed in 1X PBS (137 mM NaCl, 2.7 mM KCl, 8 mM Na_2HPO_4, and 2 mM KH_2PO_4) for 5 minutes at 300 rpm on a shaking platform. Prepared strips were then submerged in 100 μL of 1 μM DNA probe labeled with FAM at the 5' end and biotin at the 3' end for 15 minutes at 25oC and washed in a 1X PBS bath for 15 minutes. Another set of prepared strips were mounted by a 1 cm x 1cm absorbent pad and placed into dnase-free tubes containing 30 uL of DNA probe with the streptavidin-spotted end up, ensuring contact between the strip and the bottom of the tube. Following 25^{o}C incubation for 15 minutes, strips were removed from respective tubes and placed in a 1X PBS bath (137 mM NaCl, 2.7 mM KCl, 8 mM Na_2HPO_4, and 2 mM KH_2PO_4) for 15 minutes, ensuring contact between the strip and the bottom of the PBS bath. Both sets of strips were then dried in a dessicator for 4 hours at 25^{o}C for imaging. Nitrocellulose strips were imaged using the Nikon camera under green fluorescent filter at an exposure of 1000 and gain value of 2. ImageJ analysis was performed using the method described by Gavet et al. to calculate total fluorescence present at the spot with

subtraction of the background.[79] Signal-to-noise ratio was calculated with F/F_o, where F= corrected total fluorescence of the spot and F_o=corrected total fluorescence of the negative control.

Figure 18a: Streptavidin Concentration Optimization for Lateral Flow Detection. Streptavidin dilutions were spotted on nitrocellulose lateral flow strips for immobilization of biotinylated DNA probes.

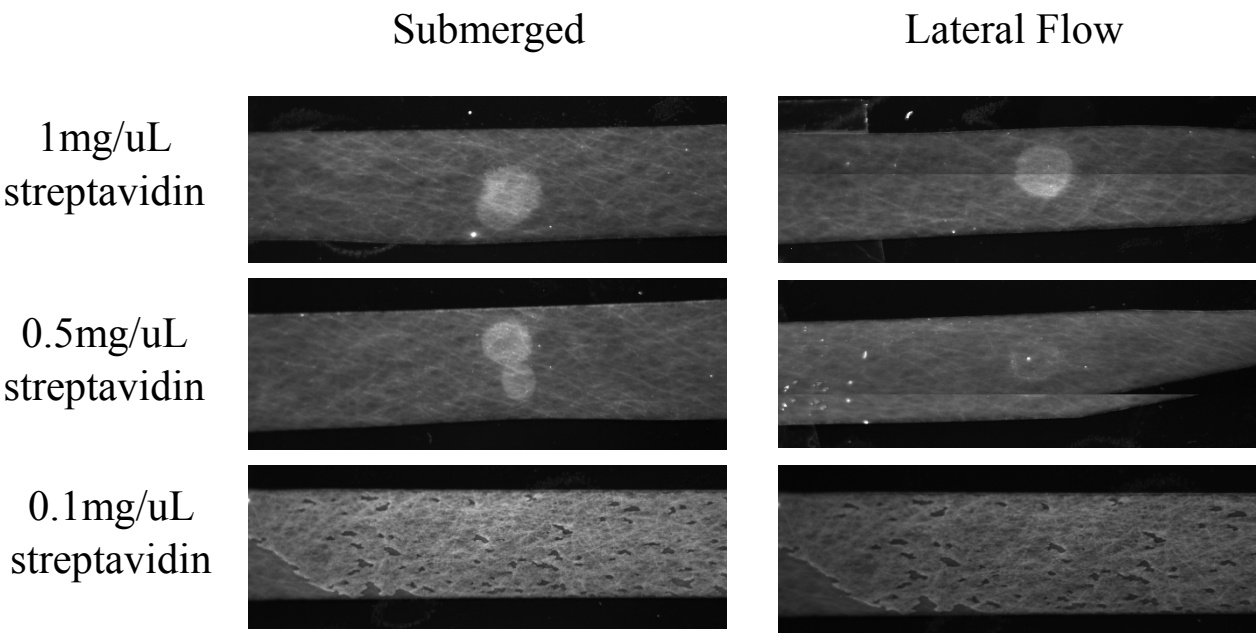

[79] Gavet, Olivier, and Jonathon Pines. "Progressive activation of CyclinB1-Cdk1 coordinates entry to mitosis." *Developmental cell* 18.4 (2010): 533-543.

Figure 18b: ImageJ Analysis of Streptavidin Optimization Testing. Corrected total fluorescence of streptavidin dilution spotting on nitrocellulose strips. Signal is measured using the method described by Gavet et al. for calculation of fluorescence through ImageJ analysis.[74] Signal-to-noise ratio is calculated as the corrected total fluorescence at 0.1, 0.5 and 1.0 mg/uL divided by the corrected total fluorescence at 0 mg/uL spotted streptavidin.

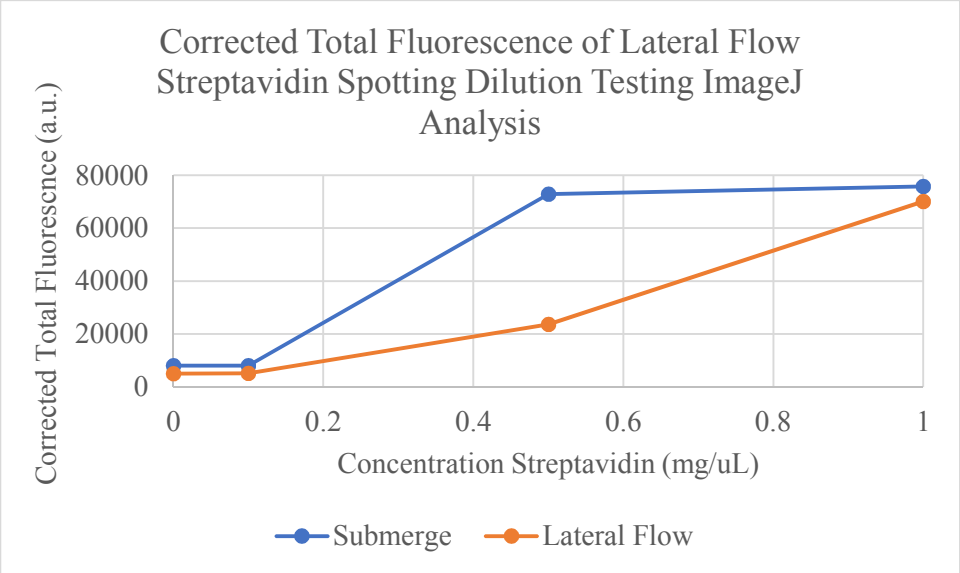

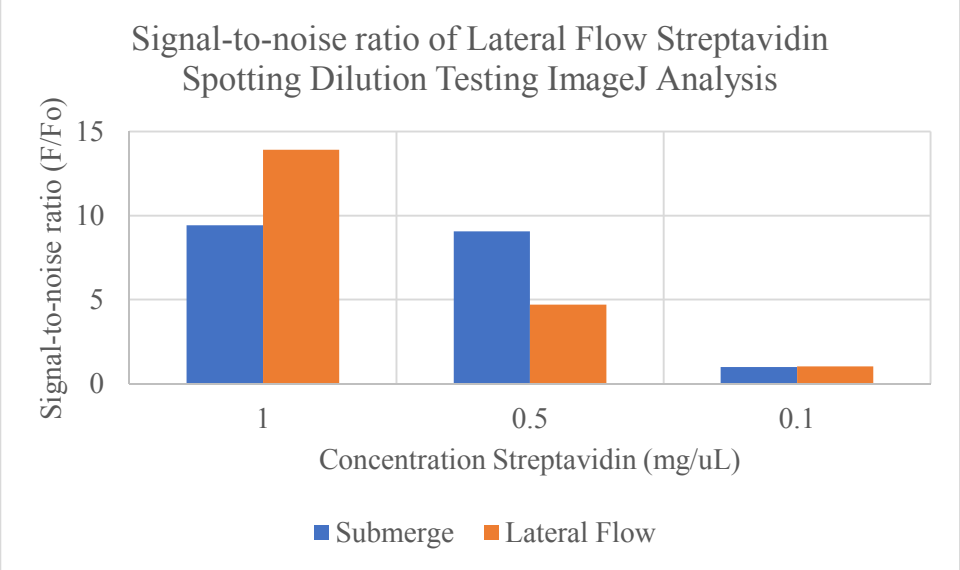

Spotted streptavidin strips demonstrated a clear increase in signal following addition of biotinylated DNA probe under both submerged and lateral flow conditions at 0.5 mg/uL and 1 mg/uL of spotted streptavidin, with an apparent saturation in fluorescent signal appearing at 1 mg/uL for both conditions. Additionally, 0.1 mg/uL demonstrated significantly lower fluorescence with poor signal-to-noise, indicating an optimal spotting concentration of 1mg/uL streptavidin for future experiments.

DNA Dilution Testing on Nitrocellulose Lateral Flow:

Nitrocellulose strips were spotted with 1 μL of 1 mg/uL streptavidin along the designated region and incubated for 2 hours at 25oC until dry. A dilution range of DNA probe labeled with FAM at the 5' end and biotin at the 3' end ranging from 0.01 μM to 1 μM were prepared and 30 μL were aliquoted into dnase-free tubes. Prepared strips were then mounted by a 1 cm x 1cm absorbent pad and placed with the streptavidin-spotted end up, ensuring contact between the strip and the bottom of the tube. Following 25^{o}C incubation for 15 minutes, strips were removed from respective tubes and placed in a 1X PBS bath (137 mM NaCl, 2.7 mM KCl, 8 mM Na_2HPO_4, and 2 mM KH_2PO_4) for 15 minutes. Strips were placed in a dessicator and dried at 25^{o}C for 8 hours and fluorescence was measured using Nikon Eclipse microscope at exposure 1000 and a gain value of 2. Images were captured using SPOT Basic Imaging Software and analyzed in ImageJ for signal quantification.

Figure 19: Lateral Flow Testing of DNA Controls. DNA standards were diluted at a range from 0.01 µM to 1 µM concentrations and incubated at 25°C for 15 minutes.

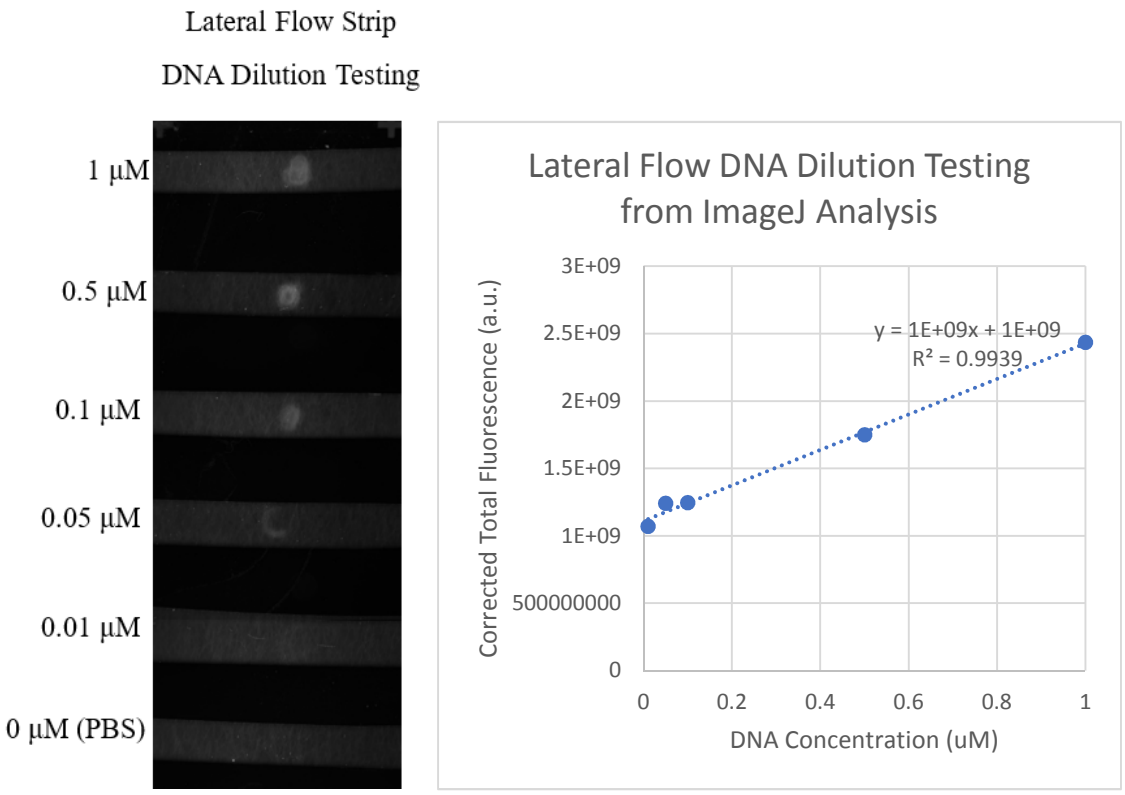

Following ImageJ analysis, DNA probe dilution testing on lateral flow strips demonstrated a linear response at all concentrations within the tested dilution range of 0.01 to 1 µM with a R^2 value of 0.9939, indicating validity of a quantitative approach to DNA measurement on the lateral flow strips. Additionally, concentrations used in the linear range fall well within the concentrations of DNA probe utilized in DSN related experiments, showing promise for future work related to incorporation of the nitrocellulose strips followed by ImageJ analysis as a viable alternative detection method of the assay for deployment in the field.

DSN-mediated Detection of SARS-CoV-2 Open Reading Frame Conserved Region on Lateral Flow:

As a proof-of-concept, an experiment was conducted to compare a standard DSN reaction to positive and negative controls to confirm compatibility with lateral flow design as a viable alternative to fluorescence measurements using a traditional reader. Samples were prepared using 100 nM 3' biotinylated DNA with a FAM fluorescent marker at the 5' end targeting the open reading frame conserved region along with 50 nM target RNA at 55^{o}C for 30 minutes with a final volume of 30 μL of 100 nM DNA probe, 50 nM synthetic target RNA, 50 mM Tris-HCl, 5 mM $MgCl_2$, and 1 mM DTT together with 0.25 U DSN. The sample was tested against a positive (DNase I digestion) and negative control (100 nM DNA probe) for DSN digestion. Signal was evaluated using ImageJ analysis as listed previously to determine change in signal intensity at the readout line of the sample.

Figure 20: DSN-mediated Detection on Lateral Flow Strip. Samples are incubated with 50 nM target RNA at 55ºC for 30 minutes followed by lateral flow testing with incubation at 25ºC for 15 minutes.

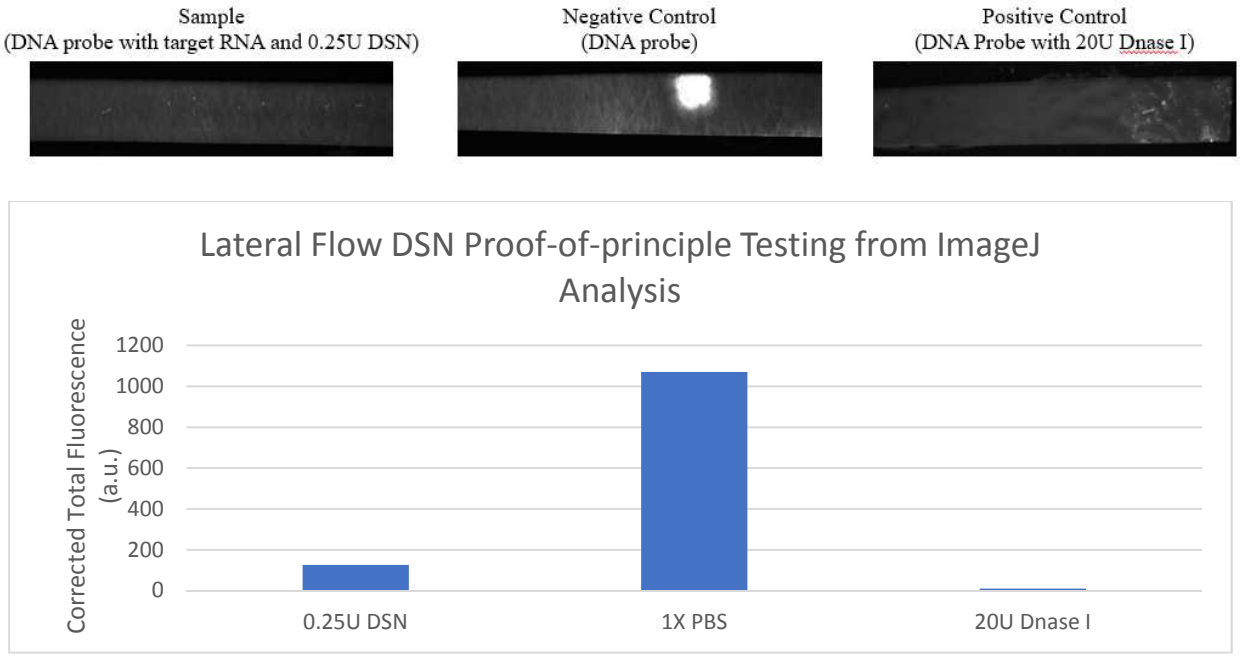

Due to the design of the probe, increase in fluorescence is inversely related to the dnase activity occurring within the reaction due to DNA cleavage resulting in separation of the biotinylated 3' end from the FAM fluorophore located at the 5' end. The negative control was expected to demonstrate the maximum fluorescent signal while samples containing DSN and DNase I should exhibit significantly lower fluorescence. These assumptions were in accordance with ImageJ analysis of the nitrocellulose strips, demonstrating significant DSN activity in the presence of complementary DNA: RNA complexes. Fluorescently tagged DNA in samples containing 0.25 U DSN and 20U DNase I with active dnase activity could also be observed passing through the nitrocellulose strip through lateral flow and being deposited at the end of the strip, indicating DNA cleavage and resulting separation from the biotinylated end of the DNA probe.

While initial experiments demonstrate compatibility of this technique with nitrocellulose-based lateral flow, further work is necessary in order to determine if the limit of detection of this technique is suitable for adaptation with the previously described assay design for SARS-CoV-2 variant discrimination. However, this is a promising approach with relevance to low-resource techniques for screening communities by providing a simple method for portable detection. Additionally, due to the simplicity of the probe design and application for lateral flow on nitrocellulose strips, the fluorescent marker is irrelevant and can be adapted into other labels such as in a colorimetric test to remove the burden of requiring a system for fluorescent detection. The use of the streptavidin-biotin complex to immobilize the probes onto the nitrocellulose surface removes the necessity for a FRET-based quencher system to evaluate DSN activity, reducing the cost of the biological reagents required and simplifying readout in multiplexed assay designs by removing the subtraction of baseline signal required when using TaqMan-based probes.

CHAPTER 3: Electro-osmotic Signal Enhancement for Molecular Detection on Latex Beads

Electrokinetic Guided Assembly of Beads with Electro-osmosis:

A key to microfluidic diagnostics is the guided movement of fluid or particles through manipulation of their physico-chemical properties, such as geometry, permittivity, conductivity, and mechanical properties.[80] Electrokinetics, or dielectrophoresis (DEP) and electro-osmosis (EO) in particular, are one such method where electric fields are used to influence assembly and characterization of polarizable particles so as to facilitate movement.[81,82] Both forces have been widely utilized in biological applications for transportation, separation, sorting, and assembly of particles and cells.[83,84,85,86] In AC electro-osmosis, nonlinear flow occurs around the polarized electrode surface resulting from the accumulation of ionic charge on the double layer of the electrode surface and the application of an external AC electric field.[87] The velocity of fluid flow within the AC electro-osmotic system has been found to be linearly dependent on the applied

[80] Hosseini, Imman I., et al. "Cell properties assessment using optimized dielectrophoresis-based cell stretching and lumped mechanical modeling." *Scientific reports* 11.1 (2021): 1-13.
[81] Barsotti Jr, Robert J., et al. "Assembly of metal nanoparticles into nanogaps." *small* 3.3 (2007): 488-499.
[82] Ohannesian, Nareg, et al. "Directed concentrating of micro-/nanoparticles via near-infrared laser generated plasmonic microbubbles." *ACS omega* 5.50 (2020): 32481-32489.
[83] Xiong, Xugang, et al. "Directed assembly of gold nanoparticle nanowires and networks for nanodevices." *Applied Physics Letters* 91.6 (2007): 063101.
[84] Subramanian, Arunkumar, et al. "Micro and Nanorobotic Assembly Using Dielectrophoresis." *Robotics: Science and Systems*. 2005.
[85] Vazquez-Pinon, Matias, et al. "Hydrodynamic channeling as a controlled flow reversal mechanism for bidirectional AC electroosmotic pumping using glassy carbon microelectrode arrays." *Journal of Micromechanics and Microengineering* 29.7 (2019): 075007.
[86] Cortez, Jennifer, et al. "Electrokinetic Propulsion of Polymer Microparticulates Along Glassy Carbon Electrode Array." *Journal of Micro-and Nano-Manufacturing* 8.2 (2020): 024504.
[87] Squires, Todd M., and Martin Z. Bazant. "Induced-charge electro-osmosis." *Journal of Fluid Mechanics* 509 (2004): 217-252.

frequency and magnitude of the strength of the applied electric field and can be described using the Helmholtz-Smoluchowski equation:

$$u = -\frac{\varepsilon}{\eta}\Delta\phi_{\mathrm{d}}\frac{\partial\phi}{\partial x}$$

Where u is described as the fluid velocity, ε is the permittivity of the fluid, η the viscosity of the fluid, ϕ is the potential of the electric field outside the diffuse double layer, and $\Delta\phi$d is the difference in potential between the outer and inner portions of the diffuse double layer.[88,89]

During application of an AC non-uniform electric field on a dielectric particle, dielectrophoresis is also exerted and can be described be the following equation:

$$\langle F_{\mathrm{DEP}}\rangle = 2\pi r^3\varepsilon_{\mathrm{m}}Re\{CM(\omega)\}\nabla|E|^2$$

$$CM = \left\{\frac{\varepsilon_{\mathrm{p}}^* - \varepsilon_{\mathrm{m}}^*}{\varepsilon_{\mathrm{p}}^* + 2\varepsilon_{\mathrm{m}}^*}\right\}$$

$$\varepsilon^* = \varepsilon_{\mathrm{r}} + i\frac{\sigma}{\omega}$$

where $\nabla|E|^2$ represents the gradient of the electric field magnitude squared, r the radius of the particle, εm the relative permittivity of the medium, and ε_m* and ε_p* are the complex permittivities of the fluid medium and particle, respectively.[82] Due to the impact of the radius r of the particle on DEP force at a relation of $\langle F_{DEP}\rangle \sim r^3$, particles of smaller radii are less impacted by DEP force and fluidic movement is dominated by electro-osmosis.

[88] Bruckenstein, Stanley. "Physicochemical hydrodynamics." *Nature* 268.5618 (1977): 298-299.
[89] Zhou, Tuo, et al. "Guided Electrokinetic Assembly of Polystyrene Microbeads onto Photopatterned Carbon Electrode Arrays." *ACS applied materials & interfaces* 12.31 (2020): 35647-35656.

Figure 21: COMSOL Simulation by Zhou et al. of DEP and Electro-osmotic Forces on 1 μm Polystyrene Beads.[85] Beads experience dominant electro-osmotic forces due to the small radii and are jettisoned into the "windows" by EO force along the edges of the electrodes. As beads are moved into the windows and cluster, they experience positive insulator DEP, resulting in attraction of more beads to the existing clusters.

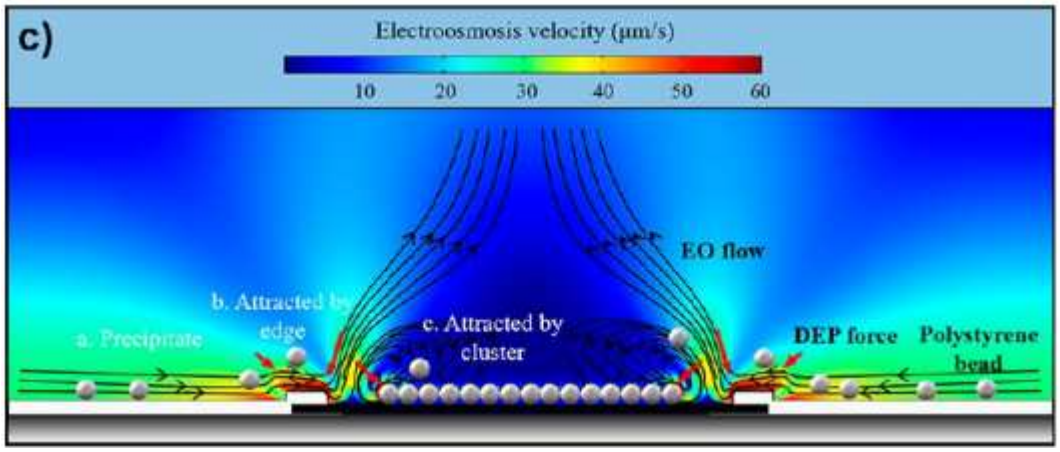

Investigation of the method for electrokinetic self-assembly by Zhou et al. utilizes a combination of guided dielectrophoresis (DEP) and AC electro-osmosis (ACEO) with glassy carbon interdigitated electrode arrays (IDEAs) to guide microparticulates to photoresist-patterned "windows", or depressed regions on the electrode. Due to the small size of 1 μm beads, fluidic movement is dominated by AC electro-osmosis with induced vortices occurring over the surface of the electrodes and at the edges of coplanar bar electrodes, driving movement of the fluid toward the edge of exposed "windows".[90,91] Once beads are driven to edge of the "windows", they pass over the outer edges of the electrodes and experience positive insulator DEP, where the beads

[90] Green, Nicolas G., et al. "Fluid flow induced by nonuniform ac electric fields in electrolytes on microelectrodes. I. Experimental measurements." *Physical review E* 61.4 (2000): 4011.
[91] Green, Nicolas G., et al. "Fluid flow induced by nonuniform ac electric fields in electrolytes on microelectrodes. III. Observation of streamlines and numerical simulation." *Physical review E* 66.2 (2002): 026305.

within the windows serve as the point of highest electric field intensity. The clustering of beads within the windows results in increasing insulator DEP force, attracting more beads toward the regions of the window where bead clusters are located. Additionally, the vortices at the edges of the coplanar bar electrodes can be manipulated to expand from the edges of the wells at decreasing frequency, resulting in greater clustering of the beads within the center of the "window".[82]

In this work, experiments were conducted in collaboration with the Kulinsky group at the University of California, Irvine with their expertise in manipulation of dilelectrophoretic and electro-osmotic forces to evaluate the bead-based post-concentration of both protein-based and molecular assays with electrokinetic assembly.

Guided Electrokinetic Assembly of Protein Conjugated Beads Through Electro-osmosis:

Electrode Preparation:

Glassy carbon inter-digitated electrode arrays (IDEA) were fabricated as described by Zhou et al. through conventional SU-8 photoresist lithography followed by pyrolysis.[84] IDEAs were fabricated on 4 in. diameter silicon wafers coated with a 1 μm thick layer of thermal oxide (University Wafer, MA, USA). SU-8 2025 photoresist (Microchem Corp. Ltd.) was then spin-coated onto the silicon wafer using a Laurell photoresist spinner (Laurell Technologies) at an initial angular velocity of 500rpm for 10 seconds, followed by an increase to 4000 rpm for 30 seconds. Following SU-8 spin coating, wafers were soft baked at 95^{o}C for 5 minutes on a Dataplate Pmc 732 hot plate (Dataplate Pmc 732 Series) followed by mask lithography using a patterned plastic mask (CadArt) with a UV flood exposure system (Oriel Instrument, Newport Corp) for 6 seconds at an energy intensity of 10 mW/cm^2. Wafers were then post-baked at 95^{o}C for 5 minutes and developed in SU-8 developer (Microchem Corp. Ltd.) to remove non-crosslinked regions from the

IDEA pattern. Following a hard bake stage at 95ºC for 45 minutes, wafers were inserted into a pyrolysis oven (Thermo Fisher Scientific) at a thermal profile of 25ºC for 2 hours, 300ºC for 1 hour, 900ºC for 1 hour, and ramp down to 25ºC. Height of the electrode fingers were measured using a Dektak 3 profilometer (Veeco Instrument Inc.) exhibiting heights between 1.5-2.0 μm and widths of 120-126 μm.

Wells were then lithographically patterned using a SU-8 photoresist coat over the pyrolyzed IDEAs. The patterned photoresist layer consists of an array with alternating well sizes of 90 × 90 μm, 100 × 100 μm, 110 × 110 μm. Wells were lithographically produced using an iron oxide mask (Front Range Photomask) and MA56 mask aligner (Karl Suss). Subsequent soft-bake, exposure, and post-exposure bake processes were adjusted to achieve a range of desired heights for the resist layer in order to create different well depths for the "windows" as listed in table 5. Following these steps, non-crosslinked regions were removed using Su-8 developer for 5 minutes and hard-baked at 95ºC for 45 minutes.

Table 5: "Window" Manufacturing Protocol for Lithography

Window Depth (μm)	Soft-bake (95ºC)	Exposure time and intensity (10 mW/cm^2)	Post-bake (95ºC)
3	2 minutes	4 seconds	3 minutes
6	3 minutes	6 seconds	5 minutes

Anti-IgG – Alexafluor-647 Bead Preparation:

1 μm carboxyl-modified latex (CML) polystyrene beads (ThermoFisher Scientific) were prepared at 2.5 ml (40mg/ml) and diluted with 10 ml 0.025M 2-(N-morpholino) ethanesulfonic acid(MES) buffer (Sigma Aldrich). Samples were then centrifuged at 3000 rpm for 20 minutes on the mySPIN 12 from Thermo Scientific (ThermoFisher Scientific). Supernatant was then removed

from the particles and resuspended in 5 ml 0.025M MES buffer at an approximate concentration of 20 mg/ml.

Bead controls were prepared according to the passive adsorption protocol listed by Thermofisher Scientific to produce a positive control consisting of conjugation of Goat anti-Human IgG Fc Recombinant Secondary Antibody, Alexafluor-647 (ThermoFisher Scientific) and a negative control consisting of conjugation of Goat anti-Human IgG Fc Cross-Adsorbed Secondary Antibody, HRP (ThermoFisher Scientific) on the aforementioned 1 μm latex beads.[92] Anti-human IgG antibody controls were prepared at a concentration of 4 μg/ml in 0.025M MES buffer and prepared at a 1:1 dilution with 500 μl of prepared latex beads. Samples were then incubated at 25°C overnight for 10 hours and centrifuged at 3000 rpm for 20 minutes. Supernatant was then removed and resuspended with 1 mL 1X PBS (ThermoFisher Scientific) and centrifuged again to sediment the particles. This wash step was repeated for a total of three washes and then blocked in 250 μl 1X StartingBlock™ (PBS) blocking buffer (ThermoFisher Scientific) for 2 hours at 25°C. Samples were then centrifuged again to sediment the particles at 3000 rpm for 20 minutes and washed in 400 μl 1X PBS. Washes were performed for a total of three washes and beads were resuspended in 1 mL 1X PBS. Prior to electro-osmosis testing on the electrodes, bead samples were immediately prepared at a 1:10 dilution in UltraPure™ DNase/RNase-Free Distilled Water (Thermofisher Scientific).

[92] Passive Adsorption Protocol, Thermofisher Scientific, https://www.thermofisher.com/us/en/home/life-science/cell-analysis/qdots-microspheres-nanospheres/idc-surfactant-free-latex-beads/latex-bead-protein-coupling-protocols/passive-adsorption-protocol.html. Accessed on 7 November, 2022.

Electro-osmosis Experimental Setup:

Following IDEA fabrication, wires were soldered to the carbon contact pads using indium and 10 μl of the 1:10 bead dilution was deposited onto the surface of the electrodes. A glass cover slide was placed over the chip to reduce evaporation of the liquid and establish a uniform plane to visualize bead facilitation by electro-osmosis. Microscopic observation was conducted using a Nikon eclipse microscope and recorded using SPOT Basic video editing program (SPOT Imaging, MI, USA). IDEA chips were connected to a function generator (Stanford Research System, CA, USA) to produce AC field at a voltage of 2V and frequency of 200 Hz.

Figure 22: Electro-osmosis of anti-IgG Conjugated Control Beads

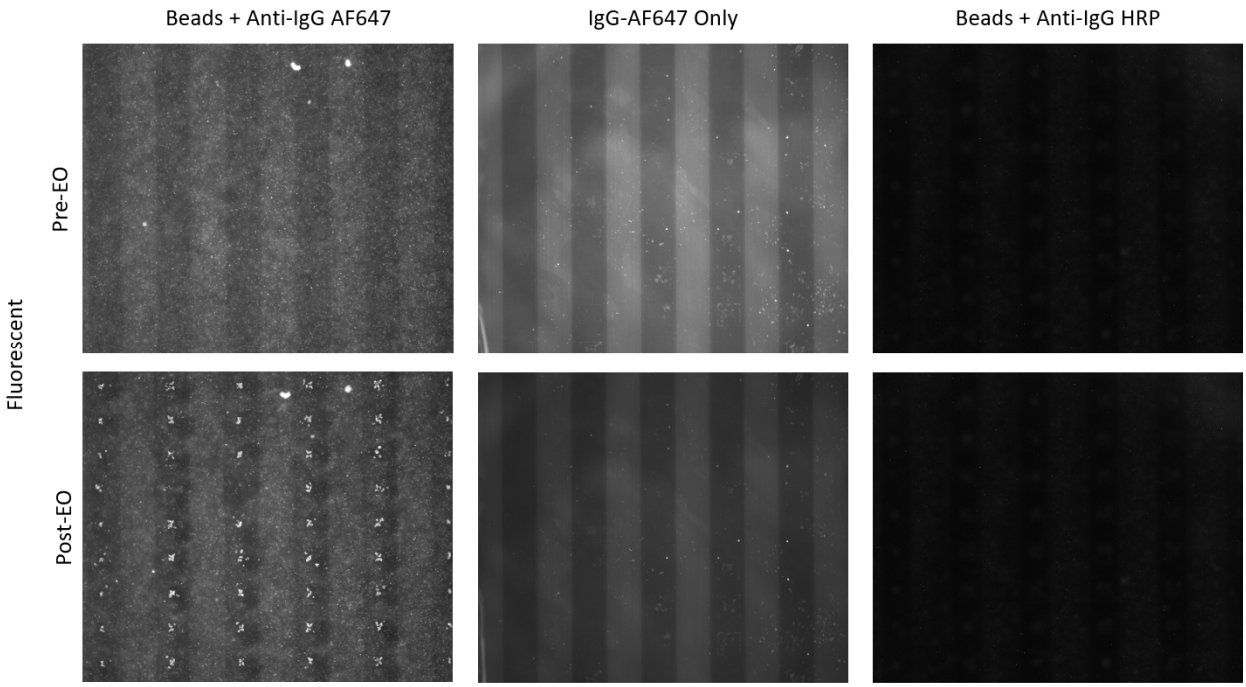

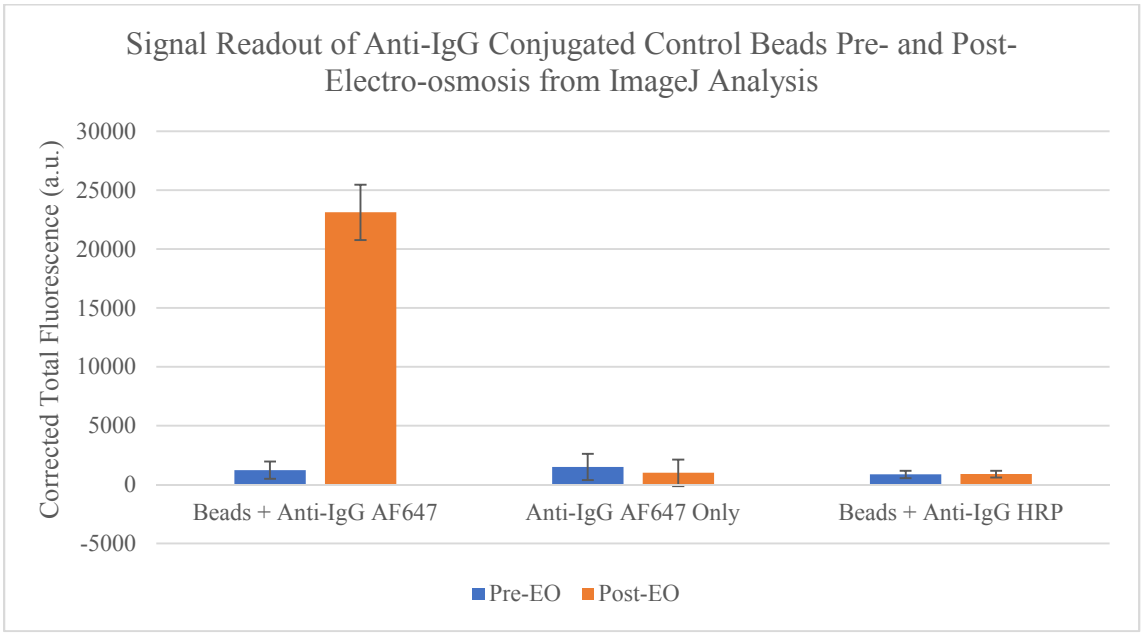

Feasibility of the electro-osmotic bead concentration technique was first evaluated three sets of controls in order to determine biocompatibility of the electro-osmotic bead concentration technique with antibody-based detection techniques. Electro-osmotic experiments were conducted

using positive control (0.4 μg/ml Anti-IgG Alexafluor-647 conjugated beads), negative control (0.4 μg/ml Anti-IgG Alexafluor-647 protein) of fluorescently conjugated protein to determine if voltage and frequency settings were optimized for specific capture of bead products in the "windows", and microscope negative control (0.4 μg/ml Anti-IgG HRP conjugated beads) to determine that bead and protein reagents used in this experiment did not exhibit autofluorescence. Images were taken of a 9x5 array prior to application of electro-osmosis at the 0 second time point and following application of electro-osmosis at the 120 second time point for comparison. ImageJ analysis was used to calculate signal within the windows by subtracting the signal of the background outside of the window from the fluorescence within each window and averaging total fluorescence.

With results reflective of expectations from a standard ELISA, electro-osmosis is biologically compatible for detection of antibody-based protein with significant localization of beads and resulting fluorescent readout within the "windows" of the electrode. Additionally, accumulation of free fluorescent protein in solution into the "windows" was negligent, Bead autofluorescence is also not evident with microscope negative control of beads conjugated with non-fluorescent anti-IgG demonstrating measurable signal comparable to that without beads in solution. Critically, through comparison of pre- and post-electro-osmosis images of sample containing fluorescently tagged protein without beads, little to no assembly occurred within the "windows" of the electrode for non-conjugated protein in solution. This was further verified using bright field visualization of the samples with deposition of particles only visible in bead-based solutions, indicating that current voltage and frequency settings are ideal for separation of unbound anti-IgG protein in solution from passively adsorbed protein on beads. Due to the ability to differentiate between beads and unbound sample in solution through guided assembly at the

electrode “windows”, the electro-osmotic technique is a promising method for highly specific detection for biological applications and can be viewed as a potential alternative to conventional washing steps in a standard ELISA assay.

Figure 23: Validation of Bead Localization at “Windows” Using Bright Field Microscope

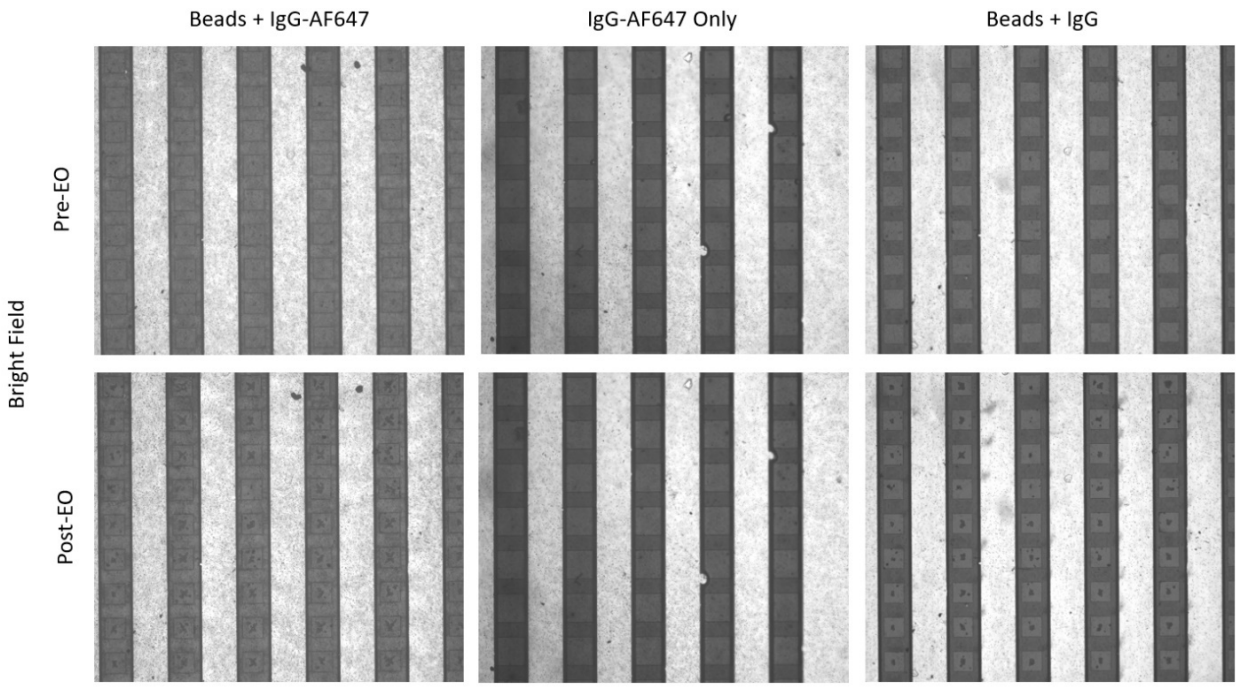

To evaluate the impact of varying protein concentrations on visualization of electro-osmotic bead concentration, controls were tested using a dilution range of 1000 to 4000 pg/ml of Alexafluor-647 conjugated anti-IgG protein during incubation with latex beads. Samples were prepared using the previously described protocol for anti-IgG protein conjugation with dilutions of 375, 750, 1500, and 3000 pg/ml with the original bead concentration of approximately 20 mg/ml. Images were taken using an exposure value of 2000 and gain value of 2.

Fluorescent signal readout was significant at all concentrations within the tested dilution range for bead passive adsorption from 1000 to 4000 pg/ml. ImageJ analysis confirmed

accumulation of beads conjugated with fluorescent protein with increases in signal following electro-osmosis. However, signal increase did not yield a linear range for the concentrations tested due to varying efficiencies in bead conjugation. Washing steps also had an apparent impact on signal calculation due to greater concentrations of unbound protein in solution, increasing background fluorescence during the imaging stage. This was reflected by greater values of corrected fluorescence intensity at the lower concentration within the dilution range of 1000 pg/ml in comparison to the corrected signal of the 2000 pg/ml sample. However, pre-electro-osmosis maintained uniform levels of minimal signal change, a clear indication of successful signal concentration following application of electro-osmosis.

Figure 24: Anti-IgG Alexafluor-647 Dilution Testing

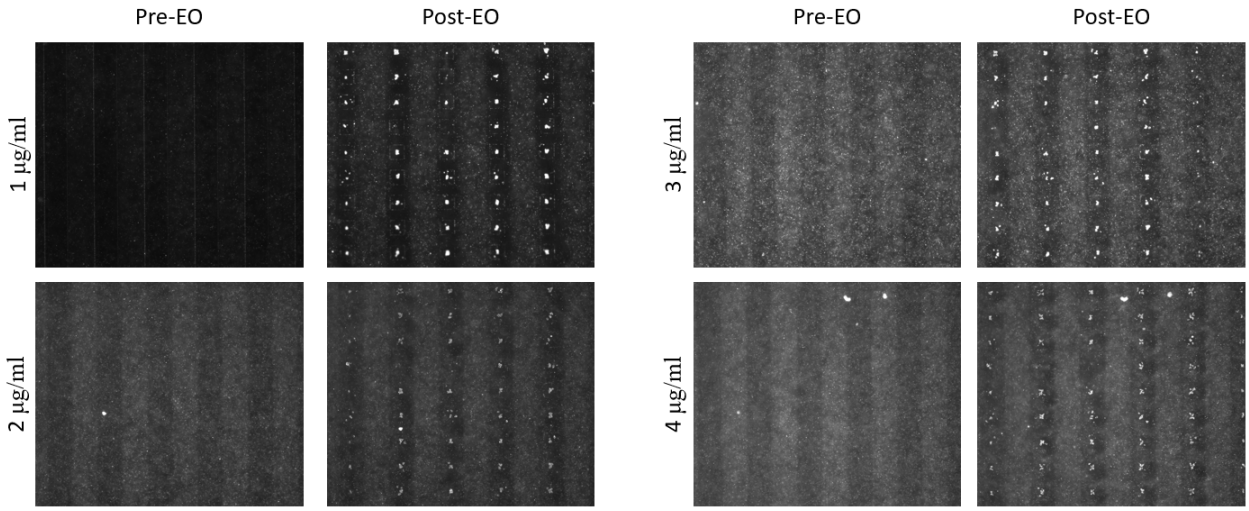

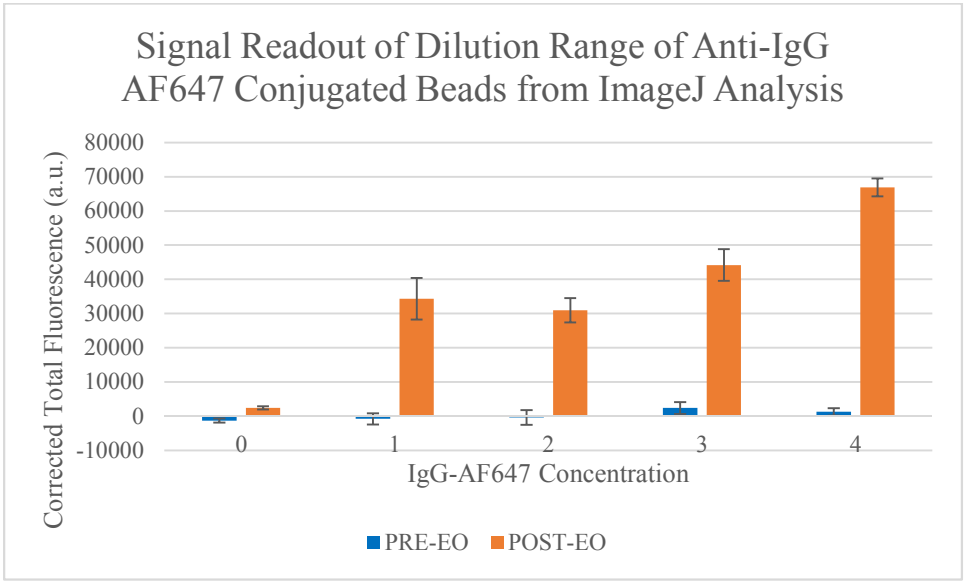

Following proof-of-concept testing of electro-osmotic concentration of fluorescence using protein conjugated beads, it is necessary to evaluate the viability of relevant biological assays with real world applications. The human tumor necrosis factor alpha (TNF-α) is the prototypic ligand of the TNF superfamily and plays a central role in inflammation, immune system development, apoptosis, lipid metabolism. TNF has been found to induce cell death in certain tumor cell lines

but can also play an oncogenic role and serves as important biomarker for inflammation-induced cancer.[93,94,95] Electro-osmotic concentration was further tested using the TNF alpha Human Matched Antibody Pair from Thermofisher Scientific (Thermofisher Scientific) due to its relevance in biomarker detection and an established protocol for implementation on the latex bead-based assay.

TNF alpha ELISA Protocol Adaptation for Latex Beads:

Pre-titrated, purified anti-Human TNF alpha coating antibody was prepared at a concentration of 0.08 µg/ml in 0.025M MES buffer and incubated at a 1:1 ratio with 500 µL of previously prepared 1 µm carboxyl-modified latex (CML) polystyrene beads (ThermoFisher Scientific) at 25ºC overnight for 10 hours and centrifuged at 3000 rpm for 20 minutes. Supernatant was then removed and resuspended with 1 mL 1X PBS (ThermoFisher Scientific) and centrifuged again to sediment the particles. This wash step was repeated for a total of four washes and then blocked in 250 µl 1X StartingBlock™ (PBS) blocking buffer (ThermoFisher Scientific) for 2 hours at 25ºC. Samples were then centrifuged again to sediment the particles at 3000 rpm for 20 minutes and washed in 400 µl 1X PBS. Wash steps were performed for a total of four washes. Recombinant human TNF alpha standard was prepared at a concentration of 2000 pg/ml in 100 µl of 1X assay buffer (8.0 g NaCl, 1.13 g Na2HPO4, 0.2 g KH2PO4, 0.2 g KCl, 5.0 g bovine serum albumin (fraction V), 1 mL Tween 20, 0.5% ProClin™ in 1ml DI H_2O) and incubated with 100 µl of the coating antibody-conjugated latex beads at 25ºC for 60 minutes. Samples were then centrifuged to

[93] Zelová, Hana, and Jan Hošek. "TNF-α signalling and inflammation: interactions between old acquaintances." Inflammation Research 62.7 (2013): 641-651.
[94] Juhasz, Kata, Krisztina Buzas, and Erno Duda. "Importance of reverse signaling of the TNF superfamily in immune regulation." Expert review of clinical immunology 9.4 (2013): 335-348.
[95] Gong, Ke, et al. "Tumor necrosis factor in lung cancer: Complex roles in biology and resistance to treatment." *Neoplasia* 23.2 (2021): 189-196.

sediment the particles at 3000 rpm for 20 minutes and washed in 400 µl 1X PBS. Wash steps were performed for a total of four washes. Biotinylated anti-Human TNF alpha detection antibody were prepared at a concentration of 1:200 in 1X assay buffer to a volume of 200 µl and incubated with the latex beads at 25^{o}C for 60 minutes. Samples were then centrifuged again to sediment the particles at 3000 rpm for 20 minutes and washed in 400 µl 1X PBS. Wash steps were performed for a total of four washes. Streptavidin-modified Alexa Fluor™ 647 conjugate (Thermofisher Scientific) was prepared to a dilution of 0.05 mg/ml in 100 µl and incubated with the latex beads for 40 minutes at 25^{o}C. Samples were then centrifuged to sediment the particles at 3000 rpm for 20 minutes and washed in 400 µl 1X PBS. Wash steps were performed for a total of four washes. Beads were then resuspended in 500 µl 1X PBS and placed in storage. Prior to electro-osmosis testing on the electrodes, bead samples were immediately prepared at a 1:10 dilution in UltraPure™ DNase/RNase-Free Distilled Water (Thermofisher Scientific).

Figure 25: TNF-alpha Conjugated Bead Fluorescence Pre- and Post-electro-osmosis

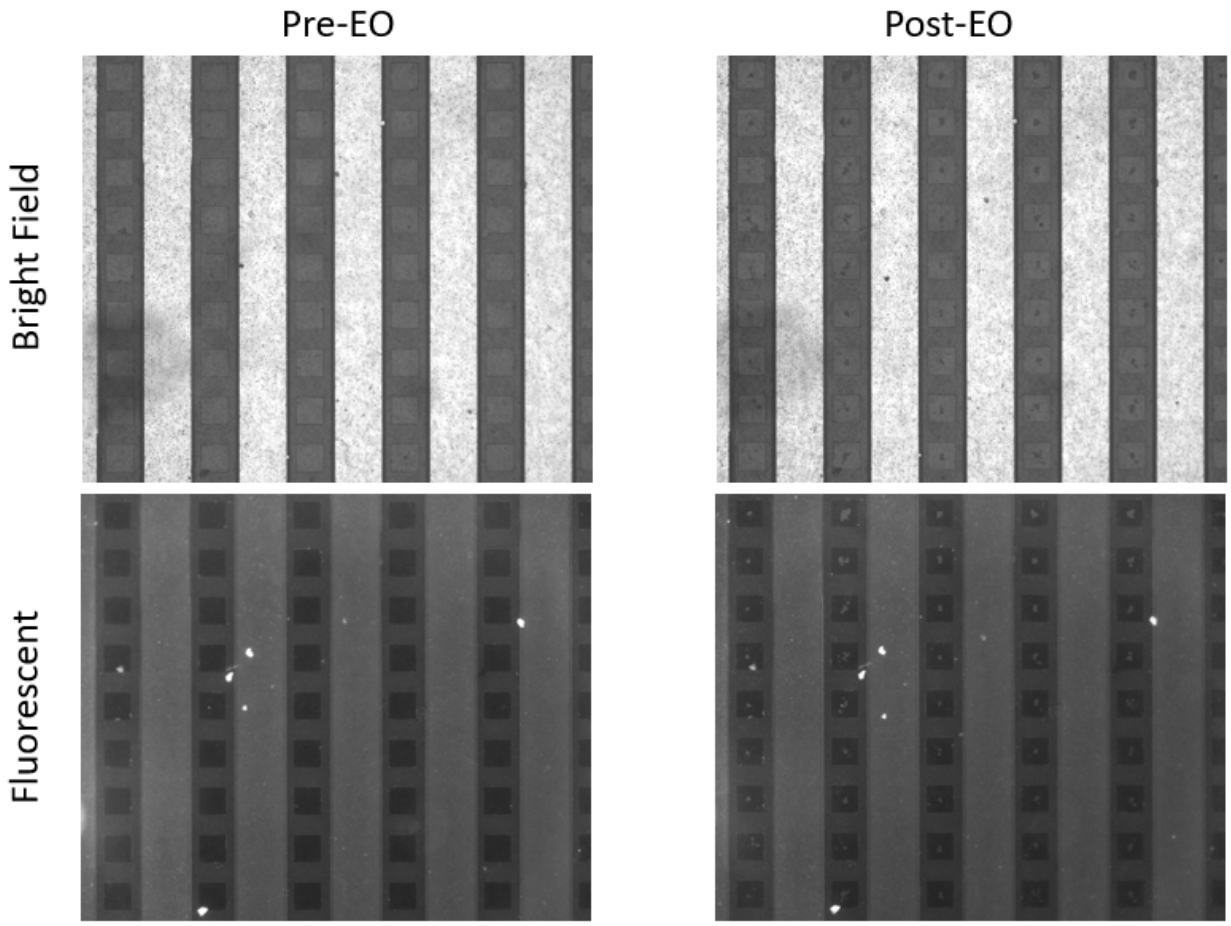

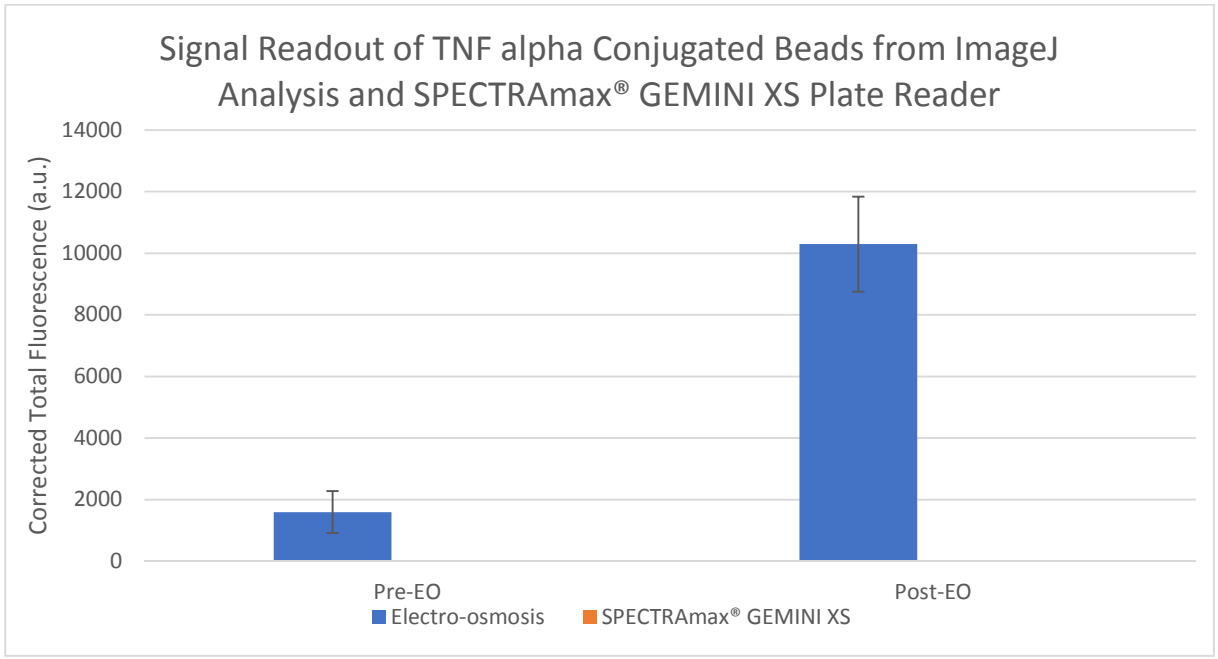

TNF-alpha conjugated beads demonstrated a significant increase in corrected total fluorescence following electro-osmosis, indicating that the ELISA was sufficiently successful. Interestingly, due to accumulation of signal within single points in the electrode "windows", signal calculations using ImageJ analysis for electro-osmotically concentrated beads demonstrated greater sensitivity in the limited sample set with a false-negative signal readout when using the SPECTRAmax® GEMINI XS plate reader. In this limited trial, electro-osmotic concentration was a superior detection technique regarding the improved sensitivity, while the readout from the fluorescent plate reader may have indicated an incorrect false-negative interpretation. In conclusion, electro-osmosis-based bead concentration is a viable strategy for signal concentration with biological assays and is a promising and potentially superior method of detection to conventional fluorescent readout in traditional machines. When utilizing an immobilization-based assay, electro-osmosis also holds several advantages over conventional detection methods including the ability to self-assemble on the electrode and improving detection, eliminating or reducing the importance of wash steps, and increased surface area in comparison to an ELISA plate surface to improve binding efficiency. While further optimization of this strategy for biochemical assays is necessary, its potential as an alternative method for detection in diagnostics is intriguing.

DSN-mediated DNA Cleavage and Detection Using Electro-osmotic Signal Concentration:

In order to determine compatibility of the DNA-based assay with electro-osmotic signal concentration technique, control trials were run by immobilizing previously described 5' FAM and 3' biotin labeled DNA probes to latex beads for detection. Streptavidin for passive adsorption on the latex bead surface was prepared at a concentration of 50 ng/ml in 0.025M MES buffer to a

final volume of 100 µl and mixed at a 1:1 ratio with previously prepared latex beads. Samples were then incubated at 25ºC overnight for 10 hours and centrifuged at 3000 rpm for 20 minutes. Supernatant was then removed and resuspended with 1 mL 1X PBS (ThermoFisher Scientific) and centrifuged again to sediment the particles. This wash step was repeated for a total of three washes and then blocked in 250 µl 1X StartingBlock™ (PBS) blocking buffer (ThermoFisher Scientific) for 2 hours at 25ºC. Samples were then centrifuged again to sediment the particles at 3000 rpm for 20 minutes and washed in 400 µl 1X PBS. Washes were performed for a total of three washes and beads were resuspended in 1 mL 1X PBS.

Following preparation of streptavidin-coated beads, 5'FAM and 3'biotin labeled DNA probes targeting the open reading frame conserved region of SARS-CoV-2 Wuhan-hu-1 strain were prepared at a concentration of 100 nM in a volume of 100 µl and incubated with prepared beads for 30 minutes at 25ºC. Prior to electro-osmosis testing on the electrodes, bead samples were immediately prepared at a 1:10 dilution in UltraPure™ DNase/RNase-Free Distilled Water (Thermofisher Scientific).

Evaluation of DNA-probe Functionalized Bead Detection:

While corrected total fluorescence following electro-osmosis was significantly lower than in previously described antibody-based experiments, post-concentration revealed 215.4% increase in signal within the windows in comparison to pre-electro-osmosis. Bright field imaging also revealed bead localization following application of electro-osmosis as expected. Plate reader analysis of functionalized beads yielded nonsignificant fluorescent signal relative to the ImageJ analysis, indicating that DNA functionalization efficiency onto the beads remained limited. Successful fluorescent analysis at concentrations relevant for DSN-based experiments indicates its

potential as a method of detection and analysis for previously described SARS-CoV-2 detection scheme. However, further testing of the linear range using DNA-based probes is necessary to determine its relevance in terms of analyte quantification and limit of detection.

Table 6: Probes and RNA for Electro-osmotic Post-concentration Testing

Taqman Probe	Target Region	5' - FAM CCAACCTCTTCTGTAATTTTTAAAC Biotin – 3'
Target RNA (Wuhan-hu-1)	ORFC	5' – GUUUAAAAAUUACAGAAGAGGUUGG – 3'
Non-target RNA (B1.1.7)	ORFV	5' – AUACUAGUUUGAAGCUAAAAGA – 3'

Figure 26: DNA Bead Post-Concentration Testing using Electro-osmosis

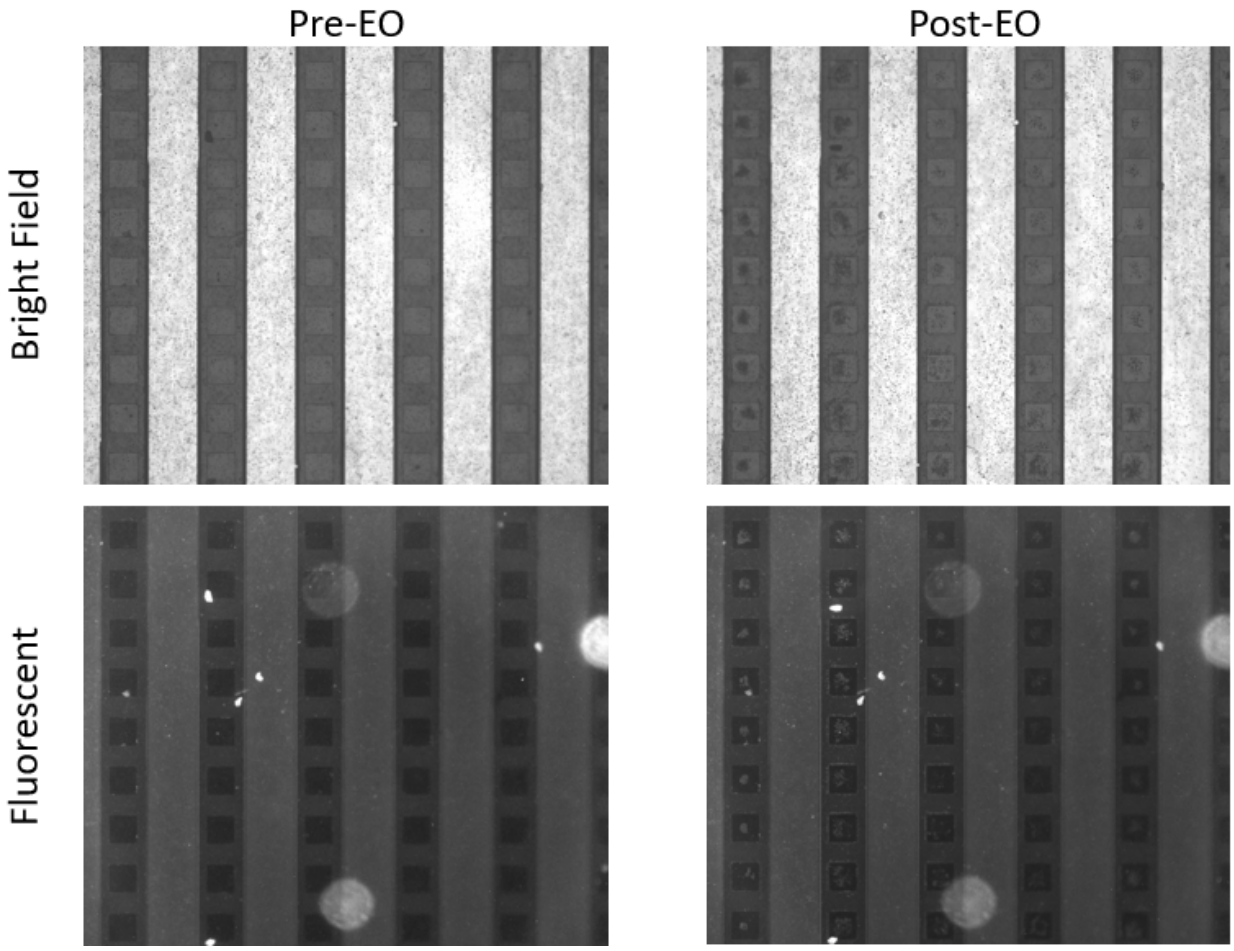

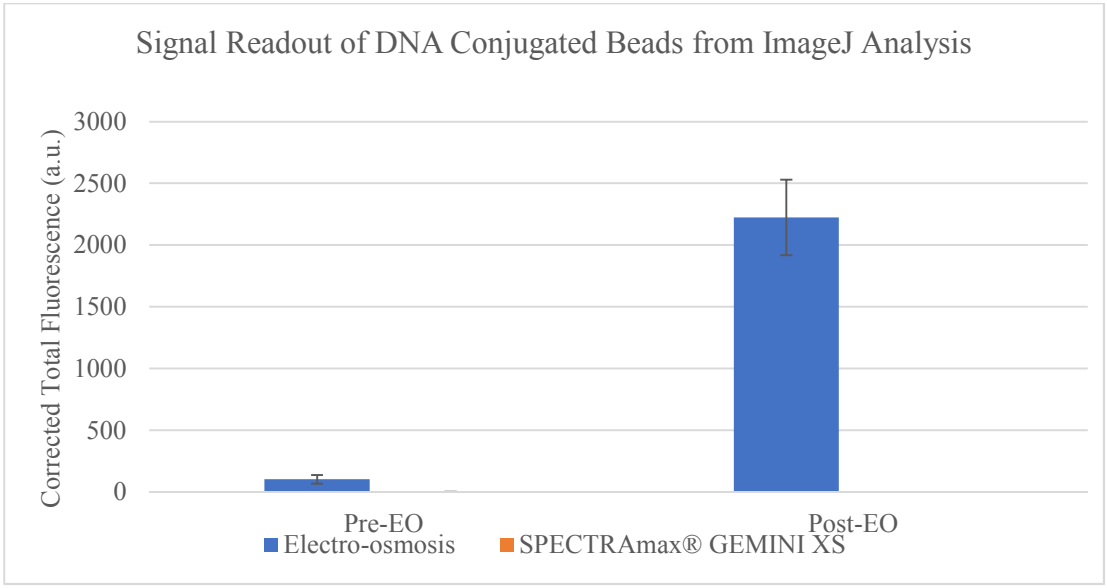

Figure 27: Electro-osmotic Post-concentration Following DSN-mediated DNA Cleavage

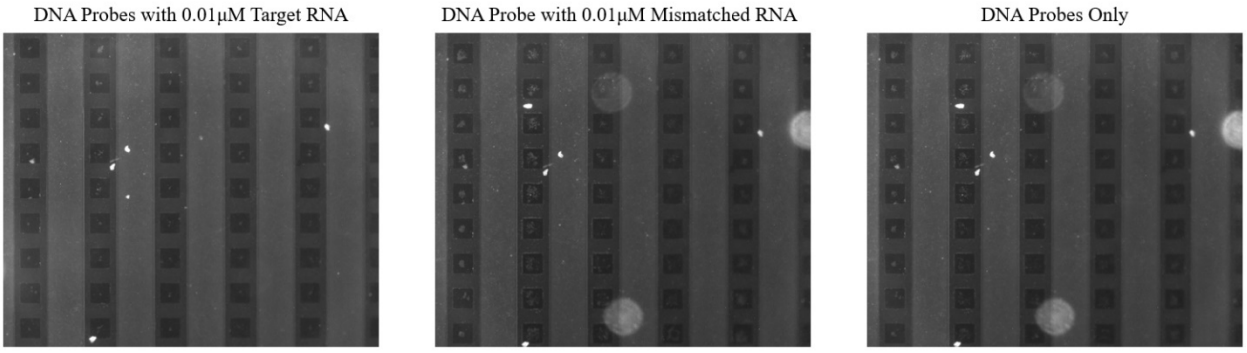

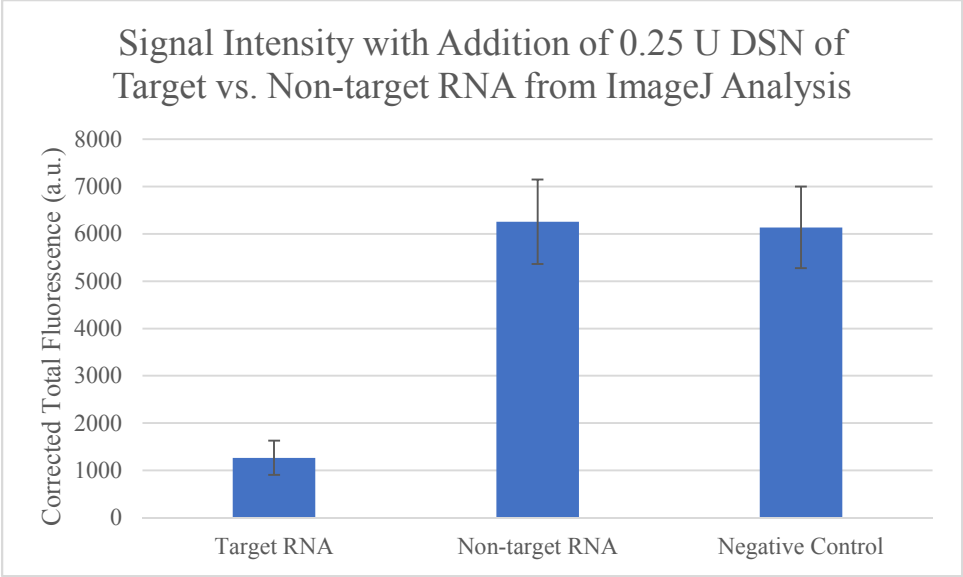

Initial trails for the DSN detection technique of SARS-CoV-2 on the electro-osmotic post-concentration platform were evaluated using biotinylated fluorescent DNA probe target the open reading frame conserved region. Samples were prepared in an RNase-free tube with 100 nM DNA probe, 10 nM RNA, and 0.25 U DSN to a final volume of 100 µl and incubated with 0.25 U DSN at 55ºC for 30 minutes. Prior to electro-osmosis testing on the electrodes, bead samples were immediately prepared at a 1:10 dilution in UltraPure™ DNase/RNase-Free Distilled Water (Thermofisher Scientific). 10 µl of diluted sample was distributed evenly onto the surface of the

electrode for electro-osmosis. As shown in figure 27, signal intensity in samples with 0.25 U DSN decreased in the presence of DNA;RNA complementary duplexes, while signal in non-complementary duplexes remained comparable to the negative control. In preliminary trials, electro-osmostic concentration of signal is a viable method for detection of the SARS-CoV-2 based reaction.

In this work, adaptation of DSN-mediated amplification for detection and differentiation of SARS-CoV-2 strains as well as traditional antibody-based ELISA kits into the electro-osmotic detection scheme was demonstrated with clear differentiation between positive samples targeting analyte and negative controls. Biocompatibility of common materials and reagents used in diagnostic assays were evaluated through testing of standard ELISA and DNA detection protocols with success reflected through detection of target analyte at improved sensitivities in comparison to standard fluorescent plate readers. The electro-osmotic post-concentration technique possesses many advantages to traditional fluorescent detection techniques including improved sensitivity in detection relative to target analyte present within a bulk solution, size exclusion and self-sorting capabilities to differentiate between non-target molecules, and dramatically smaller volumes required for detection than traditional tests such as fluorescent plate readers. Incorporation of multiple stages of signal enhancement are vital to offsetting the cost required to reach competitive sensitivities in analyte detection. Guided electrokinetic assembly is a promising approach for low-resource cost diagnostics and screening due to post-concentration of signal serving as an additional step for improving sensitivity, a key obstacle in point-of-care devices that ultimately result in inferior limits of detection to state-of-the-art techniques and associated technology.

Chapter 4: Summary and Conclusions

With an increasing number of SARS-CoV-2 variants with highly consistent genetic sequences continuing to emerge globally, it becomes increasingly important to focus our attention and resources on prevention and limiting the spread of contagion in high-risk communities. Greater availability to screening tools with sequence-based differentiation is critical for understanding global trends concerning spread and recombination of the virus to limit emergence of new variants. Providing a method of documentation for tracking mutations within the SARS-CoV-2 genome is vital to a global endeavor for understanding and minimizing impact on communities most susceptible to spread of disease.

In this work, we demonstrate a proof-of-concept of a viable low-resource cost strategy for detection of SARS-CoV-2 variants by incorporating a highly specific technique for differentiating target RNA regions using duplex-specific nuclease while achieving reasonable sensitivity using RT-RPA amplification and T7 transcription. While the sensitivity of the demonstrated assay was not at the benchmark RT-PCR level (as the sensitivity was dependent on the amplification strategy), differentiation of key variant regions was successful down to the limit of detection of this assay, indicating the potential as a screening diagnostic device while maintaining key point-of-care features such as isothermal amplification and cheap instrumentation for deployment. Incubation steps of the assay were conducted using heat blocks while endpoint fluorescent readout was measured using a plate reader, an inexpensive alternative to real-time thermocyclers used for PCR amplification and real-time detection.

Additionally, we have demonstrated the multiplexing potential of this assay through simultaneous detection of multiple synthetic RNA targets within one sample. However, the

greatest limiting factor in achieving competitive sensitivity and sensitivity to conventional approaches for molecular detection of SARS-CoV-2 is reaching relevant concentrations of amplified product for DSN recognition of the duplexes. RT-RPA in particular can be limited in simultaneous amplification of multiple regions and is highly dependent on target sequences, amplicon size and primer design for ample replication of analyte.[96]

Compatibility of this assay was further tested using nitrocellulose-based lateral flow as a low-resource cost alternative for sample analysis and patient screening. Proof-of-principle experiments were conducted to successfully detect RNA indicative of the conserved region of the open reading frame region of the SARS-CoV-2 genome. By providing a means for detection without the requirement of expensive instruments such as a fluorescent plate reader, cost of the device can be reduced and become more readily available for communities that require screening technology without requiring the expertise to handle complicated instrumentation and sample analysis. By providing a simple method for detection that could be reduced to a qualitative readout for positive infection, simplification of assay analysis while reducing cost makes this assay more attractive for large-scale screening for populations with limited access to centralized healthcare with readily available access to training and technology of state-of-the-art diagnostics.

Lastly, guided electrokinetic assembly was tested as a method of signal enhancement following DSN digestion and detection of the open reading frame conserved region of the SARS-CoV-2 virus. By utilizing multiple strategies for improvement in signal through target enhancement with recombinase polymerase amplification and signal enhancement using DSN target recycling and electro-osmotic post-concentration, sensitivity of the assay can be improved

[96] Kersting S., Rausch V., Bier F.F., von Nickisch-Rosenegk M. Multiplex isothermal solid-phase recombinase polymerase amplification for the specific and fast DNA-based detection of three bacterial pathogens. *Microchim. Acta.* 2014;181:1715–1723.

without significant contribution to cost, an attractive feature for low-resource cost diagnostics. Through proof-of-principle experiments using established ELISA assays and molecular assays, we have demonstrated compatibility of IDEA-based electro-osmostic bead concentration with biological assays and its potential as a method for improvement in sensitivity in a wide range of diagnostic approaches with antibody-based detection and molecular detection.

Present work demonstrates a novel approach for SARS-CoV-2 diagnostics that incorporates variant discrimination with the potential for success when deployed outside of the typical healthcare environment. The developed assay demonstrates promise as a method to achieve significant specificity in order to distinguish between existing and emerging SARS-CoV-2 variants while possessing flexibility with additional methods for signal amplification such as electro-osmotic post-concentration. One way of further enhancing the assay is to improve the sensitivity with incorporation of more effective upstream amplification or increasing enzyme activity without nonspecific cleavage of DNA probe. Lastly, DSN is an attractive method for RNA-based molecular detection and can be expanded beyond SARS-CoV-2 due to the nature of the enzyme requiring matched duplex recognition for significant cleavage activity toward DNA while also having minimal activity toward RNA. Due to these unique properties of the DSN enzyme, the presented technique is suitable for detection of multiple regions of the SARS-CoV-2 genome without significant adjustment to the design of the assay and can also be adapted for detection of other viruses of interest to develop a larger encompassing screening test for other illnesses. In this work, we hope to demonstrate the applicability of the DSN enzyme in clinical screening applications through a practical and relevant use in detection and differentiation of two common SARS-CoV-2 strains of interest.

REFERENCES:

1. Cascella, Marco, et al. "Features, evaluation, and treatment of coronavirus (COVID-19)." *Statpearls [internet]* (2022).
2. Song, Qi, et al. "Point-of-care testing detection methods for COVID-19." *Lab on a Chip* 21.9 (2021): 1634-1660.
3. Vasireddy, Deepa, et al. "Review of COVID-19 variants and COVID-19 vaccine efficacy: what the clinician should know?." *Journal of Clinical Medicine Research* 13.6 (2021): 317.
4. WHO Clinical Management of Severe Acute Respiratory Infection (SARI) When COVID-19 Disease is Suspected: Interim guidance. 2020. https://apps.who.int/iris/bitstream/handle/10665/331446/WHO-2019-nCoV-clinical-2020.4-eng.pdf?sequence=1&isAllowed=y (accessed 7 November 2022)
5. Ludwig, Stephan, and Alexander Zarbock. "Coronaviruses and SARS-CoV-2: a brief overview." *Anesthesia and analgesia* (2020).
6. National Center for Immunization and Respiratory Diseases (NCIRD), Division of Viral Diseases, Aug. 12 20222.
7. "Symptoms of COVID-19." Center for Disease Control and Prevention. Mar. 22, 2022
8. Giri, Anil K., and Divya RSJB Rana. "Charting the challenges behind the testing of COVID-19 in developing countries: Nepal as a case study." *Biosafety and Health* 2.02 (2020): 53-56.
9. World Health Organization. "Global atlas of medical devices." (2017).
10. Minskaia, E. et al. Discovery of an RNA virus 3′→5′ exoribonuclease that is critically involved in coronavirus RNA synthesis. *Proc. Natl Acad. Sci. USA* **103**, 5108–5113 (2006).
11. Eckerle, L. D. et al. Infidelity of SARS-CoV Nsp14-exonuclease mutant virus replication is revealed by complete genome sequencing. *PLoS Pathog.* **6**, e1000896 (2010).
12. Duffy, S., Shackelton, L. A. & Holmes, E. C. Rates of evolutionary change in viruses: patterns and determinants. *Nat. Rev. Genet.* **9**, 267–276 (2008).
13. Tao, Kaiming, et al. "The biological and clinical significance of emerging SARS-CoV-2 variants." *Nature Reviews Genetics* 22.12 (2021): 757-773.
14. Guia, R. T. et al. A human coronavirus evolves antigenically to escape antibody immunity. *PLoS Pathog.* **17**, e1009453 (2021).
15. Morel, B. et al. Phylogenetic analysis of SARS-CoV-2 data is difficult. *Mol. Biol. Evol.* **38**, 1777–1791 (2020).
16. Mavian, C. et al. Sampling bias and incorrect rooting make phylogenetic network tracing of SARS-COV-2 infections unreliable. *Proc. Natl Acad. Sci. USA* **117**, 12522–12523 (2020).
17. Rambaut, A. et al. A dynamic nomenclature proposal for SARS-CoV-2 lineages to assist genomic epidemiology. *Nat. Microbiol.* **5**, 1403–1407 (2020).
18. Volz, E. et al. Assessing transmissibility of SARS-CoV-2 lineage B.1.1.7 in England. *Nature* **593**, 266–269 (2021).
19. Allen, H. et al. Increased household transmission of COVID-19 cases associated with SARS-CoV-2 variant of concern B.1.617.2: a national case–control study. *Knowledge Hub* (2021).
20. Faria, N. R. et al. Genomics and epidemiology of the P.1 SARS-CoV-2 lineage in Manaus, Brazil. *Science* **372**, 815–821 (2021).

21. Borges, Vítor, et al. "Tracking SARS-CoV-2 VOC 202012/01 (lineage B. 1.1. 7) dissemination in Portugal: insights from nationwide RT-PCR Spike gene drop out data." *Euro. Surveill* 26 (2021): 2100131.
22. Vogels, Chantal BF, et al. "PCR assay to enhance global surveillance for SARS-CoV-2 variants of concern." *MedRxiv* (2021).
23. Morel, B. et al. Phylogenetic analysis of SARS-CoV-2 data is difficult. *Mol. Biol. Evol.* **38**, 1777–1791 (2020).
24. Jacofsky, David, Emilia M. Jacofsky, and Marc Jacofsky. "Understanding antibody testing for COVID-19." *The Journal of arthroplasty* 35.7 (2020): S74-S81.
25. Hall VJ, Foulkes S, Charlett A, Atti A, Monk EJM, Simmons R, et al. SARS-CoV-2 infection rates of antibody-positive compared with antibody-negative health-care workers in England: a large, multicentre, prospective cohort study (SIREN). Lancet. 2021 Apr 17;397(10283):1459-69.
26. Liu, Guoqiang, and James F. Rusling. "COVID-19 antibody tests and their limitations." *ACS sensors* 6.3 (2021): 593-612.
27. Lumley SF, O'Donnell D, Stoesser NE, Matthews PC, Howarth A, Hatch SB, et al. Antibody status and incidence of SARS-CoV-2 infection in health care workers. N Engl J Med. 2020 Dec 23;384:533-40.
28. Qu, Jiuxin, et al. "Profile of immunoglobulin G and IgM antibodies against severe acute respiratory syndrome coronavirus 2 (SARS-CoV-2)." *Clinical Infectious Diseases* 71.16 (2020): 2255-2258.
29. Wölfel, Roman, et al. "Virological assessment of hospitalized patients with COVID-2019." *Nature* 581.7809 (2020): 465-469.
30. Grifoni A, Weiskopf D, Ramirez SI, Mateus J, Dan JM, Moderbacher CR, et al. Targets of T cell responses to SARS-CoV-2 coronavirus in humans with COVID-19 disease and unexposed individuals. Cell. 2020 Jun 25;181(7):1489-501 e15.
31. Robbiani DF, Gaebler C, Muecksch F, Lorenzi JCC, Wang Z, Cho A, et al. Convergent antibody responses to SARS-CoV-2 in convalescent individuals. Nature. 2020 Aug;584(7821):437-42.
32. Suthar MS, Zimmerman MG, Kauffman RC, Mantus G, Linderman SL, Hudson WH, et al. Rapid generation of neutralizing antibody responses in COVID-19 patients. Cell Rep Med. 2020 Jun 23;1(3):100040.
33. Corman, Victor M., et al. "Comparison of seven commercial SARS-CoV-2 rapid point-of-care antigen tests: a single-centre laboratory evaluation study." *The Lancet Microbe* 2.7 (2021): e311-e319.
34. Arnaout, Ramy, et al. "SARS-CoV2 testing: the limit of detection matters." *BioRxiv* (2020).
35. Tahamtan, Alireza, and Abdollah Ardebili. "Real-time RT-PCR in COVID-19 detection: issues affecting the results." *Expert review of molecular diagnostics* 20.5 (2020): 453-454.
36. Liu, Guoqiang, and James F. Rusling. "COVID-19 antibody tests and their limitations." *ACS sensors* 6.3 (2021): 593-612.
37. Giri, Anil K., and Divya RSJB Rana. "Charting the challenges behind the testing of COVID-19 in developing countries: Nepal as a case study." *Biosafety and Health* 2.02 (2020): 53-56.
38. Rezaei, Meysam, et al. "Point of Care Diagnostics in the Age of COVID-19." *Diagnostics* 11.1 (2020): 9.
39. Becherer, L. et al. Loop-mediated isothermal amplification (LAMP)—review and classification of methods for sequence-specific detection. *Anal. Methods* 12, 717–746 (2020).

40. Sun, Yangyang, et al. "One-tube SARS-CoV-2 detection platform based on RT-RPA and CRISPR/Cas12a." *Journal of translational medicine* 19.1 (2021): 1-10.
41. Chen, Janice S., et al. "CRISPR-Cas12a target binding unleashes indiscriminate single-stranded DNase activity." *Science* 360.6387 (2018): 436-439.
42. Gootenberg, Jonathan S., et al. "Nucleic acid detection with CRISPR-Cas13a/C2c2." *Science* 356.6336 (2017): 438-442.
43. Gootenberg, Jonathan S., et al. "Multiplexed and portable nucleic acid detection platform with Cas13, Cas12a, and Csm6." *Science* 360.6387 (2018): 439-444.
44. Gerasimova, Yulia V., and Dmitry M. Kolpashchikov. "Enzyme-assisted target recycling (EATR) for nucleic acid detection." *Chemical Society Reviews* 43.17 (2014): 6405-6438.
45. Ye, Jiawei, et al. "Research advances in the detection of miRNA." *Journal of pharmaceutical analysis* 9.4 (2019): 217-226.
46. Shagin, Dmitry A., et al. "A novel method for SNP detection using a new duplex-specific nuclease from crab hepatopancreas." *Genome research* 12.12 (2002): 1935-1942.
47. Qiu, Xiaopei, et al. "Duplex-specific nuclease-mediated bioanalysis." *Trends in biotechnology* 33.3 (2015): 180-188.
48. Tan, Lin, et al. "Duplex-specific nuclease-mediated target recycling amplification for fluorescence detection of microRNA." *Analytical Methods* 11.2 (2019): 200-204.
49. Liu, Meiqing, et al. "SARS-CoV-2 RNA detection with duplex-specific nuclease signal amplification." *Micromachines* 12.2 (2021): 197.
50. Gong, Shaohua, et al. "Duplex-specific nuclease-assisted CRISPR-Cas12a strategy for MicroRNA detection using a personal Glucose meter." *Analytical Chemistry* 93.30 (2021): 10719-10726.
51. Liu, Meiying, et al. "Label-free optical detection of single-base mismatches by the combination of nuclease and gold nanoparticles." *Biosensors and Bioelectronics* 26.11 (2011): 4294-4300.
52. Jansson, Martin D., and Anders H. Lund. "MicroRNA and cancer." *Molecular oncology* 6.6 (2012): 590-610.
53. Xu, Fang, et al. "Ultrasensitive and multiple disease-related microRNA detection based on tetrahedral DNA nanostructures and duplex-specific nuclease-assisted signal amplification." *ACS Applied Materials & Interfaces* 8.49 (2016): 33499-33505.
54. Miao, Peng, et al. "Nuclease assisted target recycling and spherical nucleic acids gold nanoparticles recruitment for ultrasensitive detection of microRNA." *Electrochimica Acta* 190 (2016): 396-401.
55. Wang, Ye, et al. "Duplex-specific nuclease-amplified detection of MicroRNA using compact quantum dot–DNA conjugates." *ACS applied materials & interfaces* 10.34 (2018): 28290-28300.
56. Zhang, Shixi, et al. "Multiplex miRNA assay using lanthanide-tagged probes and the duplex-specific nuclease amplification strategy." *Chemical Communications* 52.99 (2016): 14310-14313.
57. Wu, Yudong, et al. "Recent advances in duplex-specific nuclease-based signal amplification strategies for microRNA detection." *Biosensors and Bioelectronics* 165 (2020): 112449.
58. Li, Xue-Mei, et al. "A dual-amplified electrochemical detection of mRNA based on duplex-specific nuclease and bio-bar-code conjugates." *Biosensors and Bioelectronics* 65 (2015): 245-250.

59. Kuang, Yuqiong, et al. "Duplex-specific nuclease-mediated amplification strategy for mass spectrometry quantification of MiRNA-200c in breast cancer stem cells." *Analytical chemistry* 91.14 (2019): 8820-8826.
60. Pang, Yuanfeng, et al. "Fe3O4@ Ag magnetic nanoparticles for microRNA capture and duplex-specific nuclease signal amplification based SERS detection in cancer cells." *Biosensors and Bioelectronics* 79 (2016): 574-580.
61. Wei, Hongjuan, et al. "Duplex-specific nuclease signal amplification-based fluorescent lateral flow assay for the point-of-care detection of microRNAs." *Analyst* 146.2 (2021): 558-564.
62. Shandilya, Ruchita, et al. "Point-of-care diagnostics approaches for detection of lung cancer-associated circulating miRNAs." *Drug Discovery Today* 26.6 (2021): 1501-1509.
63. Ying, Na, et al. "Lateral flow nucleic acid biosensor for sensitive detection of microRNAs based on the dual amplification strategy of duplex-specific nuclease and hybridization chain reaction." *PloS one* 12.9 (2017): e0185091.
64. Wang, Nan, et al. "Recent advances in the rapid detection of microRNA with lateral flow assays." *Biosensors and Bioelectronics* (2022): 114345.
65. Mercatelli, Daniele, and Federico M. Giorgi. "Geographic and genomic distribution of SARS-CoV-2 mutations." *Frontiers in microbiology* 11 (2020): 1800.
66. Ye, Jian, et al. "Primer-BLAST: a tool to design target-specific primers for polymerase chain reaction." *BMC bioinformatics* 13.1 (2012): 1-11.
67. Rosenberg, Alan H., et al. "Vectors for selective expression of cloned DNAs by T7 RNA polymerase." *Gene* 56.1 (1987): 125-135.
68. Patchsung, Maturada, et al. "Clinical validation of a Cas13-based assay for the detection of SARS-CoV-2 RNA." *Nature biomedical engineering* 4.12 (2020): 1140-1149.
69. Sun, Yangyang, et al. "One-tube SARS-CoV-2 detection platform based on RT-RPA and CRISPR/Cas12a." *Journal of translational medicine* 19.1 (2021): 1-10.
70. Altschul, S.F., Gish, W., Miller, W., Myers, E.W. & Lipman, D.J. (1990) "Basic local alignment search tool." J. Mol. Biol. 215:403-410.
71. Gordon, David E., et al. "A SARS-CoV-2 protein interaction map reveals targets for drug repurposing." *Nature* 583.7816 (2020): 459-468.
72. "Guide for Using the Fluorescence Spectraviewer." *Thermo Fisher Scientific - US*, Thermo Fisher Scientific Inc., https://www.thermofisher.com/us/en/home/life-science/cell-analysis/fluorophores/guide-fluorescence-spectraviewer.html.
73. Yin, Bin-Cheng, Yu-Qiang Liu, and Bang-Ce Ye. "One-step, multiplexed fluorescence detection of microRNAs based on duplex-specific nuclease signal amplification." *Journal of the American Chemical Society* 134.11 (2012): 5064-5067.
74. Anisimova, Veronika E., et al. "Isolation, characterization and molecular cloning of duplex-specific nuclease from the hepatopancreas of the Kamchatka crab." *BMC biochemistry* 9.1 (2008): 1-12.
75. Zhang, Kai, et al. "Sensitive detection of microRNA in complex biological samples by using two stages DSN-assisted target recycling signal amplification method." *Biosensors and Bioelectronics* 87 (2017): 358-364.
76. Trotta, Edoardo. "On the normalization of the minimum free energy of RNAs by sequence length." *PloS one* 9.11 (2014): e113380.

77. Arnaout, Ramy, et al. "SARS-CoV2 testing: the limit of detection matters." *BioRxiv* (2020).
78. Brown, Kevin A., et al. "S-gene target failure as a marker of variant B. 1.1. 7 among SARS-CoV-2 isolates in the greater Toronto area, December 2020 to March 2021." *Jama* 325.20 (2021): 2115-2116.
79. Gavet, Olivier, and Jonathon Pines. "Progressive activation of CyclinB1-Cdk1 coordinates entry to mitosis." *Developmental cell* 18.4 (2010): 533-543.
80. Hosseini, Imman I., et al. "Cell properties assessment using optimized dielectrophoresis-based cell stretching and lumped mechanical modeling." *Scientific reports* 11.1 (2021): 1-13.
81. Barsotti Jr, Robert J., et al. "Assembly of metal nanoparticles into nanogaps." *small* 3.3 (2007): 488-499.
82. Ohannesian, Nareg, et al. "Directed concentrating of micro-/nanoparticles via near-infrared laser generated plasmonic microbubbles." *ACS omega* 5.50 (2020): 32481-32489.
83. Xiong, Xugang, et al. "Directed assembly of gold nanoparticle nanowires and networks for nanodevices." *Applied Physics Letters* 91.6 (2007): 063101.
84. Subramanian, Arunkumar, et al. "Micro and Nanorobotic Assembly Using Dielectrophoresis." *Robotics: Science and Systems*. 2005.
85. Vazquez-Pinon, Matias, et al. "Hydrodynamic channeling as a controlled flow reversal mechanism for bidirectional AC electroosmotic pumping using glassy carbon microelectrode arrays." *Journal of Micromechanics and Microengineering* 29.7 (2019): 075007.
86. Cortez, Jennifer, et al. "Electrokinetic Propulsion of Polymer Microparticulates Along Glassy Carbon Electrode Array." *Journal of Micro-and Nano-Manufacturing* 8.2 (2020): 024504.
87. Squires, Todd M., and Martin Z. Bazant. "Induced-charge electro-osmosis." *Journal of Fluid Mechanics* 509 (2004): 217-252.
88. Bruckenstein, Stanley. "Physicochemical hydrodynamics." *Nature* 268.5618 (1977): 298-299.
89. Zhou, Tuo, et al. "Guided Electrokinetic Assembly of Polystyrene Microbeads onto Photopatterned Carbon Electrode Arrays." *ACS applied materials & interfaces* 12.31 (2020): 35647-35656.
90. Green, Nicolas G., et al. "Fluid flow induced by nonuniform ac electric fields in electrolytes on microelectrodes. I. Experimental measurements." *Physical review E* 61.4 (2000): 4011.
91. Green, Nicolas G., et al. "Fluid flow induced by nonuniform ac electric fields in electrolytes on microelectrodes. III. Observation of streamlines and numerical simulation." *Physical review E* 66.2 (2002): 026305.
92. Passive Adsorption Protocol, Thermofisher Scientific, https://www.thermofisher.com/us/en/home/life-science/cell-analysis/qdots-microspheres-nanospheres/idc-surfactant-free-latex-beads/latex-bead-protein-coupling-protocols/passive-adsorption-protocol.html. Accessed on 7 November, 2022.
93. Zelová, Hana, and Jan Hošek. "TNF-α signalling and inflammation: interactions between old acquaintances." Inflammation Research 62.7 (2013): 641-651.
94. Juhasz, Kata, Krisztina Buzas, and Erno Duda. "Importance of reverse signaling of the TNF superfamily in immune regulation." Expert review of clinical immunology 9.4 (2013): 335-348.
95. Gong, Ke, et al. "Tumor necrosis factor in lung cancer: Complex roles in biology and resistance to treatment." *Neoplasia* 23.2 (2021): 189-196.

96. Kersting S., Rausch V., Bier F.F., von Nickisch-Rosenegk M. Multiplex isothermal solid-phase recombinase polymerase amplification for the specific and fast DNA-based detection of three bacterial pathogens. *Microchim. Acta.* 2014;181:1715–1723.